TÉCNICO LISBOA

# Ammonia Combustion: Experiments and Modelling

**Carlos Filipe Lopes Ramos**

Thesis to obtain the Master of Science Degree in

## Aerospace Engineering

Supervisor: Prof. Mário Manuel Gonçalves da Costa

### Examination Committee

Chairperson: Prof. Filipe Szolnoky Ramos Pinto Cunha

Supervisor: Prof. Mário Manuel Gonçalves da Costa

Member of the Committee: Prof. Edgar Caetano Fernandes

**December 2018**

# Acknowledgments

Firstly, I would like to thank my supervisor, Professor Mário Costa, for all the support, guidance and perseverance that allowed me to complete this investigation on a subject that I find very important and interesting.

Additionally, I would like to thank Pedro and Rodolfo for all the partnership in all steps of the research, and Mr. Pratas for all the help and assistance throughout the experimental work. I would also like thank all the personnel at the laboratory, not only for the scientific discussions and opinions exchanged but also for the friendship that allowed me to feel welcome and integrated with everyone.

Finally, I would like to thank my family, my parents, Filipa, Kina, and Kyra that always pushed me for greater achievements and always believed in me.

# Resumo

Amoníaco é considerado uma das opções mais viáveis quanto à produção de energia sem libertação de carbono. Contudo, a falta de informação relativa às emissões da queima de amoníaco inibe a sua implementação como combustível. Assim, este trabalho centra-se em quantificar as espécies poluentes, nomeadamente $NO_x$, libertadas durante a combustão do amoníaco e das suas misturas com metano e hidrogénio, e perceber como estas concentrações são influenciadas por diversas variáveis, tais como a razão de equivalência, constituintes da mistura de combustível e quantidade de amoníaco na mistura de combustível. Foram utilizados dois queimadores distintos com misturas de amoníaco/metano e amoníaco/hidrogénio, em condições estequiométricas e pobres. Os resultados foram posteriormente comparados com modelos cinéticos recentes que lidam especificamente com a combustão de amoníaco. Os resultados experimentais mostram que a concentração de $NO_x$ aumenta à medida que a quantidade de amoníaco na mistura de combustível aumenta até 50%, diminuindo posteriormente. Adicionalmente, as emissões de $NO_x$ diminuem com a redução da razão de equivalência. Assim, a combustão ótima em termos de baixos teores de $NO_x$ ocorre para razões de equivalência reduzidas e elevadas quantidades de amoníaco na mistura de combustível. Os resultados de CO revelam a combustão completa dos hidrocarbonetos. Contudo, a presença de $NH_3$ no escape em condições de elevada potência sugere uma combustão incompleta do amoníaco. Comparações com os modelos cinéticos mostram que os padrões gerais das emissões são razoavelmente reproduzidos.

**Palavras-chave:** Amoníaco, Combustão, Emissões, $NO_x$, Experimental, Numérico.

# Abstract

Ammonia is regarded as one of the most viable alternatives to produce carbon-free energy. However, scarcity of information on the emissions of burning ammonia inhibits its implementation as a fuel. Therefore, the present work focuses on quantifying the pollutant gas species, namely $NO_x$, that are emitted from the combustion of ammonia and its mixtures with methane and hydrogen, and understanding how their concentrations are affected by several variables, such as equivalence ratio, constituents of the fuel mixture and amount of ammonia in the fuel mixture. Two different types of burners were used over a wide range of conditions, employing mixtures of ammonia/methane and ammonia/hydrogen under stoichiometry and lean conditions. The results were afterwards compared with recent chemical kinetic models that deal specifically with the combustion of ammonia. The experimental results showed that the $NO_x$ concentration initially increases as the quantity of ammonia in the fuel mixture rises up to 50%, decreasing afterwards. Furthermore, $NO_x$ emissions decrease as the equivalence ratio is reduced. Therefore, optimum combustion in terms of low $NO_x$ emissions occurs for reduced equivalence ratios and high amounts of ammonia in the fuel mixture. The CO results indicate complete combustion of hydrocarbons. However, the presence of unburnt ammonia for high thermal inputs points towards incomplete combustion of ammonia under these conditions. Comparisons with the results from the chemical kinetic models show that the overall emissions patterns are reasonably captured.

**Keywords:** Ammonia, Combustion, Emissions, $NO_x$, Experimental, Numerical.

# Table of Contents

# List of figures

# List of tables

# Acronyms

A/D – Analog to Digital

CCS – Carbon Capture and Storage

DOE – Department of Energy

IEA – International Energy Agency

SCR – Selective Catalytic Reduction

SNCR – Selective Non-Catalytic Reduction

UNFCCC – United Nations Framework Convention on Climate Change

# 1. Introduction

## 1.1. Motivation

Energy and mass are the properties that define the physics of our universe. Indeed, everything that has mass can be considered a part of a network constantly sharing energy, and, at a larger scale, our society constitutes one of those networks. As the global population rises, so do our energy demands. A look at the last years of energy statistics by the International Energy Agency (IEA) [1] proves such reality. Figure 1.1 shows how the total primary energy supply has been evolving by source.

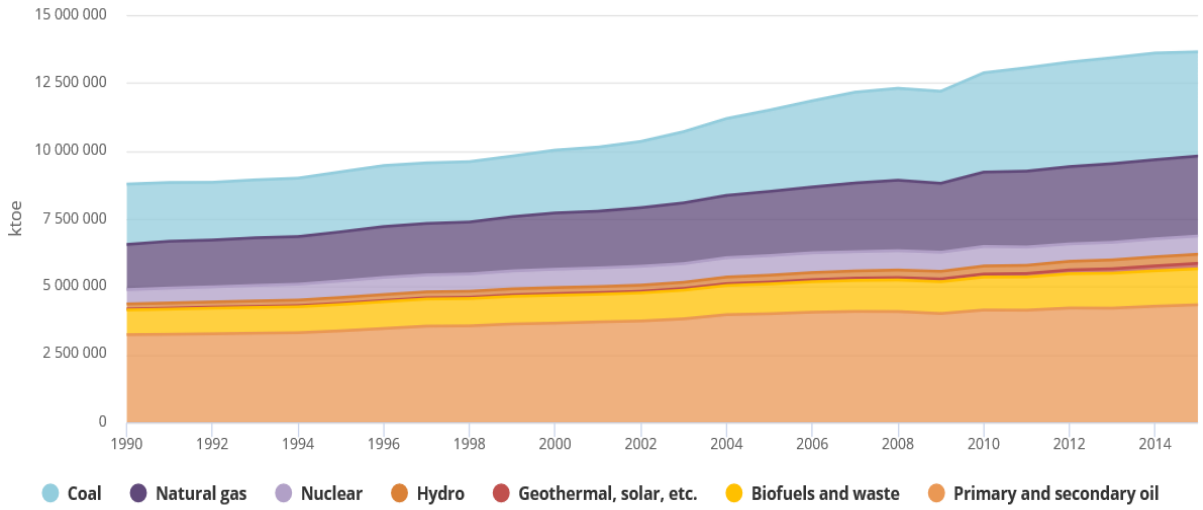


Figure 1.1 - Global total primary energy supply by source (excluding electricity and heat) between 1990 and 2015 [1].

Accounting for the different energy sources, the conclusion is that the combustion of fossil fuels constitutes the principal process of energy supply. In fact, as of 2012, about 90% of the energy used in electricity production, thermal energy and transportation results from the combustion of solid, liquid and gaseous fuels [2]. Although the tendency is for this percentage to decrease, combustion is expected to largely dominate the energy production sector for the next decades [2].

Nevertheless, the impacts of burning fossil fuels are well known: the flue gases that result from the combustion process greatly influence the biosphere and atmosphere in a negative manner, mainly due to most of them having carbon in their composition [2]. Data from the IEA corroborates the correspondence between the increase of energy demands (seen previously) and the growth in pollution [1]. Figure 1.2 shows the global $CO_2$ emissions from the combustion of fuels, from 1990 to 2015.

Additionally, fossil feedstock numbers are finite and dwindling, as the rate at which they are consumed far surpasses the rate of creation by nature. Therefore, they will eventually run out completely or stop being economically feasible [2]. It is, therefore, widely known that a change must occur in the energy sector worldwide, since the current situation is unsustainable.

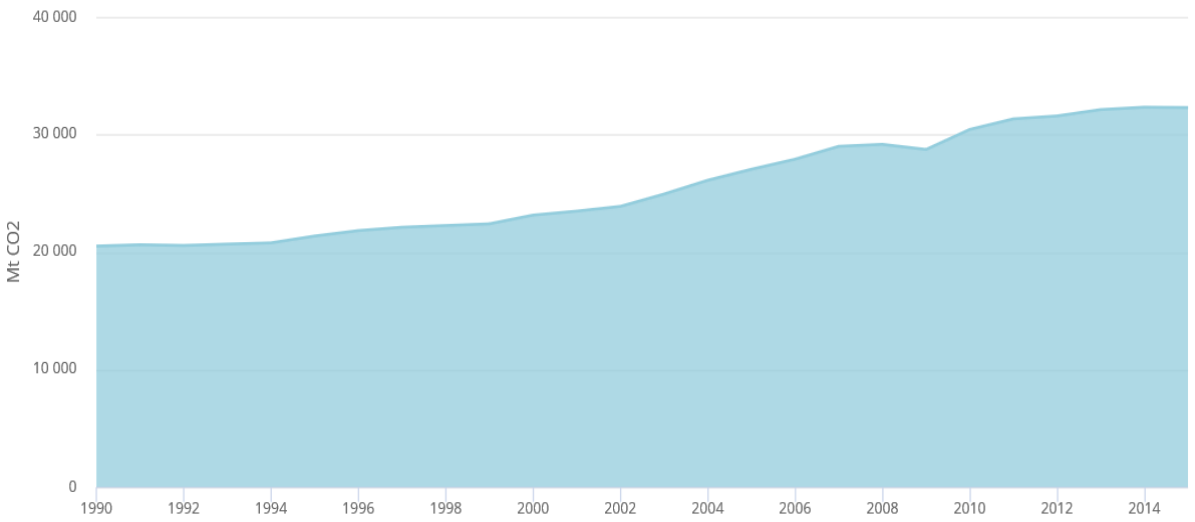


Figure 1.2 - Global $CO_2$ emissions (from combustion fuels only) from 1990 to 2015 [1].

As a proactive measure in decreasing carbon-based pollution, the United Nations Framework Convention on Climate Change (UNFCCC) created the Paris Agreement, in December of 2015 [3]. As of July 2018, 195 countries have signed the agreement, which aims to “keep the increase in global average temperature to well below 2 °C above pre-industrial levels” and “limit the increase to 1.5 °C”, among other aspects regarding adaptation and finance of members. To achieve these values, “global emissions need to peak as soon as possible”, thus existing a need to rely on “the best possible science”.

Renewable energies have an important role in helping achieve these objectives. They have been studied, commercialized and improved upon for the last decades, thus strengthening this shift towards energy sustainability. They exist in several forms, from solar and geothermal, to wind and hydropower – to name a few – and they all propose an emission-free energy production process. Although they have started to gain a fair share of the global energy supply in the last years, one aspect that defines them is their variability, as their potential is dependent on the location and time: renewable sources like wind and solar have limited availability to satisfy a highly variable energy demand. Additionally, as mentioned before, combustion processes will still represent the bulk of energy supply. This means the most cost-effective manner would be to find a suitable fuel to substitute fossil feedstock, while incurring in the least amount of changes to the current energy production processes and infrastructures. Such substitute would need to be able to supply clean and sustainable energy, in order to make frameworks like the Paris Agreement an achievable reality.

Hydrogen ($H_2$) has been considered a strong candidate for this substitution [4]. It is considered a clean energy, as its combustion does not include carbon, having the potential to only result in water and nitrogen. It is the lightest fuel and consists of the most abundant element in the universe. Jain [4] has studied the feasibility of a hydrogen-based economy where the fuel would be able to satisfy all kinds of energy demands, taking into account that it is already being used in experimental vehicles and in space programmes. Nevertheless, the author acquiesces in stating that the properties of hydrogen require additional care in production, storage and transportation. Such are the problems that limit its use in most

of the common scenarios. Reiter and Kong [5] further described the concerns of burning hydrogen: it has a high burning velocity, low ignition energy and it produces flashback easily, which is why it needs to be stored at very low temperatures or very high pressures.

Ammonia ($NH_3$) is another candidate for replacing fossil fuels. It is already widely used as fertilizer, refrigerant and chemical feedstock for the manufacture of other substances, and is now being considered as a suitable energy carrier [6]. As a component in nitrogen fertilizer production, ammonia has supported about 27% of the world's population in the last century, which corresponds to approximately 42% of the estimated total births since 1908 [7].

Ammonia is mainly produced from the Haber-Bosch process, which has been developed for more than a century, and has earned its creators Nobel prizes, individually [8]. It consists of combining hydrogen and nitrogen in a 3:1 ratio at high pressure and moderate temperature. The hydrogen can result from electrolysis (of water) or from steam reforming (of a fossil fuel, normally natural gas), while the nitrogen comes from air [8]. Ammonia is one of the world's most synthesized chemicals [5].

Furthermore, it has safer handling properties when compared to hydrogen: storage only requires relatively low pressures or temperatures, and in those conditions, ammonia contains 30% more energy per volume than liquid hydrogen. The drawback is that, as a combustion fuel, ammonia has a high ignition temperature and low flame speed, both constituting flammability challenges [5].

Bartels [9] compared how an economy based on each of these options would be sustainable and feasible. Taking into account that both energy sources would have the same benefits, the author debates whether the lower cost of production of hydrogen would suffice for it to be a frontrunner. Indeed, ammonia will always be more expensive than hydrogen since the former depends on the production of the latter, which means it will always require additional processes for its synthesis. Nevertheless, taking into account how well developed the ammonia infrastructures are, due to its prolonged use in other sectors, the lower cost of transportation and storage, and higher efficiency of ammonia gives it an economic lead over the competition.

As ammonia's potential as a sustainable energy source started to gather arguments in its favour, in 2006 the Department of Energy (DOE) of the USA conducted an analysis on its use for the transportation sector [10]. In this study, the authors investigated the key issues and disadvantages of ammonia as energy carrier for on-board vehicular hydrogen storage, i.e., a system where ammonia stored in the vehicle is converted into hydrogen, to be used in a fuel-cell. Considering the cracking difficulties, safety, and toxicity issues of this system, the DOE ended in an unfavourable note, stating that much improvement is needed. As a result, it would not fund R&D to improve ammonia fuel processing technologies, for use on-board light weight vehicles, at that time.

Nonetheless, in the last decade the focus has changed from just perceiving ammonia as a middleman for hydrogen consumption, to considering ammonia itself as a fuel. With this objective in mind, ammonia would be capable of being used in combustion engines, gas turbines and boilers, needing only slight or no modifications for existing ones, while also being compatible with fuel-cells [8].

In light of current research, the Department of Energy of the USA has changed its perspective on the matter. Consequently, it has launched a special programme that aims to develop scalable technologies for converting electrical energy into energy-dense liquid fuels that do not contain carbon. From the 16 projects included in this programme, 13 are focused on ammonia [11]. This commitment of the DOE marks a great change in the mentality of governmental institutions, in which ammonia starts being considered a rather viable alternative to fossil fuels.

A reason for this shift in perspective has been the acknowledgment that the implementation of ammonia as a fuel in the present times is already economically feasible. For example, Zamfirescu et al. [6] investigated the potential of ammonia being used in internal combustion engines and fuel-cells, which also takes into account the refrigeration potential of $NH_3$. Comparing with other conventional fuels and hydrogen, the authors concluded that ammonia is the least expensive fuel in terms of $/GJ.

Leveraging all of these insights, ammonia may represent the forefront of future clean fuels. Its applications must be studied thoroughly in order to maximise its potential, especially when it comes to combustion. Although burning ammonia may possibly result in only water and nitrogen – ideally – it must be taken into account that this scenario is still farfetched, since technologies for such are not ready yet. Thus, ammonia combustion still produces pollutants, most being known as $NO_x$ (nitric oxide, NO, and nitrogen dioxide, $NO_2$). Experimental and computational studies have focused on the flammability conditions of ammonia; however, data on $NO_x$ emissions is scarce. Therefore, if ammonia is to be implemented seriously in the energy supply sectors, more information on the emissions is needed, and the same is true for validating numerical models against experimental data.

Thus, the aim of the present thesis is to study the combustion of ammonia and its mixtures with methane and hydrogen for a wide range of operating conditions, both experimentally and numerically, in order to gather more insight into this emerging subject.

## 1.2. Literature Review

### 1.2.1. Background

Before presenting the literature review, it is important to elucidate some of the reactions that can take place in flames that include ammonia. In simple terms, ammonia ($NH_3$) reacting with oxygen ($O_2$) constitutes the basis of the combustion process. It is, however, more common to react with air, which also includes nitrogen ($N_2$). In air, the approximate ratio of $O_2$ molecules to $N_2$ is 1:3.76, thus, the reaction can be defined by the following stoichiometry [12]:

$$4\,NH_3 + 3\,(O_2 + 3.76\,N_2) \rightarrow 6\,H_2O + 15.28\,N_2 \quad (1)$$

This would mean the combustion of ammonia has the potential to result in only water and nitrogen. This is one of the most important features of $NH_3$, since such reaction would be completely "clean", regarding the products. However, the following can also happen [12]:

$$4\,NH_3 + 5\,(O_2 + 3.76\,N_2) \rightarrow 4\,NO + 6\,H_2O + 18.8\,N_2 \tag{2}$$

This is a simple explanation on how nitric oxide (NO) can be formed from the combustion of ammonia. Additionally, due to the high temperatures that occur in flames, oxidation of the nitrogen in air is also a factor, leading to further increased values of NO in the exhaust, which are not explained by the previous equation. This chemical mechanism is called "Zel'dovich mechanism", and the reactions can be summarized by the following one [2]:

$$N_2 + O_2 \rightarrow 2\,NO \tag{3}$$

Additionally, there are other mechanisms for the production of nitric oxide. Nevertheless, in ammonia combustion, the major source of NO is the $NH_3$ molecules. Nitrogen dioxide ($NO_2$) is formed from NO, and together they are the major constituents of $NO_x$, a term that is used to denominate the nitrogen oxides that contribute for air pollution. The mechanism that creates $NO_2$ is the following [13]:

$$2\,NO + O_2 \rightarrow 2\,NO_2 \tag{4}$$

If the fuel is a mixture of ammonia and another constituent, such as hydrogen ($H_2$) or methane ($CH_4$), the following equations apply:

$$\begin{aligned} &x\,NH_3 + (1-x)\,H_2 + (0.25x + 0.5)(O_2 + 3.76\,N_2) \rightarrow \\ &\rightarrow (0.5x + 1)\,H_2O + (1.44x + 1.88)\,N_2 \end{aligned} \tag{5}$$

for the case of hydrogen, and:

$$\begin{aligned} &x\,NH_3 + (1-x)\,CH_4 + (2 - 1.25x)(O_2 + 3.76\,N_2) \rightarrow \\ &\rightarrow (1-x)CO_2 + (2 - 0.5x)\,H_2O + (7.52 - 4.20x)\,N_2 \end{aligned} \tag{6}$$

for the case of methane. In these equations, $x$ represents the mole fraction of ammonia in the fuel mixture. With these two additives, the formation of $NO_x$ can also occur and it can be influenced by the ratios of the fuel constituents and other variables, as will be discussed afterwards. However, the combustion of ammonia with hydrogen does not yield $CO_2$, unlike with methane. As a consequence, the combustion of a $NH_3$-$H_2$ mixture is still carbon-free.

Nitrogen oxides are the main obstacle for implementing ammonia as a completely clean fuel, because, even though they do not contain carbon, they are still highly pollutant. Even if they are present in only small traces, they are a major participant in the occurrence of smog and contribute to the formation of

nitric acid, which is very reactive with most metals and leads to acid rain. Therefore, the formation of these species should be suppressed as efficiently as possible.

Nitrogen oxides can be minimized by altering the combustion process or implementing post-combustion methods [2]. The former is mainly used for burning hydrocarbons, where the major source of $NO_x$ is air-nitrogen. Since with ammonia combustion, the principal $NO_x$ source is the fuel itself, the most employed option is the latter [14]. There are mainly two manners of decreasing the $NO_x$ concentration in post-combustion: selective non-catalytic reduction (SNCR) and selective catalytic reduction (SCR) [2].

SNCR involves the introduction of ammonia (or urea) in the location where NO is located, to expedite its conversion into $N_2$ and $H_2O$. The reactions that occur are simplified as [14]:

$$4\,NO + 4\,NH_3 + O_2 \rightarrow 4\,N_2 + 6\,H_2O \tag{7}$$

On the other hand, SCR promotes the conversion of NO with the use of a catalyst, which includes secondary reactions, although the end products are the same [14].

Lastly, another danger of burning ammonia is when the combustion is incomplete. The presence of unburnt $NH_3$ at the exhaust is dangerous, since ammonia is considered highly toxic [8]. Therefore, these emissions should also be inhibited, through altering the combustion processes or implementing post-combustion treatments. The latter are commonly used by employing catalysts to convert any leftover ammonia into other innocuous species [13].

### 1.2.2. Ammonia Combustion Studies

As mentioned before, ammonia constitutes the focus of investigations on its feasibility as a complete alternative to fossil fuels in combustion processes. Although this interest has been gathering more attention and supporters in recent years, combustion of ammonia is not exactly new.

Remounting to 1809, Henry [15] conducted the first documented case of ammonia combustion. At the time, the constituents of ammonia had already been theorized. The author resourced to burning the substance, as a method to determine its composition. Although the specific burner is not specified, Henry was the first to report the difficulty of burning ammonia, which would only occur in a narrow interval of ratios of $NH_3$ to $O_2$.

However, more than a century was needed to observe an application of ammonia combustion in a practical environment. In 1945, Kroch [12] published his work on using this chemical as fuel for motor buses in Belgium. In the course of the 2nd World War, the author explained that diesel would stop being supplied to civilian buses as of April 1942, due to war-time efforts. Since liquefied petroleum gas was not available in sufficient quantities, and using compressed coal gas alone was not feasible due to its low energy density, the solution was to adapt the motor buses to a combustion system based on ammonia. The author noted that coal gas was also used as an additive, because of ammonia's resilience to burning by itself. The author expressed his initial concern in the combustion resulting not only in water,

but also in nitric oxide, which would lead to the existence of nitric acid in the exhaust. However, after a year and thousands of miles driven, no trace of corrosion was present on the parts of the motor in contact with the flue gases. Additionally, wear and tear were not worse than what could be found in diesel and gasoline engines.

This application spawned several studies that sought to investigate the properties of ammonia combustion and its applications, should fossil fuels suffer a supply shortage. The 1960's were the stage for important studies that defined the initial flammability conditions in which ammonia could combust. Supported by the US Army, Starkman and Samuelsen [16] recognized the difficulty of burning the chemical, so they investigated the properties of the reactions taking place in a CFR engine. The authors proved that slow flame speed was the main contributor to low flammability, and noted that decomposition of $NH_3$ prior to the combustion was the most important variable for successful ignition. It was also noted that the NO concentrations at the exhaust were quite high, comparing to other fuels, and could not be explained only by the Zel'dovich Mechanism. Thus, the authors had observed the incomplete conversion of the ammonia molecules, and the consequent formation of nitric oxide (equation 2).

In the same year, Verkamp et al. [17] conducted experimental studies in the same vein as the last mentioned, although in a flat-flame burner. The authors noted that, not only ammonia burned considerably slower than hydrocarbon fuels, but also the range of equivalence ratios for stable flames was much narrower. As a result, ammonia could not be used alone in conventional gas turbine burners unless the ignition-system energy was increased and the fuel was injected in gaseous state. The authors further studied the inclusion of additives in the fuel. However, none was capable of improving the flame stability to the extent required. The last objective was to study the effect of pre-dissociation, having concluded that a mixture using 28% dissociated ammonia had stability and ignition properties similar to those of methane, which corroborates the findings of the previous study of Starkman and Samuelsen [16].

Pratt [18] followed suit and analysed scaling of gaseous ammonia combustion in gas turbines. The author took the information gathered and constructed a performance map for these combustors, to define the most efficient conditions of operation. Once again it was shown that the main problem of burning ammonia is the slow chemical reaction between this substance and air, aggravated by the much less effective mixing of the constituents, comparing to more common fuels. To increase flame stability, apart from using additives or resourcing to cracking ammonia, Pratt recommended the use of smaller nozzle orifices to increase the velocity of the fuel injection, thus allowing for better mixing.

Although a few other studies from this time period exist, the investigations presented here thus far summarize the principal conclusions made in the twentieth century, regarding the combustion of ammonia. Nevertheless, in this century, work in this matter can be considered scarce, since the low cost of using carbon-based fuels kept the overall interest low [6]. Awareness for the use of ammonia as fuel started expanding in the twenty-first century, due to its potential as a clean and combustible energy source.

In more recent years, ammonia has been featured in combustion studies with the intent of understanding the formation of nitrogen-based radicals and other species. In these studies, only small quantities of ammonia were fed to the burners. Konnov et al. [19] studied the use of methane flames doped with ammonia – the latter representing 0.5% of the fuel, in volume. Their goal was to analyse the formation of fuel-bound $NO_x$ in a perforated plate burner at atmospheric pressure. The authors concluded that the emissions of nitrogen oxides peaked around stoichiometric conditions, decreasing for lower and higher equivalence ratios. Although a rather small amount of ammonia was used, this behaviour would become consistent throughout several studies and across different types of burners, as will be discussed.

Brackmann et al. [20] also studied ammonia-doped methane flames, using 5200 ppm of ammonia in volume of fuel. The burner chosen was a porous-plug McKenna-type burner, which created a flat, one-dimensional flame on the top. This study was more geared towards understanding the role of amidogen (NH) radicals in the formation of nitric oxide. The authors concluded that $NH_3$ was a key species in the formation of both $N_2$ and NO from the increased amount of nitrogen atoms introduced by the ammonia. Also worth of mention was the shift of the flame downstream, when ammonia was injected.

Barbas et al. [21] analysed the impact of small amounts of ammonia present in the oxy-fuel combustion of methane, measuring the carbon monoxide (CO) and nitric oxide emissions, in a flat-flame burner. The authors concluded that an increase in the excess oxygen coefficient generally decreased the amounts of both CO and NO present at the exhaust, independently of the oxidizer composition. However, in air firing, the NO emissions were higher than those from the oxy-fuel conditions. Additionally, HNO was also found to be the main intermediate species in the formation of NO.

Some studies also focused on the application of ammonia in compression-ignition (CI) and spark-ignition (SI) engines, where normally diesel and gasoline are used, respectively. Reiter and Kong [5] investigated the combustion and emission characteristics of a CI engine using blends of ammonia and diesel as fuel, with little modification to the injection system for ammonia to be introduced in the gaseous state. Using constant engine power and varying the diesel amount, it was found that the most favourable fuel efficiency was found for ratios around 1:1 of $NH_3$ to diesel. However, not only were the carbon monoxide and hydrocarbon emissions higher than they would be for independent diesel use, $NO_x$ emissions were also significantly high, especially when ammonia amounted for more than 40% of the total fuel energy. The conclusion was that fuel-bound nitrogen was the primary source of nitric oxide. In contrast, soot emissions were reduced significantly for these conditions of higher ammonia quantity. The authors also noted that, although the overall ammonia conversion was approximately 100%, $NH_3$ could still be found at the exhaust in values between 1000 and 3000 ppm. Therefore, the authors concluded that, for the setup used, employing only ammonia as fuel would necessitate post-combustion treatment, as $NH_3$ concentrations at the exhaust would not be within the safe limits.

Mørch et al. [22], on the other hand, tested blends of ammonia/hydrogen in an SI engine, using different proportions of the two constituents. Their conclusion was that these mixtures are a suitable replacement for SI engines in terms of efficiency and power. It was found that most $NO_x$ emissions occurred for high hydrogen content and excess air ratio ranging from 1.1 to 1.4. Although these emissions are similar

between the mixtures used and gasoline, the authors proposed SNCR to reduce the values encountered. The SNCR system could resource to the ammonia that is already on board.

Other researchers carried out studies on swirl burners. These combustion rigs are characterized by their use of a rotational flow to increase the mixing of the constituents, thus being a representation of the flows that exist in gas turbines. Valera-Medina et al. [23] experimented on an atmospheric pressure swirl burner, with both ammonia/methane and ammonia/hydrogen fuel blends. The authors achieved stable flames with low emissions by applying strong swirling flows for both mixtures. Nevertheless, they recognized that ammonia combustion in this type of burners suffered from the same difficulties documented in the previous literature. Consequently, there was only a narrow interval of equivalence ratios where good stability with low emissions and high temperatures was attainable. Figure 1.3 presents the $NO_x$ emissions obtained in this study, as a function of the equivalence ratio, for ammonia/methane fuel mixtures. These results showed a maximum of around 2600 ppm for an equivalence ratio of 0.9, and slightly lower values for fuel-lean conditions. However, at stoichiometry and under fuel-rich conditions, the values decreased to values below 250 ppm. It is worth noting that, although these results are for a mixture of methane and ammonia, the authors did not specify what the respective ratios were. As such, it could be either 80% or 66% of ammonia in volume of fuel, the rest being methane, according to the test parameters mentioned.

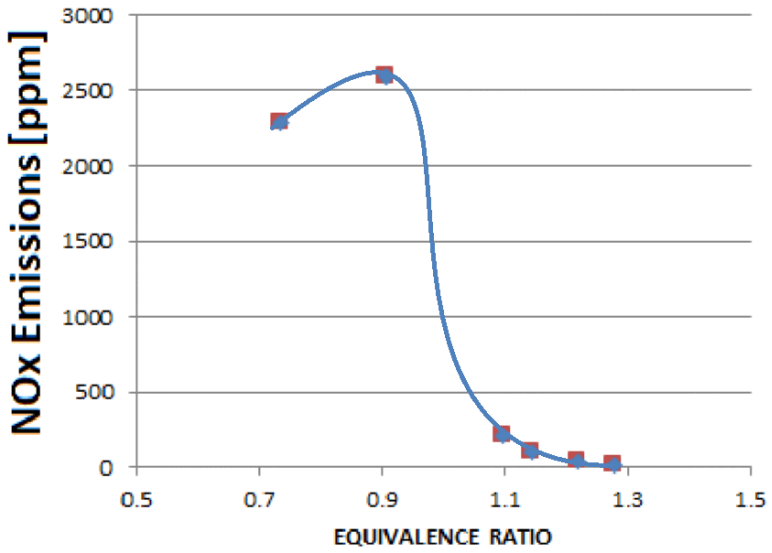


Figure 1.3 - $NO_x$ emissions as a function of the equivalence ratio from a methane/ammonia fired swirl burner, adapted from [23].

Also employing swirl stabilized flames, Hayakawa et al. [24] were confronted with the same $NO_x$ pattern for ammonia-air flames. The authors extended the findings of [23] for pure ammonia combustion, noting that, for fuel-rich conditions, not only the NO concentration decreased, but also the $NH_3$ values at the exhaust increased. Figure 1.4 shows the NO and $NH_3$ concentrations obtained in this study, as a function of the equivalence ratio. On further inspection, there is an equivalence ratio in fuel-rich conditions for which NO and $NH_3$ emissions are of the same order of magnitude.

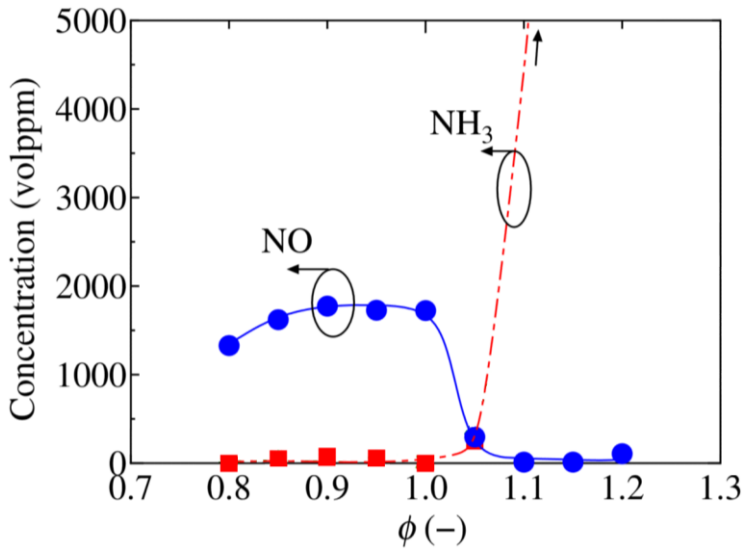


Figure 1.4 - NO and $NH_3$ concentrations as a function of the equivalence ratio from a pure ammonia fired swirl burner, adapted from [24].

The comparison between Figure 1.3 and Figure 1.4 may point towards a consistent trend, in which, when changing from fuel-lean conditions to fuel-rich, $NO_x$ emissions rise until they reach a peak around stoichiometry. Afterwards, emissions drop significantly by around one order of magnitude. It should be noted that these two graphs correspond to two different flames, one of ammonia/methane (Figure 1.3) and other of pure ammonia (Figure 1.4). Additionally, this pattern had already been observed in the analysis of [19], in which the authors only used 0.5% of ammonia in volume of fuel.

Kurata et al. [25] also investigated swirling flows, although in a larger 50 kW class gas turbine. The authors varied the power from 18.4 kW to 44.4 kW while using ammonia/methane blends and pure ammonia. Their findings revealed that, when using pure ammonia, there were two separate combustion zones. The primary combustion zone was characterized by fuel-rich and fuel-lean regions. The authors theorized that $NH_3$ was released from the fuel-rich region while the fuel-lean region released NO. In the secondary combustion zone, the unburnt $NH_3$ reacted with the NO, thus leading to increased NO conversion. For ammonia-air blends, $NH_3$ emissions were mostly found to be lower than 500 ppm, although there were some peaks of around 1600 ppm. When employing ammonia/methane mixtures, the unburnt $NH_3$ emissions dropped, while NO emissions rose considerably. In the authors' theory, the conversion ratio of NO in the secondary combustion zone decreased with the addition of $CH_4$, since ammonia was being withdrawn. For that reason, in order to achieve low emissions, the authors recommended burning large quantities of pure ammonia to generate both rich and lean fuel mixtures in the primary combustion zone. Figure 1.5 shows the emissions measured by the authors for ammonia/methane flames with a thermal input of 31.4 kW. Note that these results are in function of the energy ratio of ammonia in the fuel mixture. Also, although there were rich and lean regions in the combustor, as aforementioned, the authors did not disclose the global equivalence ratio.

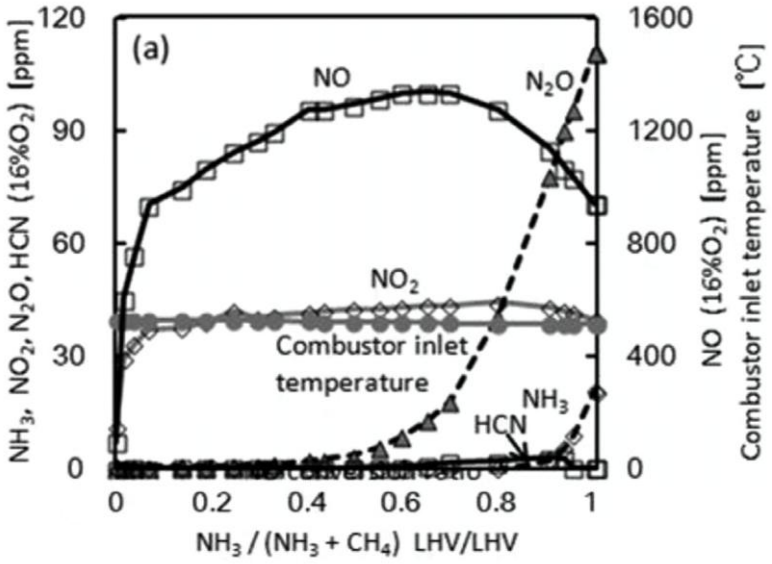


Figure 1.5 - Concentrations of various gas species and combustor inlet temperature as a function of the amount of ammonia in the fuel mixture in a gas turbine, adapted from [25].

In these results, the $NO_2$ emissions can be seen as approximately independent of the ratio of ammonia in fuel, steadying at around 40 ppm. The NO, on the other hand, can be seen rising from nearly non-existence to more than 800 ppm as soon as ammonia is introduced. It keeps increasing slightly until a ratio of 0.7 of ammonia in fuel energy is achieved. After this peak, it decreases, until it reaches around 900 ppm for pure ammonia-firing. This latter part of the pattern is consistent with the authors' previously mentioned theory: the increased ammonia concentration leads to more unburnt $NH_3$, thus reducing the NO emissions through SNCR. Also, since $NO_2$ is more or less constant, this means the $NO_x$ emissions will have the same pattern as the NO, although with a vertical shift upwards.

Xiao et al. [26] conducted a numerical simulation which corroborated the results found in Figure 1.5. The authors studied ammonia/methane flames for different equivalence ratios, employing a computational model of a homogeneous reactor with a one dimensional, premixed, freely propagating flame. Figure 1.6 shows the results for the NO emissions as a function of $NH_3$ mole fraction in the fuel mixture, for three different equivalence ratios. Neither power nor flowrates were specified. As can be seen, the NO emissions in Figure 1.5 and the NO emissions for stoichiometry in Figure 1.6 are qualitatively rather close – the patterns are very similar. As for the influence of equivalence ratio on NO emissions, it appears to be in accordance with [23] and [24], the peak being around stoichiometry, while emissions for fuel-lean and fuel-rich are lower.

The study of Nozari et al. [27] resulted in a graph analogous to Figure 1.6 but for mixtures of ammonia and hydrogen. The numerical model employed here was also a one dimensional, premixed, freely propagating flame. The authors investigated conditions similar to those of [26], for an equivalence ratio of 0.5. Figure 1.7 shows the $NO_x$ measurements as a function of the energy ratio of ammonia in the fuel mixture.

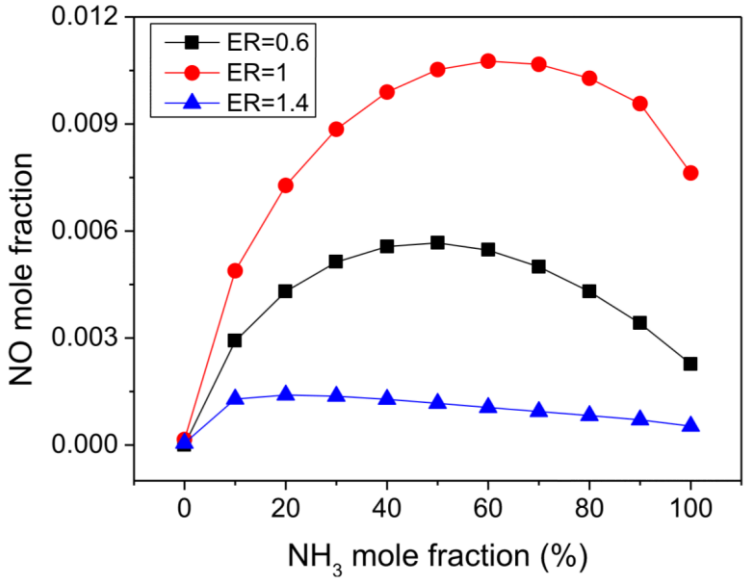


Figure 1.6 - Predicted NO mole fraction as a function of the $NH_3$ mole fraction in the fuel mixture for various equivalence ratios [26].

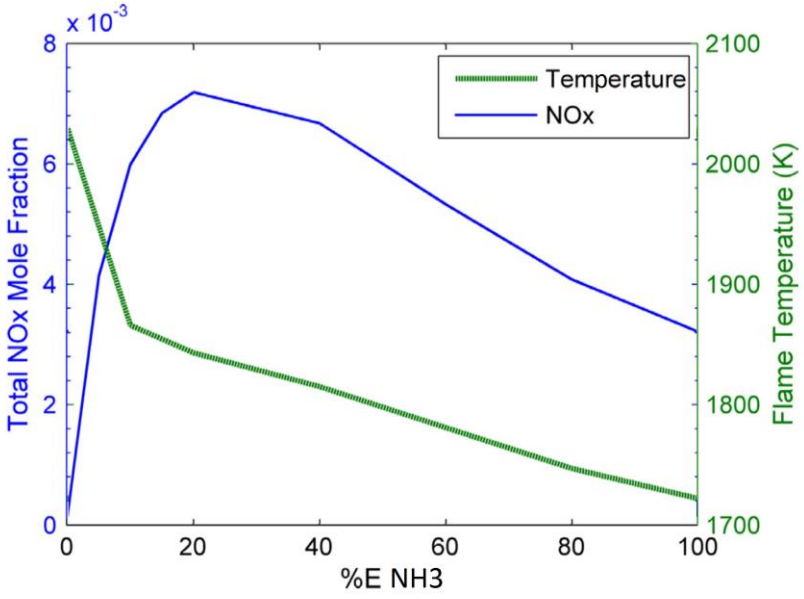


Figure 1.7 - Predicted $NO_x$ mole fraction and flame temperature as a function of amount of ammonia in the hydrogen/ammonia mixture for $\phi$ = 0.5, adapted from [27].

From the results of Figure 1.7, the similarities with Figure 1.6 are observable. As ammonia is introduced, $NO_x$ emissions rise quickly from practically zero and peak at around 20% of ammonia in energy fuel, starting to decline afterwards. Although not quantitatively comparable, Figure 1.6 and Figure 1.7 represent the same type of $NO_x$ pattern with respect to increasing ammonia substitution, and they do so for two distinct mixtures: ammonia/methane and ammonia/hydrogen, respectively.

Nozari et al. [28] studied ammonia/hydrogen mixtures employed in a silicon-carbide (SiC) porous-media burner. The authors conducted stability tests to ascertain the flammability conditions of mixtures with varying amount of ammonia. After establishing upper and lower stability criteria, the authors concluded

that this kind of burners is capable of efficiently combusting mixtures, which contain moderate to high fractions of ammonia. However, the authors did not show any emission measurements for this burner, so no comparisons can be made regarding $NO_x$. Lastly, a decrease in stability is still observed when increasing the amount of $NH_3$, which is a result of the lower flame speed of the mixture, as the authors stated.

Taking everything discussed thus far into account, it is evident that the difficulties of burning ammonia are a consistent challenge. As mentioned before, Starkman and Samuelson [16] had already proved the slow flame speed to be the main contributor for such problem. Hayakawa et al. [29] expanded the knowledge on this subject by investigating how the laminar burning velocity of ammonia/air premixed flames behaves with pressure and equivalence ratio variations. The burner employed was a constant volume, cylindrical combustion chamber. They concluded that the laminar burning velocity decreases as the initial pressure rises. Additionally, the flame speed has a peak value for an equivalence ratio of about 1.1, regardless of the pressure applied. For the conditions studied, the maximum value for laminar flame velocity was found to be of approximately 7 cm/s, for an equivalence ratio of 1.1 and an initial pressure of 0.1 MPa (very close to atmospheric pressure). This value is rather low when compared to commonly used hydrocarbons, which record a maximum value of about 35 cm/s.

The same conclusion was made by Duynslaegher et al. [30], who performed the same type of studies as in [29], albeit numerically, with a one-dimensional, premixed, and freely propagating flame model. In accordance to the previous article mentioned, laminar burning velocity was found to peak at an equivalence ratio of 1.12. The authors also concluded that only the variation of equivalence ratio influences the NO formation, while the pressure variation does not affect it. Furthermore, NO emissions as a function of equivalence ratio were found to have a similar pattern to those already found in [23] and [24], as previously discussed.

The work mentioned so far has focused on the research of burning ammonia as fuel, since it is the focus of this thesis. However, there is great potential in employing $NH_3$ as an energy source through a multitude of processes. Valera-Medina et al. [31] have conducted an extensive review about the use of ammonia in not only combustors, but also in power cycles, fuel-cells, carbon capture and storage, and even in micro-thrusters for propulsion. This demonstrates the high interest of the scientific community in developing clean, ammonia-based energy production.

### 1.2.3. Chemical Kinetics Models for Ammonia Combustion

The previous studies have investigated into the properties of ammonia combustion, in order to achieve a better understanding on the complex processes that characterize it. However, only a fraction has studied ammonia substitution at an industrial level, due to the costs involved. Numerical investigations have an advantage in this regard, since many conditions and variables can be studied without employing expensive experimental devices. As a result, these studies represent the most cost-effective way of designing the ammonia gas turbines of the future for the best performance. If these computational efforts

are able to reflect existing experimental data correctly, they are of utmost importance for scaling combustion to a larger magnitude.

There are several mechanisms that aim to replicate the chemical reactions that take place when ammonia is burning, and the differences between them are mainly focused on the selection of species and reactions that each author introduced. When developing these schemes, the authors take into account two commonly contrasting aspects: the time it takes to run the calculations versus how close the mechanism is able to replicate the intermediary reactions and experimental values. They can also be focused in specific conditions: for example, some are to be used for gas turbine simulation, which means they will excel for high temperatures and pressures. The following list of numerical schemes is not extensive, however, it reflects the main mechanisms that have already been validated against experimental data, either from the own authors or others.

One of the first accounts of modelling nitrogen chemistry in combustion was published in 1989 by Miller and Bowman [32] dealing with the mechanisms and rate parameters of N-oxides formation and removal processes, and fuel nitrogen conversion, among other aspects. It differentiated the several formation paths of NO that were known at the time, and it served as a basis for the creation of the first ammonia-dedicated mechanisms. Nevertheless, the authors warned that the scheme developed was tailored for the experimental results they had at the time, and, consequently, they discouraged the use of their numerical work outside of the specified conditions.

Twenty years later, Konnov [33] presented a mechanism based on his work with ammonia-doped methane flames, as was previously discussed [19]. It was developed for the combustion of small hydrocarbons with N-based compounds, featuring a revised implementation of the NO formation routes, based on his previous findings. This mechanism proved quite popular, according to [26], in which Xiao et al. mentioned that it offered “satisfying performance especially on the prediction of $NO_x$ emission and propagation compared with most of the mechanisms available”.

Konnov’s mechanism went on to be studied and improved upon by several researchers. Duynslagher et al. [34] elaborated an improved mechanism – based on Konnov’s – for flames of ammonia, hydrogen, oxygen and argon. It was modelled and validated for low pressures. For the conditions considered, not only the improved mechanism rendered a simulation closer to the experimental data available, but also the computational costs were considerably less, when compared to the predecessor.

Xiao et al. [26] also improved upon Konnov’s mechanism. In this case, the authors did so for ammonia/methane combustion in industrial conditions (high pressure and temperature). It was found that the original scheme performed poorly in ignition delay chemistry studies, hence the need to alter it. Against experimental data, the resultant model proved effective for calculating ignition delay times, flame speed and emissions for high pressure settings.

Dagaut et al. [35] proposed a mechanism for modelling the formation of nitrogen oxides in the combustion of fuels containing atoms of H, C and N. The authors stated that the kinetics of the oxidation of hydrogen cyanide (HCN) developed a major role in the process. However, no comprehensive model dedicated to such chemistry was available at the time. Based on the existing literature, the authors

gathered an extensive list of the reactions that included this intermediate species. The authors validated the resultant mechanism against a wide variety of conditions, from low to high pressures, and from intermediate to very high temperatures, achieving an overall good agreement across all settings.

Mathieu and Peterson [36] conducted a research on ammonia-air flames heavily diluted in argon (98-99% Ar), with the objective of validating numerical mechanisms for high pressure conditions. Comparing their experimental data with the literature, Dagaut's model proved to be the one that best predicted the results, although a significant difference still existed. As a result, the authors took that scheme and added several subsystems and reactions to better simulate these diluted air-fired ammonia flames. In the end, although the differences between the mechanisms were slim regarding ammonia oxidation, the improved model offered significant enhancements to the modelling of $NO_x$ and $N_2O$ data, for the conditions considered.

Xiao et al. [37] took the work done by Mathieu and Peterson and adapted the model to the combustion of ammonia/hydrogen fuel mixtures, at the same high pressure settings. Validated against literature data, this new scheme proved to be better at predicting $NO_x$ emissions, laminar burning velocity and ignition delay times, compared to the models of Mathieu/Peterson and Duynslagher et al. The authors noted, however, that the latter was not intended to predict high pressure scenarios, thus being an unfair comparison.

Song et al. [38] proposed a chemical kinetics model for the oxidation of ammonia at high pressure and mild temperatures. The objective was researching which intermediate species have the most impact on the formation of OH radicals, and how these affect NO emissions. It was found that $NH_2$ and HNO are the primary species that influence the presence of NO at the exhaust.

Otomo et al. [39] expanded upon the mechanism by Song and co-workers by adding important reactions to $NH_2$, HNO and $N_2H_2$. Although the original scheme proved the relevance of these compounds, Otomo and co-workers found that it was lacking certain dynamics between these intermediate species. Additionally, the authors extended the mechanism to predict both ammonia/air and ammonia/hydrogen/air flames. This recent kinetics scheme proved to be usable in a wider range of conditions and demonstrated better agreement with experimental data, regarding laminar flame speeds and ignition delay times.

One mechanism that has been thoroughly studied is the one by Tian et al. [40]. The authors experimentally studied several premixed flames of $NH_3/CH_4/O_2/Ar$ at low pressure and stoichiometry, and developed a chemical kinetics mechanism based on existing reactions in the literature. The mechanism proved capable of achieving a good agreement with the experimental data.

Despite being initially tailored for low pressure conditions, Tian's mechanism has been applied successfully to a myriad of contrasting situations. Kumar and Meyer [41] conducted a study on $NH_3/H_2$/air mixtures across different equivalence ratios and ratios of hydrogen in fuel energy. Comparing the experimental results of laminar flame speed with mechanisms from the literature, only Tian's correctly predicted the values for all equivalence ratios. In other investigation, Xiao et al. [42] applied several numerical models to the ignition delay study of $NH_3/CH_4$/air flames at high pressures. Once

again, Tian's model proved to be the best at agreeing with experimental data, especially at high fractions of ammonia in fuel. For that reason, the authors recommended the use of this numerical scheme for most combustion studies on gas turbines.

One last mechanism worth mentioning was created by Okafor et al. [43]. The authors performed a research on ammonia/methane air-firing at standard temperature and pressure, varying the relative amount of ammonia in the fuel mixture and the equivalence ratios. Having first established that Tian's model had potential in the conditions considered, especially in the calculation of NO profiles, the authors improved the mechanism to better predict the gas species and flame speeds at lower ammonia fractions. They did so by resourcing to subsystems implemented in GRIMech3.0, a mechanism already proven quite popular for hydrocarbon combustion. In the end, not only did Okafor's mechanism agree with Tian's for high amounts of ammonia, it also agreed with the GRIMech3.0 mechanism for lower $NH_3$ fraction in fuel and for pure methane flames, thus being a more complete mechanism for these mixtures.

## 1.3. Objectives

The present work is focused on studying the emissions from the combustion of ammonia and its mixtures with methane and hydrogen, and its underlying mechanisms. The motivation for such is the demonstrated potential of $NH_3$ for satisfying global energetic needs, while not contributing for the increase of carbon-based pollution. $NO_x$ emissions are a major concern inhibiting a wide acceptance of ammonia as fuel. However, information on the subject is still scarce and lacking. Experimental values on $NO_x$ concentrations are needed to develop future reactors and processes with no pollution. Therefore, the main objective of this thesis is to contribute with quantitative data on how several variables influence the gas species concentrations at the exhaust, namely for $NO_x$, CO and $NH_3$.

To achieve this, an experimental and numerical investigation has been conducted. The objectives of the experimental work have been delineated as to evaluate the gas and temperature emissions in two distinct burners: a flat-flame burner and a porous-media burner. For the former, a fuel mixture of ammonia and methane was used, and the proportions of each fuel constituent and of air were altered, to evaluate the influence of ammonia fraction and equivalence ratio on emissions. For the porous-media burner, two types of mixtures were studied to evaluate the effect of different fuel constituents. The blends selected here were ammonia-hydrogen and ammonia-methane.

In the numerical part of the work, the objective is to assess how current numerical mechanisms predict the combustion scenarios that were experimentally studied. Therefore, the experimental data gathered was evaluated against chemical kinetics simulations, resourcing to Cantera.

The final objective is to understand the impacts of a feasible implementation of ammonia in the energy sector, while recognizing the potential contribution that the present work has in that regard. To do so, the current carbon-polluting sectors in the global economy were discriminated and the potentiality of ammonia completely substituting fossil fuels was discussed. A vision of a future ammonia-based energy

sector was presented, considering the high flexibility of ammonia for supplying power through many different processes.

In the end, this thesis aims to contribute to the future establishment of ammonia as a clean and feasible energy source.

## 1.4. Thesis Outline

The present thesis is organized into four chapters, of which the present one constitutes the introduction. Chapter 2 describes in detail the experimental setup, the measuring techniques and respective uncertainties, the experimental procedure, and the chemical kinetic model. In chapter 3, the test conditions are disclosed, the experimental and numerical results are presented and discussed, and the practical impacts of this work are debated. Finally, chapter 4 summarizes the conclusions of this study and recommends future directions for research on ammonia combustion.

# 2. Materials and Methods

The investigation presented herein has been conducted at Instituto Superior Técnico, in the Combustion Laboratory of IDMEC. This chapter describes the materials and methods employed in the research. Section 2.1 describes the experimental apparatuses used, which include the burner setups and the measuring equipment/techniques. Additionally, information regarding the experimental uncertainties involved is discussed in section 2.2. Finally, the experimental procedure and the numerical method employed are discussed in sections 2.3 and 2.4, respectively.

## 2.1. Experimental Setup

The research has been conducted in two distinct burners, which offer different conditions regarding flame stabilization and emissions: a flat-flame burner and a porous-media burner. The measuring equipment and corresponding techniques are, however, similar for both setups.

### 2.1.1. Flat-Flame Burner

Figure 2.1 shows the diagram of the flat-flame burner setup. It can be divided in three parts: the fuels, burner and measuring/sampling systems.

The fuels system is composed by the gases used in the combustion. Two compressed cylinders are used, one of $NH_3$ (10 bar, ≈20 °C) and another of $CH_4$ (50-70 bar, ≈20 °C). At the exit of each cylinder exists a safety valve, which also controls the output pressure. The $CH_4$ flow is controlled by a digital flowmeter, while the $NH_3$ flow is controlled by an analogue rotameter. After combining these two fuel constituents, the air, which is supplied by the compressor and controlled by an analogue rotameter, is also added into the mixture. The latter is then fed into the burner intake at around 1 bar of pressure and ambient temperature (around 20 °C). Note that all flow controller properties are discussed in section 2.2.1.

The burner is of the flat-flame type. It has been used in other studies, namely in [21], although it is here presented with some modifications. As can be seen in Figure 2.1, the base of the burner is an inverted cone fixed on a mount, with a hollow interior featuring two different diameters. It is made of stainless steel and it is actively cooled around the perimeter covering the flame position, resourcing to tap water. The interior is filled with small alumina spheres and several transversal stainless steel meshes, to achieve uniformity of flow in the cross-section. A hollow quartz cylinder sits on top of the base, allowing for entrainment of the flame and external observation. It has 50 cm of length, external diameter of 4.5 cm and internal diameter of 3.3 cm. Along the perimeter of this tube, a ceramic wool has been tightly placed: this thermal insulator allows for significantly reduced heat loss. On the top of the quartz tube rests a stainless steel chimney: it serves to decrease the amount of air that can enter through the top, thus allowing for more accurate reading of the flue gases. Its opening is just enough to allow for the positioning of the probes.

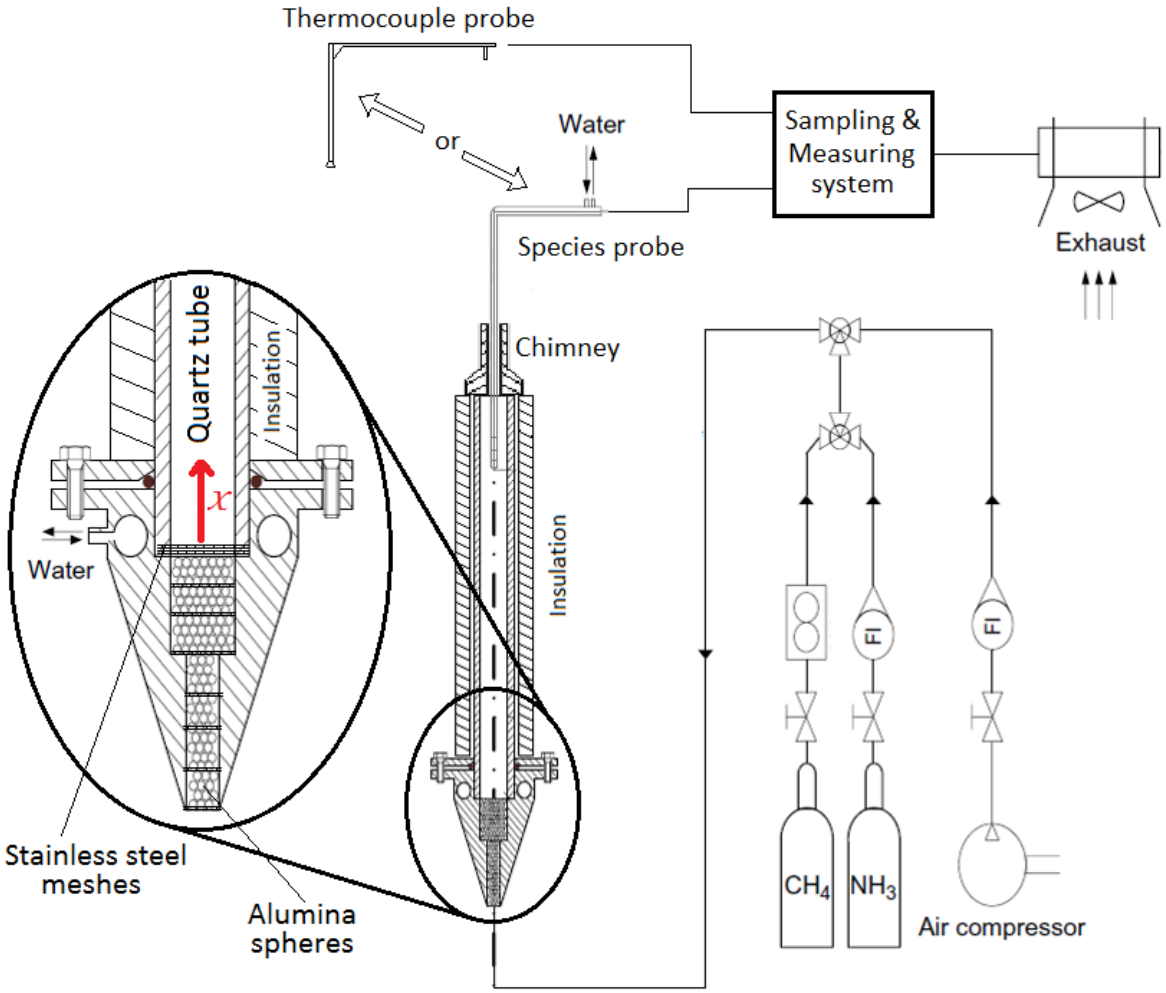


Figure 2.1 - Schematic of the flat-flame burner setup.

The thermocouple or species probes can be placed along the vertical axis of the burner, both of which are connected to the sampling and measuring system. Only one of the probes can be placed at a time, however, being supported from the top, above the burner. The gases that are not aspirated by the species probe are afterwards collected by the laboratory exhaust. The flue gases are directly sent to the latter, if the species probe is not being employed.

### 2.1.2. Porous-Media Burner

Figure 2.2 shows the diagram of the porous-media burner setup. It is similar to the previous setup, although with the addition of hydrogen as a fuel constituent and the change in burner.

Once again the setup is divided in the fuels, burner and sampling/measuring systems. The first part is the same as the one from the flat-flame burner, with the difference that there is the choice between using hydrogen or methane. The hydrogen is stored in a gas cylinder (10 bar, ≈20 °C) and its flow is controlled by an analogue rotameter. The flowmeter is the same for the $CH_4$; however, for air and ammonia, the rotameters are different. Since more power is used in this burner, extended ranges for the flow

controllers are also a necessity. Either the $H_2$ or $CH_4$ are combined with the ammonia, to which the air from the compressor is added. The mixture is then fed to the intake of the burner.

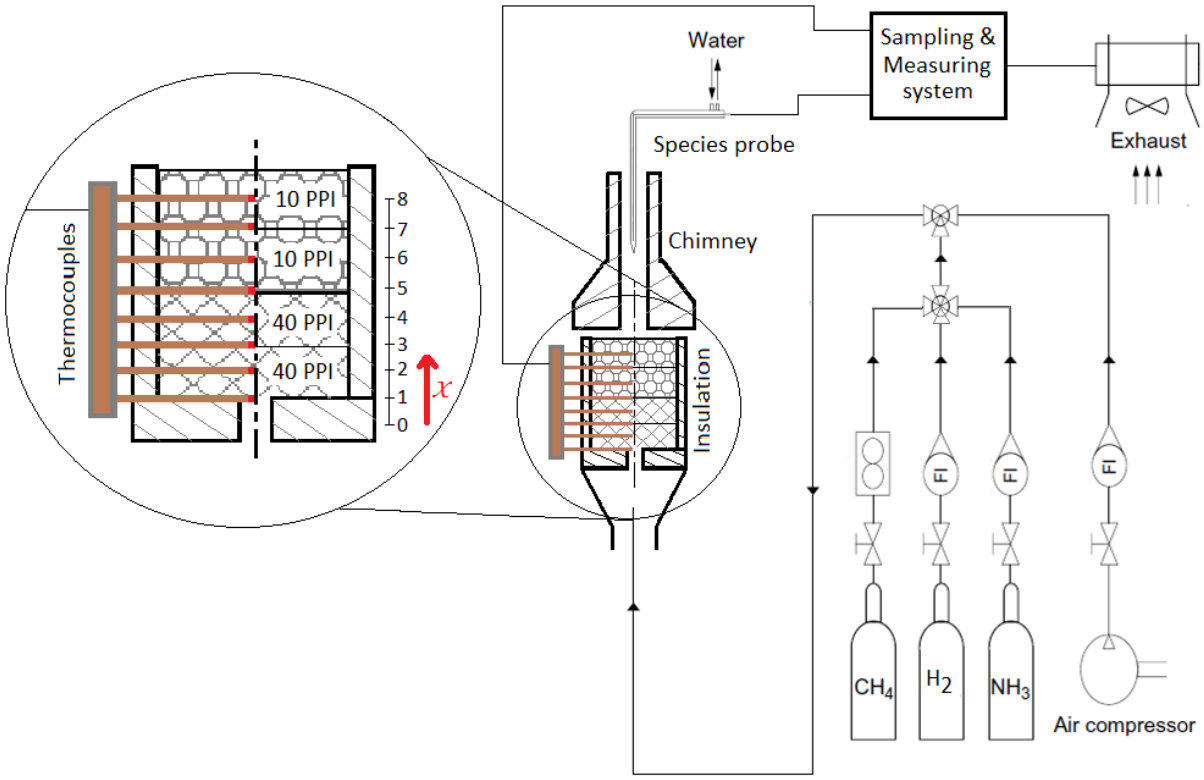


Figure 2.2 - Schematic of the porous-media burner setup.

The burner is based on the work conducted by Carvalho et al. [44] and Francisco et al. [45], although here it presents some changes. It consists of a cylindrical porous-media at the core, surrounded by the aforementioned ceramic wool, which is in turn placed in a stainless steel cylindrical container, fixed on a table. The ceramic core is characterized by 4 layers of porous foams made of alumina ($Al_2O_3$) and zirconia ($ZrO_2$). Each layer has a diameter of 70 mm and a height of 20 mm, resulting in a total of 80 mm of height. The two bottom layers have 40 pores per inch (ppi), while the top two have 10 ppi. Both regions have a volumetric porosity of 80%, however. The differences in number of pores per inch are because of quenching distance and preventing flashback: since there are more pores per inch in the bottom section, they are smaller than the pores existent in the top region. As a result, a flame is expected to stabilize in the top layers, and if flashback were to occur, the smaller distances between walls in the bottom region are more likely to extinguish the flame.

In the bottom of the core, another insulating plate is placed, with a centre channel through which the premixed gases enter. In the top of the burner, a chimney is placed to prevent air from the outside from entering the burner. The only opening in this chimney is at the top to allow for the gas species probe to be placed, through which the flue gases are collected for further analysis. The uncollected gases are aspirated into the laboratory exhaust. Additionally, eight thermocouples are placed through the burner wall, measuring temperatures inside, along the centre axis.

### 2.1.3. Measuring Equipment and Techniques

The measuring system is comprised of the probes, pumps, filters, analysers, analogue to digital converters, and computers running dedicated software. For better organization, it has been divided in several parts: gas analysers (for measuring of $NO_x$, $O_2$, CO and $CO_2$), GASTEC system (for measuring $NH_3$), and thermocouples (for measuring temperature).

#### 2.1.3.1. Gas Analysers

Figure 2.3 shows the diagram for the sampling circuit of the gas analysers. The objective of this system is to measure $NO_x$, $O_2$, CO and $CO_2$.

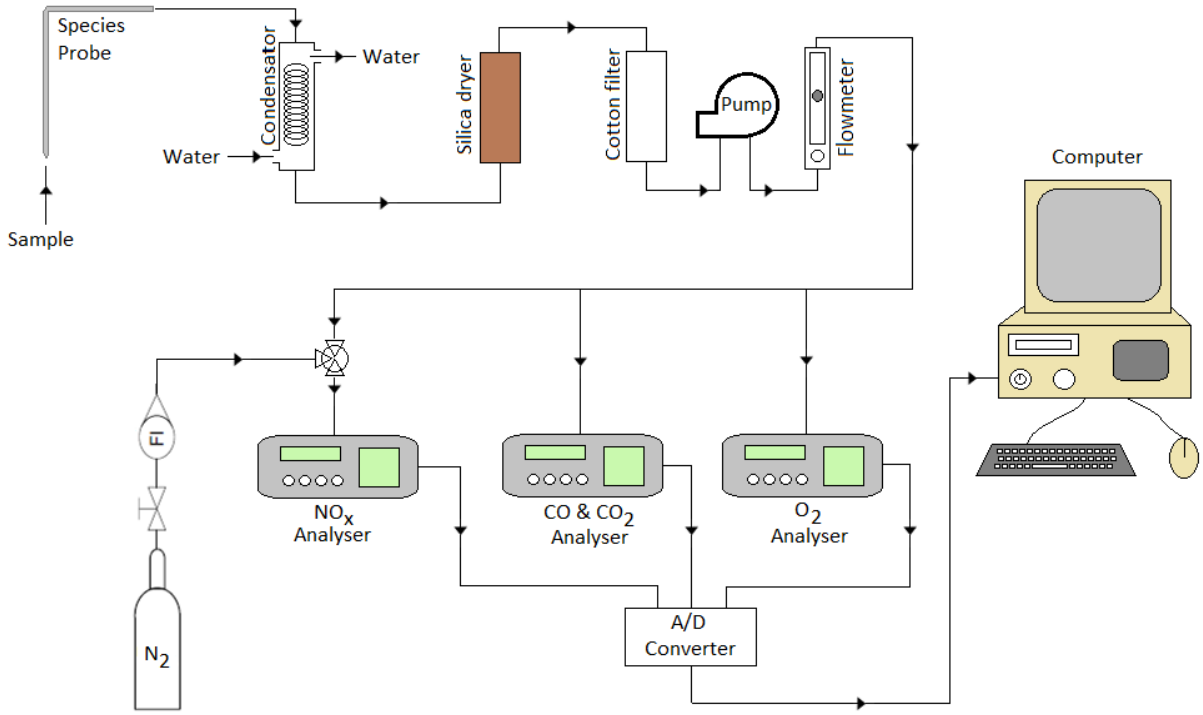


Figure 2.3 - Schematic of the gas sampling system.

The gases are initially collected with an L-shaped probe placed at the exit of the burner chimney. The probe is made of stainless steel and is hollow, with two concentric channels. Figure 2.4 shows the dimensions of this probe. The inner channel is for gases to be sampled and is opened at both ends. The outer channel is for running water, so that the probe is cooled and it does not melt when subjected to high temperatures. The probe is supported on a screw-driven vertical linear slide for axial positioning, with an uncertainty of 0.5 mm. The tip of the probe is placed at a distance of either 30 cm from the flame (for the flat-flame burner) or 20 cm (for the porous-media burner). These distances were chosen as a balance between not being too close to the flame (so that most reactions have already taken place by the time the flue gases are sampled) and not being near the exit (so that outside air is not aspirated by the probe).

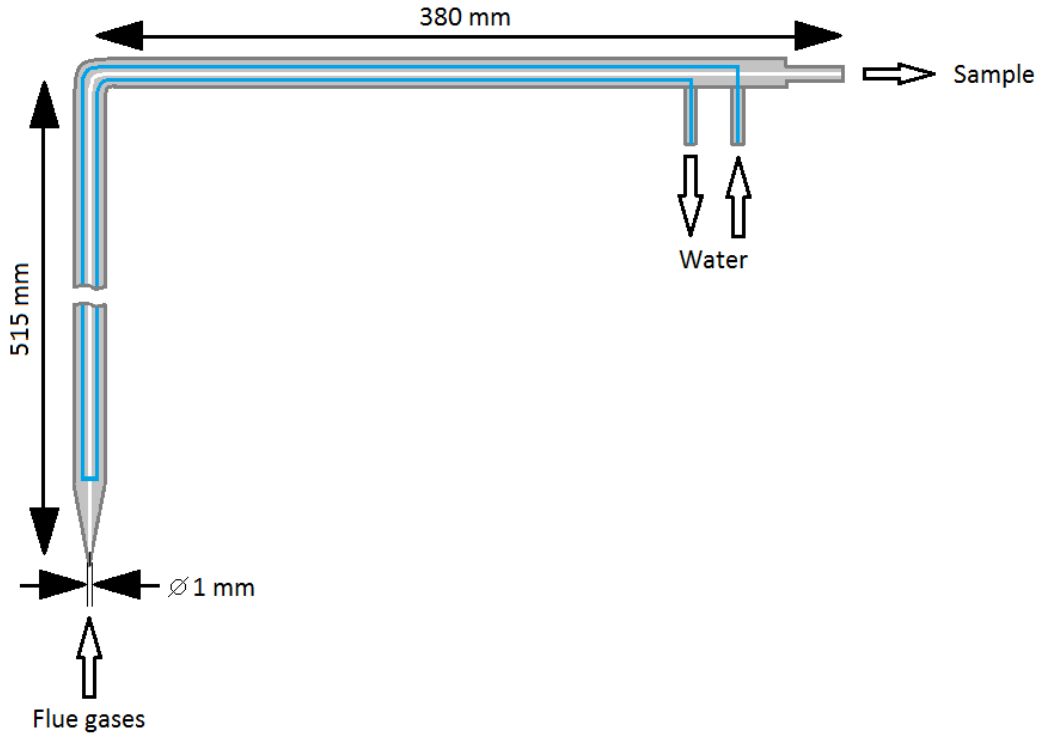


Figure 2.4 - Schematic of the gas species sampling probe.

The sampled gases are cooled as they travel within the probe. Afterwards, they pass through a condenser, a silica dryer and a cotton filter, to remove particles, humidity and other condensates. This circuit ensures that the samples are clean and dry, thus allowing the analysers to show the concentration values in a dry reference basis. Additionally, all ducts are in polytetrafluoroethylene (vulgarly known as "Teflon"), which is chemically inert and does not tamper the sample. The gases move on through the pump, which maintains a constant sampling flow, a flow meter, and are then pushed into the analysers. There are three different types of analysers, one for $NO_x$, one for $O_2$, and another for both CO and $CO_2$. Table 2.1 summarizes the characteristics of the gas analysers.

Table 2.1 - Characteristics of the gas analysers.

| Gas Species | Brand/Model | Analysis Method | Value Range |
|---|---|---|---|
| $NO_x$ | Horiba PG-250 | Chemiluminescence | 0 – 2500 ppm vol. |
| $O_2$ | Horiba CMA-331 A | Paramagnetism | 0 – 30% vol. |
| CO | Horiba CMA-331 A | Nondispersive infrared | 0 – 5000 ppm vol. |
| $CO_2$ | Horiba CMA-331 A | Nondispersive infrared | 0 – 50% vol. |

One thing that needs mentioning is the use of dilution to overcome the range of $NO_x$ measurements. Initial testing and predictions pointed to emissions superior to 2500 ppm, which is verified in the results section. To surmount this fact, a cylinder of $N_2$ (80 bar, ≈20 °C) controlled by an analogue rotameter is coupled to the intake of the analyser. When $NO_x$ measurements are needed, $N_2$ is mixed into the gas at a known flow, thus diluting the sample and allowing for the use of an extended measuring range. Since the sample is already cooled when this mixture takes place, there are no reactions with the added nitrogen. The specifications regarding the dilution process are further explained in subsection 2.2.3. The use of this process means that $NO_x$ cannot be measured at the same time as the other species: sampling $O_2$, CO and $CO_2$ while also applying dilution would introduce an unnecessary uncertainty. Hence, $NO_x$ measures are not taken simultaneously with others.

All analysers send an electric analogue signal that is converted into digital by an acquisition board (Data Translator DT 9802), at a sampling frequency of 100 Hz. The acquisition board is connected through USB to a computer, which runs a dedicated programme (HP VEE-LAB v5.02) to collect the transmitted data. Using the script selected for the present research, the sampling period is of 30 seconds for each measurement. Therefore, each value measured is itself the mean average of a total of 3,000 instantaneous measurements. Nevertheless, all the assessments carried out in this work are a result of many repetitions to ascertain the reproducibility uncertainties and to achieve better precision.

#### 2.1.3.2. GASTEC System

The analysis of $NH_3$ is not conducted in the same way as for the other gas species, a different system is used, from GASTEC, which is comprised of gas detector tubes and a pump. It has already been used in the literature with success [46]. Figure 2.5 shows a schematic of the GASTEC sampling system.

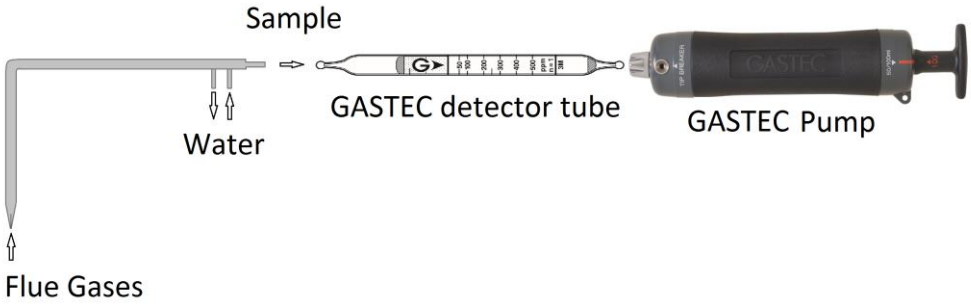


Figure 2.5 - Schematic of the GASTEC sampling system.

The same species probe mentioned before is used. It is positioned at the exit of a burner using the vertical mount. At its output, a detector tube is placed secured to a precise handheld pump. The general sampling pump mentioned before was not used in this case because the total volume of the gases collected has to be concisely controlled. Additionally, the filters were also not employed after the species probe because there is a considerable pressure drop associated, which the handheld pump was not capable of overcoming.

The detector tube is a thin glass tube, which is hermetically sealed out of the box. The concept of measuring with these tubes is related to simple chemistry. Inside the detector cube is a particulate matrix with a bonded reagent ($H_3PO_4$) that is especially sensitive to $NH_3$ and will react with it if there is any contact. If reaction occurs, then the matrix will shift colours gradually.

For consistency, a specific handheld pump is used (model GASTEC GV-100), which has two possible pump-strokes: a full stroke pulls 100 mL, while a half-stroke pulls 50 mL. After breaking both glass tips, the tube is inserted in the opening of the pump, facing the correct way, according to the indications on the glass. The open tip is connected to the exit of the species probe. When a measurement is to be taken, the lever on the pump is pulled back to create a negative pressure and push the exhaust gas through the probe and into the tube. If $NH_3$ is present, the matrix in the tube changes colour gradually, starting from the front of the tube to the back. The amount of colour-shifting that occurs can be translated into a value with the aid of a calibration scale printed on the glass, which allows for a direct measurement of the concentration of $NH_3$ in the flue gas. Figure 2.6 shows the difference between positive detection – tube b) – and an unused tube for comparison – tube a). The absence of $NH_3$ in the sample would render the same result as in the unused tube.


Figure 2.6 - GASTEC detector tubes: a) unused tube, b) positive detection of 400 ppm vol. of $NH_3$.

The detector tubes are rated for specific measurement ranges, which also depend on the amount of gas being pulled by the pump. The model being used (GASTEC No.3M) can measure between 50 and 500 ppm if used with a full stroke. If a half-stroke is employed, the range is between 500 and 1000 ppm. However, for lower concentrations there is also a possibility of using up to 5 full strokes, which allows to test for ammonia presence for values lower than 50 ppm, since the detection limit in that case reaches a minimum of 2 ppm of $NH_3$. Nevertheless, this last method is only a qualitative assessment, since the discoloration of the detector tube is general and not a contrasting boundary of colours.

#### 2.1.3.3. Thermocouples

The temperature sampling system is different for each burner. Figure 2.7 shows the system for the flat-flame burner setup. The probe used for this setup is a thermocouple, one of the simplest instruments for measuring temperatures. It functions by using two different metals alloys that are fused together at a specific point called “hot junction”. This results in an electric potential difference at each end, which is dependent on the temperature of the junction: this is known as the “Seebeck effect”. Although the use of this technique may interfere with the flow, it is the most cost-effective manner of conducting reliable temperature measurements. The thermocouple employed in this system uses a platinum anode and a cathode made from an alloy of platinum with 13% rhodium – this is commonly known as a Pt/Pt-13%Rh thermocouple, type R. Its measuring range is from -50 °C to 1760 °C, to which corresponds a range of

potentials going from -0.226 mV to 21.096 mV, respectively, according to International Thermocouple Reference Tables [47]. The thermocouple is deployed within a probe for increased accessibility. Figure 2.8 presents the dimensions of such probe.

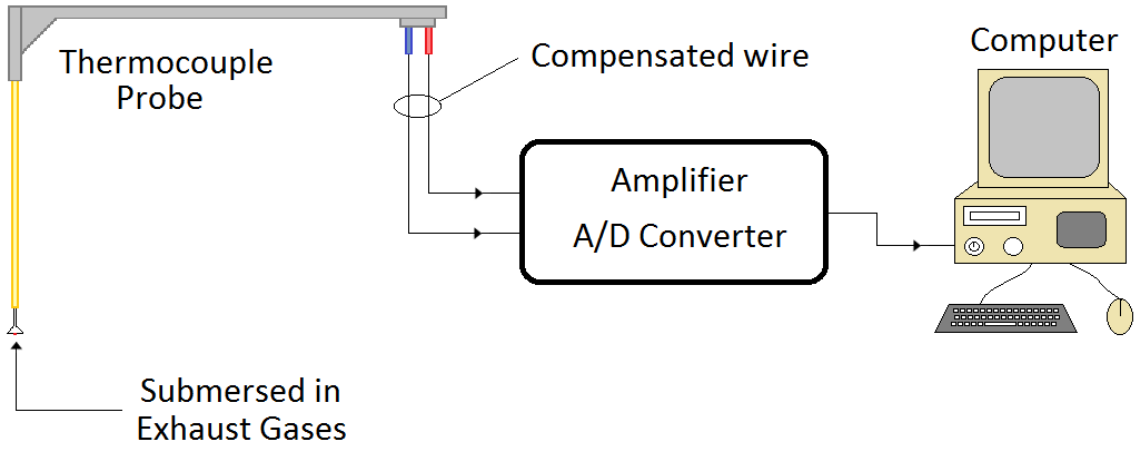


Figure 2.7 - Schematic of the temperature measuring system for the flat-flame burner setup.

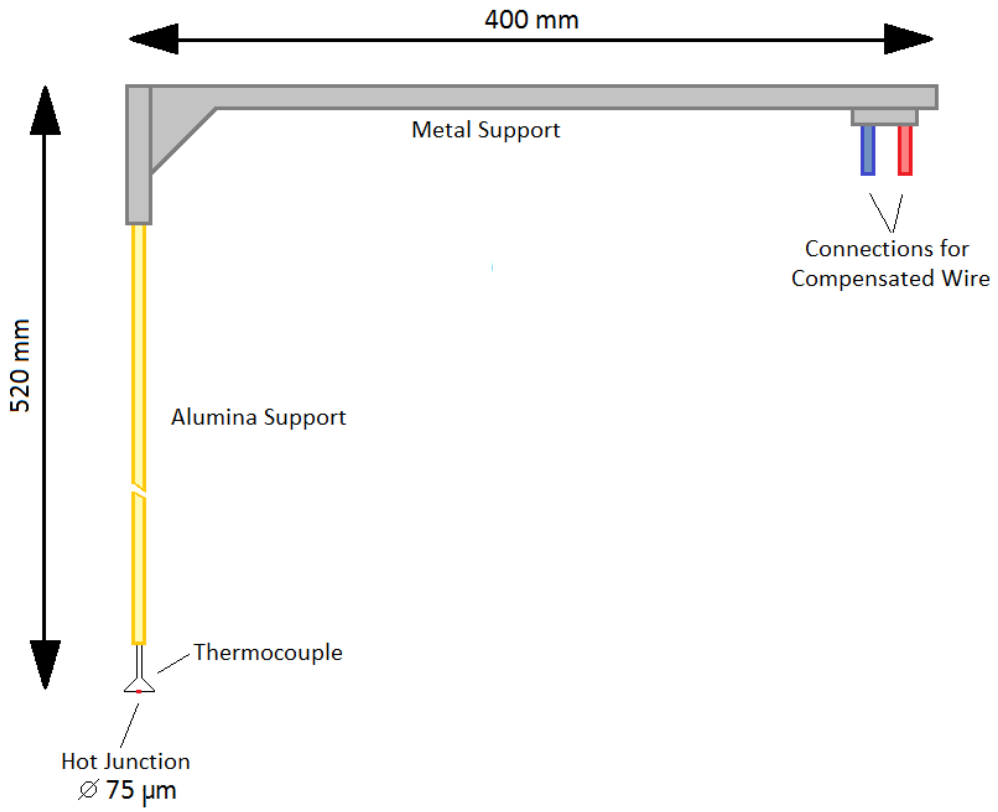


Figure 2.8 - Schematic of the thermocouple probe for the flat-flame burner setup.

The probe is placed in the same vertical mount as before, which allows for one-dimensional vertical positioning with an uncertainty of 0.5 mm. The probe itself has two parallel wires of the same materials as the thermocouple, one made of platinum and another of the Pt-13%Rh alloy (diameter of 0.5 mm, each), running parallel through a ceramic tube (6 mm of diameter, 520 mm of length), with no point of contact in between, in order to carry the signal. They are only connected in the exposed end of the tube, where the hot junction is located, thus, this is where measurements are taken. The other two ends of the wires are attached directly to a signal conditioning board (Data Translation 5B37-R-05), through a compensated wire that has the same electric conductivity than the materials used in the thermocouple. The board amplifies and filters the signal received, which is afterwards converted from analogue to digital at a rate of 100 Hz. The signal is then passed through USB to a computer running the aforementioned programme (HP VEE-LAB v5.02), in which the sample period for each measurement is, once again, 30 seconds.

Figure 2.9 shows the temperature sampling system for the porous-media burner setup. The thermocouples are placed on the side of the burner, going through the wall. Therefore, the hot junction of each one rests on the vertical symmetry axis of the burner, measuring the temperature in the middle. They are stacked vertically and are positioned so that four thermocouples are located in the interfaces between the ceramic layers and the other four measure temperatures in the middle of each layer. Each thermocouple is also of type R, which means they have the same properties and response to temperature as the thermocouple used for the flat-flame burner. The eight thermocouples are connected to an acquisition and amplification board (Agilent 34970A Data Acquisition/Switch Unit), running at 100 Hz, which in turn is linked to a computer through USB. The computer has a specific programme, called “Agilent BenchLink Data Logger 3”, which allows for real time monitoring of the temperatures at the thermocouples. Additionally, when conducting experiments, the programme can be used at the start to automate the temperature measurements. In such case, it takes a measurement for all thermocouples simultaneously every 5 seconds until it is told to stop. In the end, it generates a datasheet with the timestamp and the correspondent temperatures, which are used for the final data analysis.

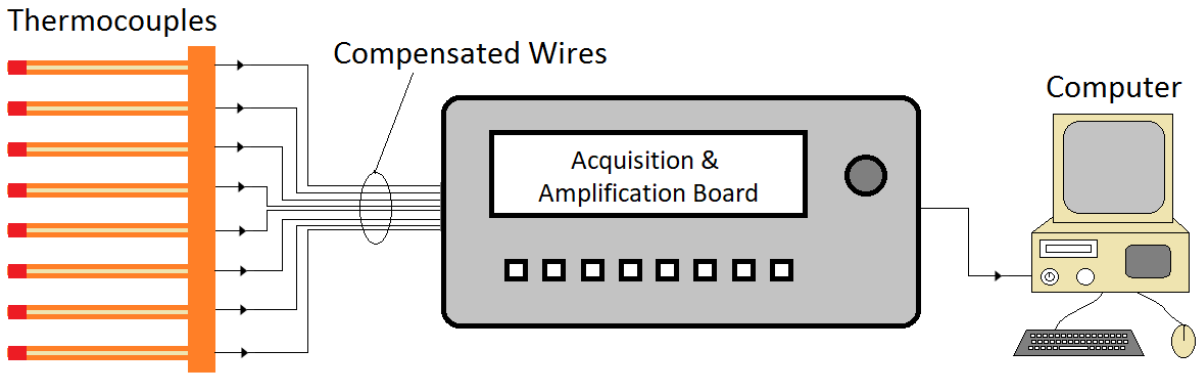


Figure 2.9 - Schematic of the temperature sampling system for the porous-media burner setup.

## 2.2. Experimental Uncertainties

### 2.2.1. Flow and Equivalence Ratio

The uncertainties related to the measurements of gas flows should be studied in order to assess if the equivalence ratios that are set up experimentally differ significantly from the real values. The same is true for the quantities of ammonia in the fuel mixture. Table 2.2 shows the flow controllers used for each scenario and the respective uncertainties (disclosed by the manufacturers). Note that some species use different controllers, according with the burner used.

Table 2.2 - Flow controllers used in the experimental setup and respective properties.

| Gas | Burner | Flow Controller Brand | Range (up to, L/min) | Relative uncertainty (respective to full scale) |
|---|---|---|---|---|
| Air | Flat Flame | Aalborg | 12 | ± 2% |
| Air | Porous-Media | Abb | 54 | ± 5% |
| $NH_3$ | Flat Flame | Aalborg | 3.14 | ± 2% |
| $NH_3$ | Porous-Media | Abb | 8 | ± 5% |
| $CH_4$ | Both | Tylan | 10 | ± 1% |
| $H_2$ | Porous-Media | Aalborg | 6.255 | ± 2% |

Taking into account the relative manufacturer-specified uncertainties, the absolute error involved with setting a specific percentage of ammonia in the fuel mixture can be calculated according to:

$$e_{\%NH_3} = \pm \left| \frac{V_{NH_3}}{V_{NH_3} + V_{CH_4}} - \frac{V_{NH_3} \pm e_{NH_3}}{\left(V_{NH_3} \pm e_{NH_3}\right) + \left(V_{CH_4} \pm e_{CH_4}\right)} \right| \quad (8)$$

where $V_{NH_3}$corresponds to the volumetric flow of $NH_3$ and $e_{NH_3}$is the absolute error of the controller measuring said flow. The nomenclature is analogous for the elements with $CH_4$ in subscript. The elements of methane are to be substituted by the equivalent terms for $H_2$ when calculating the error for that specific fuel mixture. Measuring the value of that error for all conditions, it was found that there is an average absolute error of ± 4.4% when calculating $\%NH_3$ for the flat-flame burner. For the porous-media burner, the absolute error has an average of ± 5.3% for $NH_3$-$CH_4$ mixtures and ± 3.2% for $NH_3$-$H_2$ blends. Bearing in mind these values, when selecting which experimental settings should be measured, any two adjacent conditions should be separated by a difference of at least 10% of $NH_3$ in the fuel mixture, so that the separation is clearly defined and no uncertainties overlap.

The same investigation can be made for the values of equivalence ratios. In this case, the absolute differences between intended and experimental equivalence ratios can be calculated by the following equation:

$$e_{\phi} = \pm \left| \phi_{intended} - \frac{AF_{stoich}}{\left( \frac{V_{Air} \pm e_{Air}}{(V_{NH_3} \pm e_{NH_3}) + (V_{CH_4} \pm e_{CH_4})} \right)} \right| \quad (9)$$

The nomenclature is the same as for equation 8. Once more, the elements with $CH_4$ have to be substituted by the equivalent terms for $H_2$ when calculating the error for $NH_3$-$H_2$ blends. The discrepancies were calculated for all conditions and burners. For the flat-flame burner, the maximum calculated difference between intended and experimental equivalence ratios was of ± 0.07, for $\phi$ = 1.0. The differences decreased for lower $\phi$, with the average discrepancy being of around ± 0.05, when considering equivalence ratios in the interval [0.8; 1.0]. Therefore, for a clear separation between the equivalence ratios considered for the experimental work, the difference between adjacent $\phi$ should be of at least 0.1. For the porous-media burner, the maximum error is of around ± 0.08, for $\phi$ = 0.8, regardless of the fuel blend considered.

Note that these instrumental uncertainties are constant for the respective burners. Therefore, they will not be represented in the graphs of chapter 3.

### 2.2.2. Temperature

For both burners, the temperatures are measured by the same type of sensors: type R thermocouples. Although different sizes are employed, the response to temperature variations is mostly independent of the dimensions, and so is the inherent measurement uncertainty. For this kind of thermocouple, the standard measure uncertainty is either ± 2.5°C or ± 0.25% of the correspondent measurement, whichever is greater [48]. According to the range of temperatures present in this work, this means the theoretical uncertainty reaches a maximum of ± 4 °C. However, a greater indicator of the measurement uncertainty of the experiment is to evaluate the data gathered across several repetitions and assess the reproducibility of the values. Taking into account all experimental conditions for the flat-flame burner, the average reproducibility uncertainty for this case is of approximately ± 2.4%, with the maximum being under ± 5%. For the porous-media burner, the average reproducibility uncertainty is a bit higher, at ± 7%, due to increased temperature variations between measurements.

On another note, the vertical positioning of the thermocouple probe in the flat flame setup resources to a measuring tape, which has 1 mm as the smaller scale division. Therefore, there is an uncertainty of ± 0.5 mm in the displacement of the probe.

One last aspect of the thermocouples used that should be taken into account is their composition, which is mainly based in Platinum. This element is a well-known catalyst that promotes oxidation of ammonia [49]. Therefore, if unburnt ammonia reaches the thermocouple wire, the possible chemical reaction may influence the temperatures being measured. This effect ought to be taken into account, although the

possibility of this aspect being a major influence in measurements is not a commonly observed phenomenon.

### 2.2.3. Gas Species Concentration

The concentrations of the species in the exhaust gas are measured with two different methods: the gas analysers and the GASTEC system.

The documentation of the gas analysers states that the repeatability uncertainty is of ± 0.5% of the full scale used. This results in the following values:

- ± 12.5 ppm vol. for $NO_x$ measurements;
- ± 0.05% vol. for $O_2$ measurements;
- ± 25 ppm vol. for CO measurements;
- ± 0.25% vol. for $CO_2$ measurements.

Nevertheless, a calibration for all analysers was conducted to make sure the reference values are measured correctly and to ascertain both their accuracy (deviation from reference value) and precision (deviations among measurements). For calibrating $O_2$, air was used as reference (21% $O_2$ in volume, approximately). For the remainder, a compressed cylinder with a gas mixture specific for calibration was used. Its contents were 150 ppm of $NO_x$, 750 ppm of CO and 8% of $CO_2$, the rest being nitrogen. After several repetitions, all measurements showed a deviation of less than 3% from the reference value, for all species.

However, for the scenario of measuring $NO_x$, the addition of $N_2$ to the sample may introduce an experimental error. To ascertain the effect of the dilution, three reference conditions were analysed – combustion of ammonia/methane blends with 5% of ammonia at 200, 300 and 400 W of power in the flat-flame burner. The choice for low concentration of ammonia in fuel was to allow for the analysis of $NO_x$ within the 0-2500 ppm scale without dilution. Measurements were taken with and without the addition of $N_2$, which was injected at a flow rate of 3 L/min. This allowed for the calculation of the effective dilution factor (ratio between $NO_x$ values without and with dilution) and the assessment of the deviations from this value for different scenarios. Although the flow controller has an inherent measurement uncertainty of 3% (specified by the manufacturer), this value should not be relevant for this case since the dilution is not measured as a function of the value displayed in flow controllers, but as a function of the measures in the analysers, which is where $NO_x$ is to be measured.

Accordingly, it was found that, if the flow controller was regularly checked to make sure the intended flow was passing through, the dilution factor changed insignificantly throughout the experiments. The average dilution factor was of 2.61, while the reproducibility uncertainty in the measurements of the latter is less than 0.5%. The conclusion is that the aforementioned accuracy of the $NO_x$ measures should be maintained, as there is no quantifiable influence of the sample dilution in the results.

The dilution effect was afterwards analysed in the porous-media burner and with the calibration mixture of gases, independently, which corroborated the initial findings.

Having ascertained the accuracy of the gas analysers, the precision of the data is assessed through several repetitions of the experimental conditions, to ascertain the best estimates for the reproducibility uncertainties. The emissions of $NO_x$, $CO_2$ and $O_2$ showed similar results for the reproducibility uncertainties, which were between ± 4% and ± 5.5%, and did not show any dependence on the type of burner or condition. The emissions of CO showed a higher average reproducibility uncertainty of around ± 18%. This is due to the fact that these emissions are rather low for all the investigated conditions, in which the maximum was never above 70 ppm. Therefore, the reproducibility uncertainty is more reactive to even small variations of the results. Overall, these results show that the data is precise and repeatable.

The next equipment to be discussed is the GASTEC system. The model of the detector tubes used is No.3M, designed to measure ammonia within a range of 50 to 500 ppm, although this interval can be expanded, as was previously mentioned. The relative standard deviation in the documentation of the manufacturer is 5% of each measurement, which means it could reach a value of up to ± 50 ppm, considering a maximum measure of 1000 ppm. However, since the scale printed in each tube has markings relatively distant from one another, there could be some bias in translating the colour-shifting into an actual number, which would lead to further errors.

To circumvent this subjectivity, after a measurement, each tube is photographed, and the picture is then imported into a computer to process the scale and result in pixels, thus eliminating an inaccuracy that could be introduced by the observer. As a means to assess real-world standard deviations, several repetitions for each condition were conducted. The best estimate of the reproducibility uncertainty was determined as ± 16%, which is considered very acceptable, taking into account the nature of this method.

## 2.3. Experimental Procedure

The procedure for conducting combustion experiments can be divided in several parts: preparation, ignition, measuring and power-down phases. There are some differences according to the burner being used; nevertheless, the flow of steps is similar for both.

### 2.3.1. Flat-Flame Burner

For the preparation phase, the gases being used are supplied to the burner in a safe manner. Therefore, after turning on the $CH_4$ digital flowmeter and making sure that all flow controllers are closed, the compressed cylinders are opened, using the valves to maintain an exit pressure of 1 bar. The air compressor is turned on and the air valve is also set for the same pressure. The exhaust ventilation is turned on, making sure that there is flow being sucked into the exhaust inlet. The water tap is also opened for cooling the species probe and the burner. After making sure that all connections are secure and no gas is being discarded to the environment, the ignition can take place.

Ignition takes place with $CH_4$ as the only fuel. At this time, the burner does not have any chimney or tube on top and is in direct contact with the atmosphere. Methane starts being supplied at around 0.5 L/min using a lighter to ignite the flame. At this point, the flame is only burning with ambient air. The compressed air can be supplied by opening the corresponding rotameter. The quartz tube can then be placed on top of the burner, entraining the flame. Adjustments to the flow controllers are made to reach the stabilization condition, in which 300 W of $CH_4$ is burned at stoichiometry. This corresponds to the values of 54 (cL/min) in the $CH_4$ flowmeter and 21.5 (mm of height) in the air rotameter. To achieve stability, this condition is maintained for around 20 minutes, which proved to be more than enough in the initial tests. While the burner is warming up, all the necessary measuring equipment can be turned on. This includes the analysers, the pump/filter system, the computers and/or the chromatograph. Every necessary connection should be made and/or checked. This allows the instruments to also achieve stability.

When a stable stage is achieved for both the instruments and the burner, measurements can start taking place. First, the initial testing condition is established. The initial amount of $CH_4$ is always the same as the one introduced for achieving stability; however, if the equivalence ratio being studied is not 1, then the air rotameter must be changed for the desired value. The chimney is put in place and either the species probe or the thermocouple is placed in the initial position. For the species probe, this is a fixed location and it remains still throughout all measurements. The thermocouple probe is to measure temperature profiles, so its place changes gradually in the vertical axis, as measurements are made for each condition. A waiting interval occurs until the flame achieves stability in the new condition.

Afterwards, measurements can start. By using the species probes, measures can be taken by either the gas analysers or the GASTEC system. If using the thermocouple probe, a measure must be taken for each vertical position, lowering or rising the probe until the complete profile is done.

After finishing the study of this condition, ammonia can be introduced. Nonetheless, it should always be introduced gradually, increasing the percentage of ammonia in fuel volume by 10% each time. First, the $NH_3$ rotameter is opened in the desired position, and only then the amount of $CH_4$ is reduced until 300 W of power is once again established. To maintain the flame stable, it is of utmost importance to always increase the ammonia before decreasing the methane.

Measurements can take place for the new condition after it stabilizes. Upon finishing, ammonia is increased again, by following the previous description. This process is repeated until the maximum amount of ammonia with a stable flame is achieved.

When all measurements intended are finished, the installation can be powered down. First, it starts by increasing the methane to around 0.5 L/min, regardless of the final ammonia condition, to stabilize the flame further. Ammonia feed is then cut at the exit of the compressed cylinder, to drain the circuit of ammonia. Once the $NH_3$ rotameter shows no flow, it can be closed. The same is done with the $CH_4$, by cutting the feed at the cylinder exit. Once there is no more flow, blow-off occurs and the flame is extinguished. The $CH_4$ and air flow controllers can now be closed. Water is still left running for a while to cool down the probe and the burner. All measuring instruments can be powered off and disconnected.

Once the installation is cool, the quartz tube, the chimney and the probe utilized can be taken off and stored. After making sure that every compressed cylinder is closed, the air compressor and exhaust ventilation can be powered down, thus concluding the session.

### 2.3.2. Porous-Media Burner

In the case of the porous-media burner, the preparation phase is similar as the previous one, although some flow controllers are different, as explained in subsection 2.2.1. Additionally, the $H_2$ compressed bottle is connected to the burner, and should also be opened at 1 bar, making sure the flow controller is closed. The remaining steps are the same, as described in 2.3.1.

Here, ignition also resources to $CH_4$ as the only fuel. Since the flame cannot be seen directly when it enters the ceramic core, the thermocouple system should already be running from the beginning to allow for constant monitoring of the flame position, thus ensuring a safe ignition. Additionally, this means the temperature measurements are automatic for the complete duration of the session, needing only to cross-reference the timestamps of the results with the time at which the correspondent condition is stable.

Methane is initially fed at around 1.5 L/min and ignition is made with a lighter on top of the ceramic core. The initial diffusion flame sits completely above the ceramic. The air needs to be opened very slowly, starting off at around 10% (read in the air rotameter) and increasing 5% every 2 minutes until more or less 30% is achieved. This is to allow the flame to steadily move upstream and into the porous-media. Once the flame is completely inside the core, a stabilization condition is established, by feeding 2 L/min of $CH_4$ and positioning the air rotameter at 40%. The chimney is placed on top of the burner and the species probe is positioned inside it, making sure the water tap is opened, for cooling. The burner is left to warm up for at least 20 minutes, always making sure the flame is in the middle of the ceramic core by constantly observing the temperature profile. In the meantime, the rest of the measuring equipment can be turned on and thoroughly connected.

After achieving stability, an initial measuring condition of 1200 W of power must be set, dependent on which fuel will be studied: either ammonia/methane or ammonia/hydrogen blends. If the focus is ammonia/methane, ammonia can be introduced, by opening the rotameter to the desired position. Afterwards, the methane and air flows are corrected for the current condition, re-establishing the power value of 1200 W and the equivalence ratio of 0.8. After letting the flame stabilize for at least 10 more minutes, measurements can start taking place. The time for each valid condition is recorded, to allow for comparisons with the results file of the thermocouple system. The species probe aspirates the exhaust gases for further processing. After the needed values are saved, the next condition can be established. Once again, the ammonia amount is increased first, and only then is the methane flow reduced, to maintain the total power constant. After the new condition is stable, measurements can once more take place. This process is repeated until the highest possible amount of ammonia in the fuel mixture is achieved.

If the fuel being studied is an ammonia/hydrogen blend, methane is not switched directly with hydrogen. Firstly, ammonia is introduced and methane is reduced, in the same way as if methane/ammonia mixtures were to be studied, until a mixture of 50% ammonia and 50% methane at 1200 W is achieved. At this time, the $CH_4$ is gradually phased out as the $H_2$ is introduced, with the aim of reaching a 50% ammonia/50% hydrogen blend at 1000 W. These steps are to make sure the flame shifts fuels in a steady manner. The ammonia and hydrogen are afterwards increased to achieve 1200 W. Hydrogen introduction can move the flame upstream, so caution in observing the temperature profile is of utmost importance. If the flame starts receding past the lower thermocouples, the air flow should be momentarily increased, so that the flame moves downstream. After stabilizing this initial condition, measurements are taken, moving on to the following condition afterwards. This is repeated until the last condition.

For powering down the installation, the process is the same as specified for the flat-flame burner: Increase the methane flow (even if using $H_2$), drain the ammonia (and the hydrogen, if that is the case) and, lastly, close off the $CH_4$ and air. After blow-off, the measuring equipment is turned off and disconnected. After cooling down, the water tap is closed and the compressor and ventilation are shut down. Finally, the probe and chimney can be taken off.

## 2.4. Numerical Method

As was mentioned before, numerical models are specifically important for designing combustors. However, validation against real-life results is of utmost importance for their correct application. To assess how the experimental values obtained in this work fare against existing mechanisms, a numerical, chemical-kinetics simulation was conducted. This computational work yields information on the combustion mechanism and the intermediate states, thus describing the characteristics of the reactions taking place.

The software employed here is Cantera [50], an open-source library with the necessary functions and objects to solve chemically reacting laminar flows. It does so by automating all thermodynamic, transport and chemical calculations. It is used as an add-in code library to be used in programming languages – Python was chosen for this study due to its ease of use and wide support. Cantera has already been employed in other numerical studies with success [26], [37].

The documentation repository at Cantera's website provides several tutorials on how to operate the library. The code used in this work is based on these tutorials, although it was completely revamped for the present scenarios. The programme code employed is dependent on the installation characteristics, which means two sets of code were written. Nevertheless, all programmes consist of a one-dimensional, laminar, premixed flame, held in place by the burner.

The code for the flat-flame burner is the most complex one, due to the impossibility of measuring the temperature inside the flame. Consequently, two scripts are used: the first is named "burner_flame" and predicts the adiabatic temperature in the immediate vicinity of the flame. To do so, all the conditions, mixture proportions and geometry serve as input, allowing for the calculation of the transport and energy

equations in equilibrium, outputting the temperature profile. The second script, “flame_fixed_T”, takes the predicted temperatures in the area of the flame and stitches them with the experimental temperatures measured for the same conditions, thus creating a hybrid numerical/experimental profile. This allows for the calculation of the final energy and mass transport equations along the vertical axis, yielding the final predictions for the concentrations of the products.

For the porous-media, the temperatures in the middle of the reactor are experimentally measured, which means there is no necessity of predicting temperature profiles in beforehand. Therefore, only a version of the “flame_fixed_T” script is used, with the according conditions and mixtures as input. The calculations along the vertical axis occur in the same manner as before. However, special attention is taken regarding the geometry of the burner. In fact, there is no module in Cantera to characterize the burner as made of a porous material, and no other options are suitable without extensive work being put into them. Taking into account that the development of reactor models is outside the scope of this work, a simplification was made by using the generic burner model already employed in the flat-flame burner. Nevertheless, the porosity was taken into account and only the effective “open space” is considered for the burner volume.

For Cantera to be able to calculate all the combustion steps, there is the need to run a mechanism. This is a file with a list of reactions that take place, along with all the species involved and corresponding reaction rates. This serves as the “recipe” for how Cantera should calculate all the necessary equilibrium equations. In section 1.2.3, several studies on different mechanisms were discussed, noting how they are different from one another. Since running the numerical simulation for all mechanisms is impractical, due to computational costs and time constraints, a choice was made to use only the three most relevant to the conditions being dealt.

The mechanism from Miller and Bowman [32] is outdated by today’s standards, and the authors discouraged its use for conditions different than the ones they studied. Duynslagher’s model [34] was also developed for low pressures, which means it would not fare well for the atmospheric pressure used in this work. The Xiao mechanisms, either for methane/ammonia [26] and hydrogen/ammonia [37], showed great potential, however, the authors did not disclose the mechanisms for compatibility with Cantera. On the other hand, the mechanism from Song et al. [38] and its derivative by Otomo et al. [39] could not predict methane/ammonia blends in any convincible manner for the conditions at hand, according to the initial tests. Comparing two of the most used mechanisms, Konnov’s [33] and Tian’s [40], according to the review by Kumar and Meyer [41], the latter could outperform the former in a wide range of conditions, taking into account the proximity to experimental data. The mechanism by Okafor et al. [43] has its basis in Tian’s, and showed great potential for predicting flames which include ammonia and either hydrogen or methane. It also presents a great opportunity to study how an evolved model compares against the original. Finally, the last two mechanisms discussed in section 1.2.3 were from Dagaut et al. [35] and Mathieu and Peterson [36]. Although the latter is based off of the former, Mathieu and Peterson’s mechanism proved to be inadequate for the modelling of $NO_x$ and $N_2O$ data in the presence of methane, lacking many carbon-based reactions.

Therefore, the three models used in the chemical kinetics simulation are the Tian, Okafor, and Dagaut mechanisms. However, due to different convergence issues regarding each type of burner, two different sets were used: the Okafor and Dagaut models were used for the flat-flame burner, while the mechanisms of Okafor and Tian were employed for the porous-media burner.

# 3. Results and Discussion

In this chapter, all results gathered throughout the experiments are presented and thoroughly discussed. The experimental conditions and resultant data are discussed for both the flat-flame burner and the porous-media burner, in sections 3.1 and 3.2, respectively. In section 3.3 the practical impacts of this investigation are discussed, in vision of the future roles of ammonia as a fuel.

## 3.1. Flat-Flame Burner

### 3.1.1. Test Conditions

Initial testing in the flat-flame burner with mixtures of ammonia and methane proved to have potential for achieving stable flames. However, the same could not be said for mixtures of ammonia and hydrogen, since these flames would almost always produce flashback for a wide range of conditions. Due to these limitations, it was set that this burner's usage would focus on analysing the effect of an increasing amount of ammonia in the fuel mixture, for different equivalence ratios, in premixed flames of ammonia/methane/air.

The following stage was to set the power output, which would be fixed to reduce the number of variables being studied. Previous researches on this installation used thermal powers of up to 1.5 kW [21]. However, in the case of ammonia blends, these values proved to be quite high, since in the preliminary tests the flame would always produce a blow-off at minimum amounts of ammonia, regardless of the equivalence ratio. This could only be overcome by reducing the power by about three times. Still, flame stability could only be certain for low values of ammonia in fuel volume, when in the vicinity of 500 W. On the other hand, the power of 300 W proved to be a good balance between being able to stabilize the flame and at the same time reaching high percentages of ammonia in the fuel mixture. Additionally, for lower values, no influence was detected in the stability of the flame. Therefore, 300 W was the final power set.

Afterwards, the equivalence ratios were chosen. While searching for the best power value, an initial conclusion was drawn: a higher equivalence ratio meant that an increased amount of ammonia could be injected. However, the installation was not capable of working under fuel-rich conditions, due to the high possibility of unburnt ammonia escaping through the exhaust. A compromise was set between these toxicity concerns and the objective of achieving the highest amount possible of $NH_3$ in the fuel mixture, thus setting the maximum equivalence ratio as $\phi = 1$. At this value, 70% of ammonia in the fuel mixture could be stably achieved. Decreasing the equivalence ratio from stoichiometry to fuel-lean, it was found that for values of $\phi = 0.7$ and lower, the percentage of ammonia in the fuel mixture could only go up to 40%, before occurring blow-off. Fuel blends with a minimum of 60% of methane are not as relevant, since the presence of carbon in the mixture is still overwhelming. As a result, a lower limit of the equivalence ratio was set to $\phi = 0.8$, where the highest possible amount of ammonia was 50% of

total fuel mixture volume. To allow for further comparisons, an intermediate condition was also set as $\phi$ = 0.9, for which stable flames of ammonia are possible with up to 60% of ammonia in the fuel mixture.

For each considered equivalence ratio, the flames studied ranged from pure methane (0% $NH_3$) to the maximum possible amount of ammonia, in intervals of 10% of ammonia percentage in total volume of the fuel mixture. This interval was chosen due to the flow uncertainties discussed in 2.2.1. Table 3.1 summarizes the experimental conditions of the flat-flame burner.

Table 3.1 - Experimental conditions for the flat-flame burner.

| Power | Equivalence ratio | Ammonia in the fuel mixture (% in volume) |
|---|---|---|
| 300 W | $\phi$ = 1.0 | 0, 10, 20, 30, 40, 50, 60, 70 |
| | $\phi$ = 0.9 | 0, 10, 20, 30, 40, 50, 60 |
| | $\phi$ = 0.8 | 0, 10, 20, 30, 40, 50 |

Therefore, the total number of studied flames in this burner was 21. For each one, temperature profiles were taken along the vertical axis of the quartz tube and gas species concentration measurements were made at 30 cm from the flame.

To make sure the correct values of flow are used for all constituents throughout the experiments, an Excel spreadsheet was created, which contained the stoichiometry equations of ammonia/methane blends and the specifications of the flow controllers. The equivalence ratio, ammonia fraction in the fuel mixture and power are used as input, and the output is the combination of values to be set in each controller, already adjusted to each scale.

Since the quartz tube employed in the installation was transparent, photographs of each flame were taken to assess the colour-shift that occurs as the presence of ammonia in the fuel mixture grows. The pictures were taken at an angle of about 30° from the vertical centreline, without the insulation placed around the quartz tube. An SLR camera (Canon EOS 700D) was used, with a focal distance of 50 mm, aperture of $f$/5, shutter speed of 1/20s and ISO of 6400. Figure 3.1 shows the flames studied for the equivalence ratio of $\phi$ = 1. Note that there is no discernible difference in colours when comparing between equivalence ratios with the same amounts of ammonia.

The colour for pure methane is noticeably not entirely blue, although it is not due to incomplete combustion, as the results will show. It is because of the incandescence of the steel mesh immediately below the flame. Nevertheless, a blue aura can still be seen in the periphery. The introduction of ammonia clearly changes the dominant pigment of the flame towards an increasingly whiter colour.

It is worth noting that, although reflections can be observed on the inside of the quartz tube, the flames are flat and above the burner.

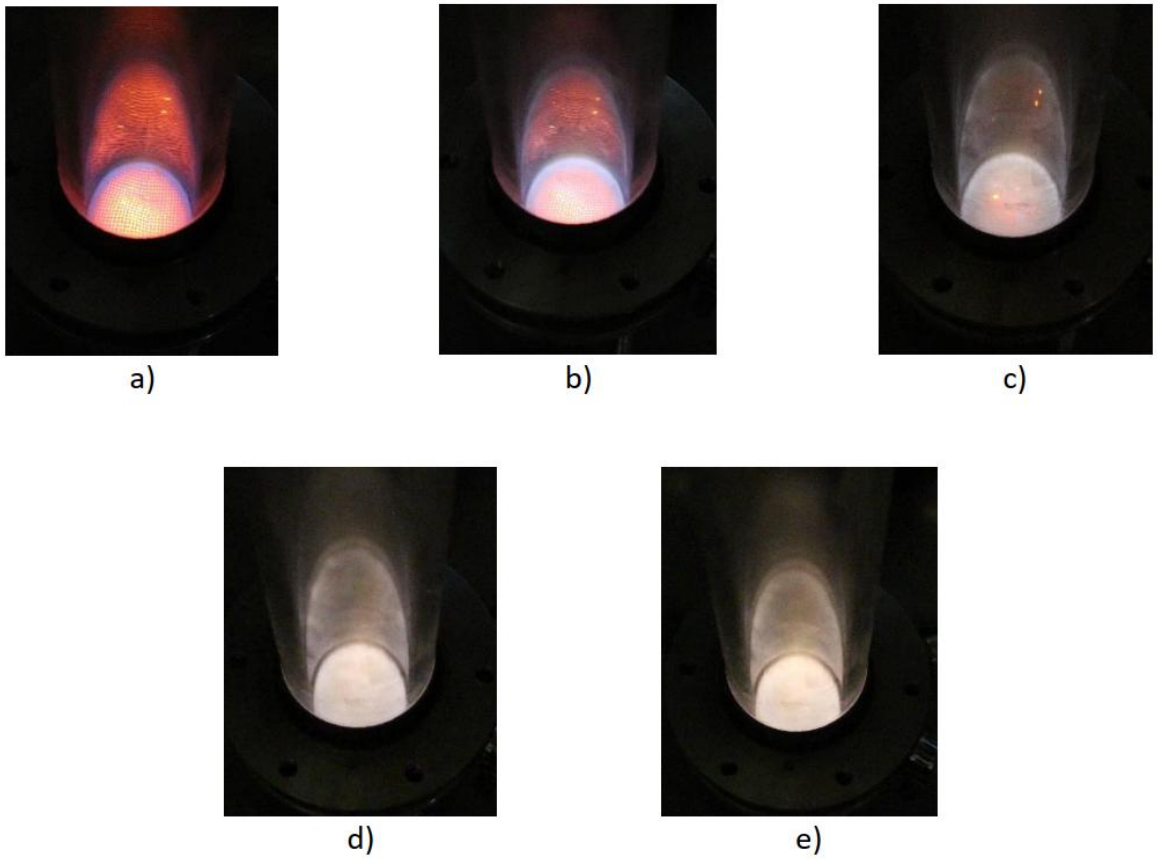


Figure 3.1 - Still photographs of the flames, taken at an angle of about 30° from the vertical centreline, for various proportions of methane/ammonia in the fuel mixture, for a thermal input of 300 W and $\phi$ = 1. a) Pure methane, b) 20% of $NH_3$ in the fuel mixture, c) 40% of $NH_3$ in the fuel mixture, d) 60% of $NH_3$ in the fuel mixture, e) 70% of $NH_3$ in the fuel mixture.

### 3.1.2. Temperature

It was observed throughout the experiments that the flame geometry remained the same: a plane disc hovering above the burner. This simplicity and steadiness resulted in consistent temperature gradients along the axis of the quartz tube.

The temperatures were measured vertically along the quartz tube, at a distance from the flame starting at 2.5 cm. The next distance was at 4 cm, and from then on until 40 cm from the flame, the temperatures were measured at an interval of every 2 cm. Measurements were made for each equivalence ratio at a time, starting from pure methane and progressively increasing the amount of ammonia in the fuel mixture. Figure 3.2, Figure 3.3 and Figure 3.4 represent the results taken for each equivalence ratio, representing the temperature as a function of the axial distance, where each curve constitutes a different percentage of ammonia in the fuel mixture. Note that the vertical bars represent the standard deviation concerning the repetition of the samples. Additionally, it can be observed that the flames corresponding to 10% and 30% of ammonia in the fuel mixture are not represented. This was to minimize overlapping of the results, and there is no general loss of information.

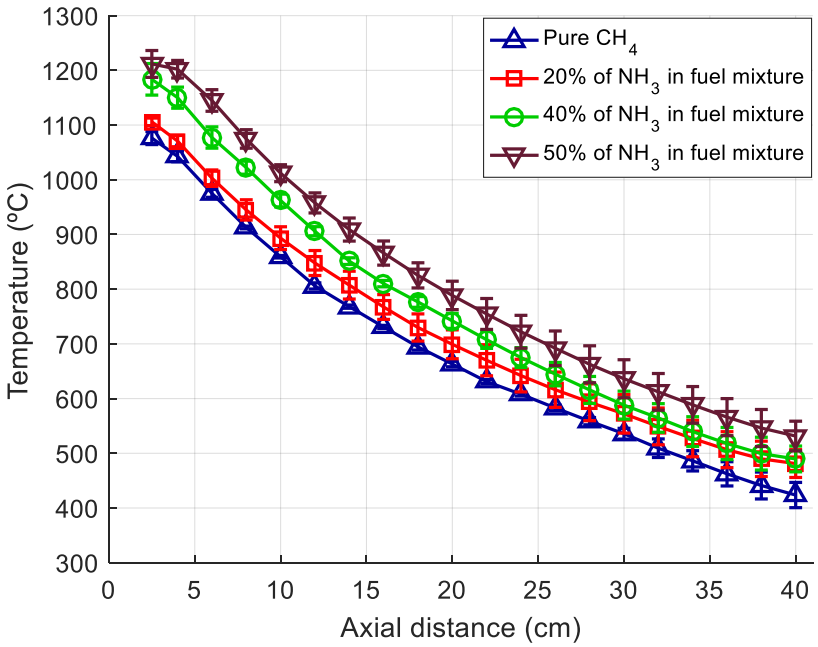


Figure 3.2 - Temperature as a function of the axial distance for a thermal input of 300 W and $\phi$ = 0.8.

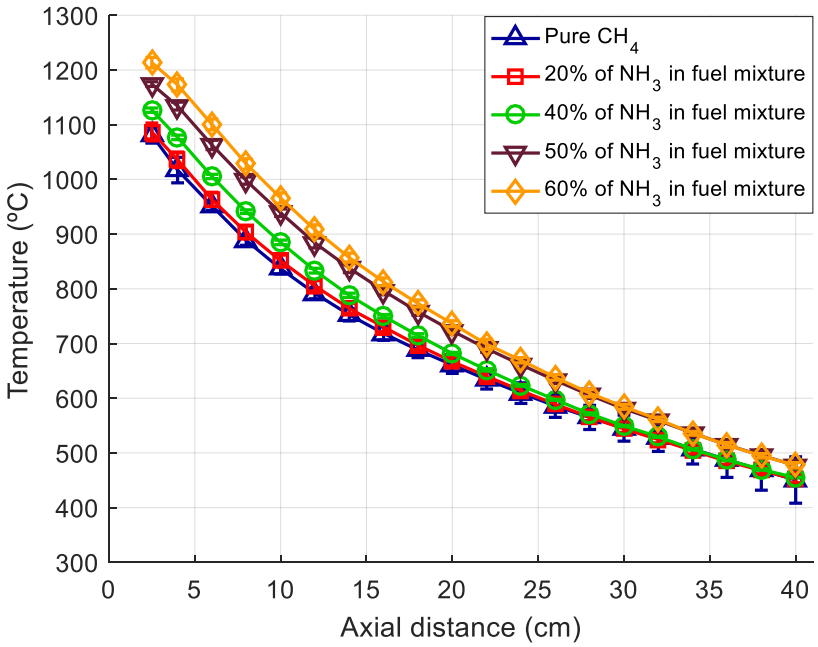


Figure 3.3 - Temperature as a function of the axial distance for a thermal input of 300 W and $\phi$ = 0.9.

The three figures show the same overall temperature gradient: all curves reveal a decrease in temperature as the distance to the flame increases. This trend is expected, since the heat loss increases as the gases travel upwards.

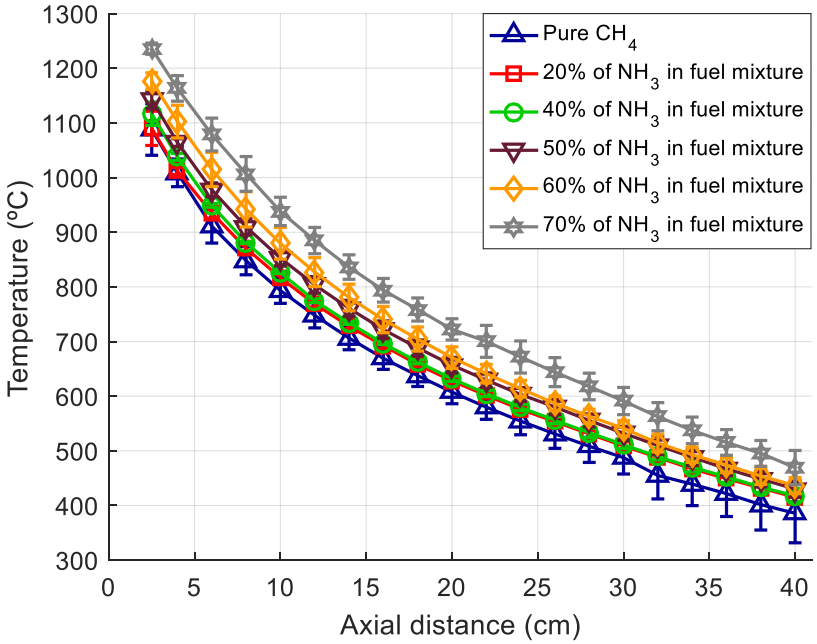


Figure 3.4 - Temperature as a function of the axial distance for a thermal input of 300 W and $\phi$ = 1.

The increase in ammonia fraction in the fuel mixture leads to an increase of the temperature across the complete profile, regardless of the equivalence ratio considered. This is an apparent contradiction of the expected behaviour. The combustion of methane has a heat release of about 890 kJ/mol, whereas the combustion of ammonia releases approximately 380 kJ/mol [51]. Thus, in theory, if the total fuel volume is kept constant, as ammonia concentration increases in the fuel mixture, the heat release would be progressively smaller, thus leading to lower temperatures. In the case being studied, the fixed property is power. This already takes into account the different heat releases of both individual combustions, so the amount of energy being released is constant, regardless of the proportions of the fuel constituents. However, since the specific energy and energy density of methane are more than double those of ammonia, respectively, this means that, as the fraction of ammonia increases, more total mass and volume are being injected in the burner, to maintain the value fixed for power. Thus, the same energy release being spread amongst more mass would lead to a lower specific internal energy. Therefore, even in this scenario, the temperatures should still decrease, as ammonia fraction in the fuel mixture increases. This is the opposite behaviour of what is presented in the results.

The probability of these values being a result of errors in the experimental procedure must be discussed. Indeed, as was mentioned before, the sequence of measurements for each equivalence ratio was in the order of increased amount of ammonia, which coincides with the order of increasing temperatures. As a result, the question arises if the burner was already in thermal equilibrium at the time of taking measures. If not so, the temperature would be explained by the warming up of the burner, as the experiments developed. However, several aspects point against this occurrence. Firstly, the burner was left to warm up at least for 20 minutes before each sampling session. In that interval of time, the temperatures were monitored to assess when a steady-state was achieved. The conclusion was that 10 minutes were enough for the temperatures to equalize. That time was doubled in order to make certain

that equilibrium was met in every repetition. Thus, the temperatures for pure methane were measured for a thermal balance. Furthermore, between conditions, the burner was also left to warm up after setting the corresponding fluxes in the flow controllers, while the temperature was also monitored. What was observed was that the temperatures started increasing significantly as soon as the fuel proportions were changed. Measurements only resumed when the temperatures stabilized once more. Therefore, to the best of the operators' abilities, all temperatures were measured for thermal equilibrium, sans any systematic error that has escaped this analysis. Additionally, the use of the aforementioned Excel spreadsheet ascertained the use of the correct values for the flow controllers to maintain a fixed power. Lastly, experiments were conducted with different flow controllers to exclude the hypothesis of malfunctioning hardware, and no differences in the overall results were found.

This assessment of the operator-induced error being negligible is also corroborated by the reproducibility uncertainty represented by the vertical bars. Some uncertainties overlap the other curves for distances further away from the flame, which is expected, since in those positions the heat loss has a greater impact due to the proximity to the exit – hence the larger spread of values. However, as an overall evaluation, the represented uncertainties mostly overlap only for adjacent curves. The result is that the conditions at both ends of the spectrum – maximum and minimum amount of ammonia for each equivalence ratio – have a well-defined separation of about 150 °C, regardless of equivalence ratio. Without more information, and considering the absence of a significant experimental error, the conclusion drawn from this data is that a certain mechanism leads to the temperature increase as ammonia is progressively introduced, which is not explained simply by the heat release of the individual combustions of methane and ammonia.

An initial supposition was that the increase of the global mass flow, as ammonia is introduced, resulted in a reduced residence time of the gases in the quartz tube, which would mean less heat is lost to the walls confining them. Nevertheless, this phenomenon will most likely have underwhelming effects, since it should not be able to produce such a difference in temperatures, considering the low power and mass fluxes being used.

Another possibility worth discussing is the measuring errors that are introduced with the use of thermocouples. These probes are an intrusive means of measuring temperatures, since they interfere with the flow of the gases and withdrawn energy from them. Brackmann et al. [20] observed the comparison between intrusive and non-intrusive temperature measurements in mixtures with ammonia. They concluded that thermocouples, in most conditions, measured temperatures significantly lower than their non-intrusive counterparts.

The most probable aspect when it comes to thermocouple interference in the temperature measurements of ammonia combustion is the possibility of occurring catalysis. As was mentioned in section 2.2.2, since the thermocouple is made from platinum, it is plausible that any ammonia in contact with the probe may suffer catalytic reduction on the surface of the wires, which is an exothermic reaction [49]. As ammonia in fuel increases, saturation may start to result in an incomplete combustion, and the outcome is a progressively stronger presence of unburnt ammonia in the exhaust. Consequently, the rate at which catalysis occurs would increase, releasing more energy directly into the thermocouple wire

and leading to higher measured temperatures. If this were the case, the temperature differences would be virtual, since they would not portray the combustion reactions, but instead a catalysis-induced error. This theory will be further investigated when the $NH_3$ concentrations at the exhaust are disclosed.

Finally, one last hypothesis has to do with differences in heat lost through radiation. Since there are varying amounts of ammonia and methane, the consequent concentrations of combustion products should change accordingly. Variations in the concentration of carbon-dioxide are rather relevant, from a thermal radiation point of view. Comparing with other flue gases, carbon-dioxide is known to have a higher emissivity, hence the fact that is considered a greenhouse gas and major responsible for the global warming effect. Although it is complex to calculate the emissivity of gaseous blends, Mateus [52] proved that exhaust gases at temperatures of about 1200 °C that result from the combustion of pulverized coal suffer a decrease in global emissivity of up to 25%, if the $CO_2$ concentrations decreased from around 20% to 0% (in volume of flue gases). This results in a substantial difference in radiated power. Therefore, as methane in fuel decreases and ammonia increases, the concentration of carbon-dioxide at the exhaust should start to decline, thus reducing the total emissivity of the exhaust mixture. If this were the case, the energy lost through radiation would be gradually less, which would explain how temperatures for ammonia-rich flames are higher. This hypothesis will be verified further when the $CO_2$ results are presented.

Continuing with the analysis of the temperatures gathered, the same data can be shown in a different manner, to individualize the influence of the equivalence ratio. Figure 3.5 shows the temperature profiles as a function of the axial distance for pure methane as fuel, where each curve represents a different equivalence ratio. Figure 3.6 represents the same relationship but for 50% of $NH_3$ in the fuel mixture.

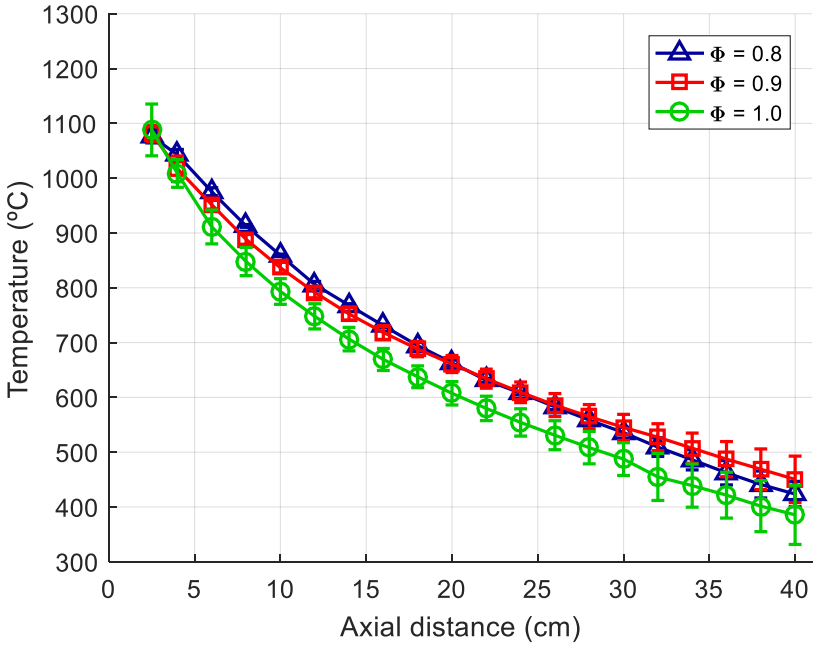


Figure 3.5 - Temperature as a function of the axial distance for pure methane firing with a thermal input of 300 W.

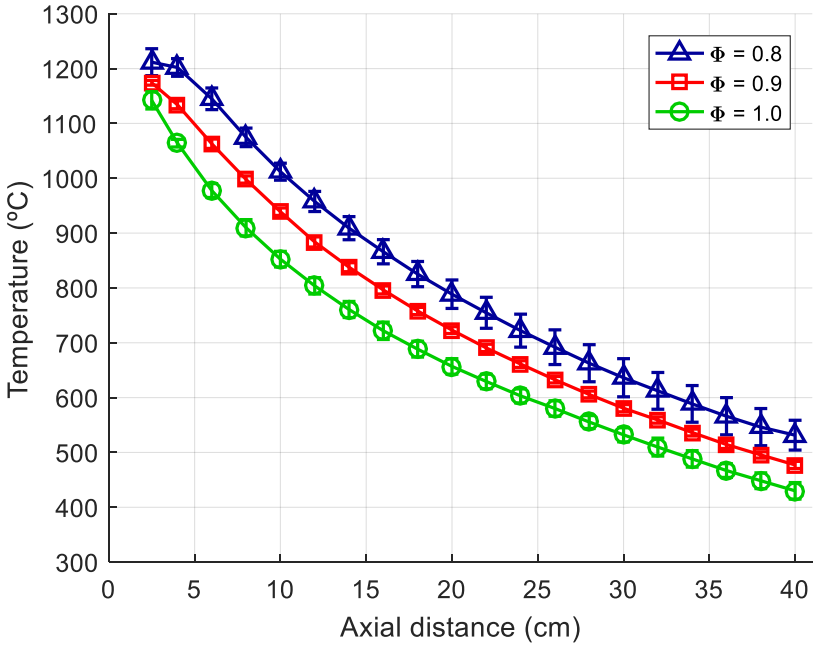


Figure 3.6 - Temperature as a function of the axial distance for a fuel mixture with 50% of $NH_3$ with a thermal input of 300 W.

From these graphs, another apparently conflicting pattern is observed: when in the presence of ammonia, for the same fuel constituents' proportions, as the equivalence ratio decreases, the temperature values increase. In theory, the adiabatic flame temperature has a maximum for near stoichiometry conditions, decreasing as the equivalence ratio is reduced [2]. And, at first glance, the same should happen here: in each graph, the fuel constitution and power are the same for each $\phi$, the only variable is the amount of air. Consequently, if the air increases as the equivalence ratio is reduced, the total mass flow increases, although the heat release is the same. Therefore, the specific internal energy should reduce, along with the temperatures. Thus, the results are contradictory once more.

In this case, however, the previously discussed possibility of significant experimental errors (due to not achieving thermal equilibrium) is even more illogical, since each curve in each graph was taken at a different occasion, within more or less the same interval of time, which means they had approximately the same amount of time to warm up. Observing the uncertainty bars, it is also clear that the reproducibility of each curve is concise and their separations are well-defined, since little overlapping is shown. Therefore, this argument is not applicable.

It should also be pointed out that the previous hypothesis of the interference of the thermocouple probe is more difficult to apply in this case. Regarding any possible $NH_3$ catalysis at the thermocouple, the increased concentration of the oxidizing agent would mean there would be less unburnt ammonia, hindering catalytic reactions. Concluding, thermocouple interference does not appear to be a consistent justification to the patterns encountered.

On the other hand, this phenomenon may be once more explained by taking a look at radiative heat loss. Since, all equivalence ratios are for fuel-lean or stoichiometry, conversion of hydrocarbons should

be mostly to $CO_2$, resulting in negligible CO. Therefore, the difference in equivalence ratios should mostly regard the dilution of the same flue gases. As a result, for the same ammonia quantity, as the equivalence ratio decreases, the overall $CO_2$ concentration should also decrease, since more $N_2$ is present. This would result in a lower emissivity of the exhaust gases, and, consequently, less heat lost through radiation, thus explaining the apparent temperature increase. This will be discussed along the presentation of the $CO_2$ results. As an addition, as the mass flow increases with the decreasing equivalence ratios, the residence time of the gases is reduced, which also decreases the heat loss to the walls, complementing the previous explanation.

Another aspect to bear in mind is the behaviour observed for pure methane. Although, apparently, there is still some discernible pattern of increasing temperature with decreasing equivalence ratio, the profiles are rather close and within the uncertainties of one another. As the amount of ammonia increases, the curves progressively separate and the effect of the equivalence ratio becomes more apparent. Thus, this points to a mechanism driven by the introduction of ammonia. This further strengthens the possibility that the difference in exhaust gas constitution may be the reason behind the patterns observed.

Once more, the results point towards a more complex situation that is not explained simply, revolving around an intricate chemistry due to the presence of both ammonia and methane. The numerical analysis of the combustion may supply some answers. As was explained in section 2.4, to reproduce the experimental data gathered for this burner, the measured temperature profiles are stitched together with a prediction of the temperatures in and around the flame, which are impossible to measure with the material at hand. Figure 3.7 represents an example of the profiles that serve as input for Cantera.

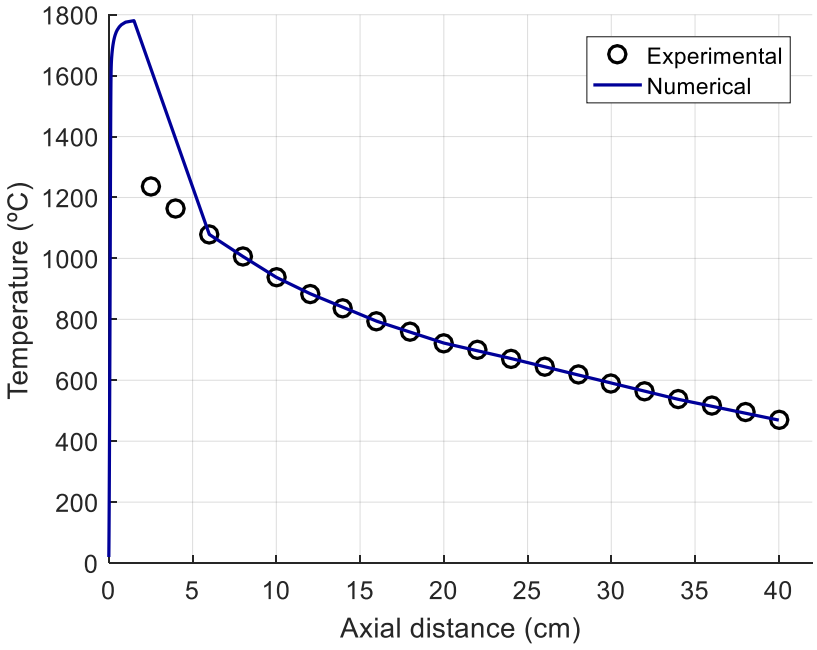


Figure 3.7 - Axial temperature profile used in Cantera, and the corresponding experimental values for a fuel mixture with 70% of $NH_3$ with a thermal input of 300 W and at $\phi$ = 1.

Although experimental temperature measurements are made starting at 2.5 cm from the flame, some values closer to the flame could not be implemented due to non-convergence of the predicted profile. Thus the predicted temperatures are used until a distance of 6 cm from the flame, whereas the experimental values are used beyond that distance (inclusively). This is consistent for all conditions and is used to calculate the numerical results in the following section.

### 3.1.3. Gas Species Concentration

The concentrations of the exhaust species were measured resourcing to two methods. Both of them resourced to the sampling probe placed at a distance of 30 cm from the flame. Note that the following results for all gas species concentrations – both experimental and numerical – are corrected for 6% of $O_2$ (with the exception of oxygen itself). Figure 3.8 shows the concentrations of $NO_x$ for the flat-flame burner as a function of the amount of ammonia in fuel mixture. Each curve represents a different equivalence ratio.

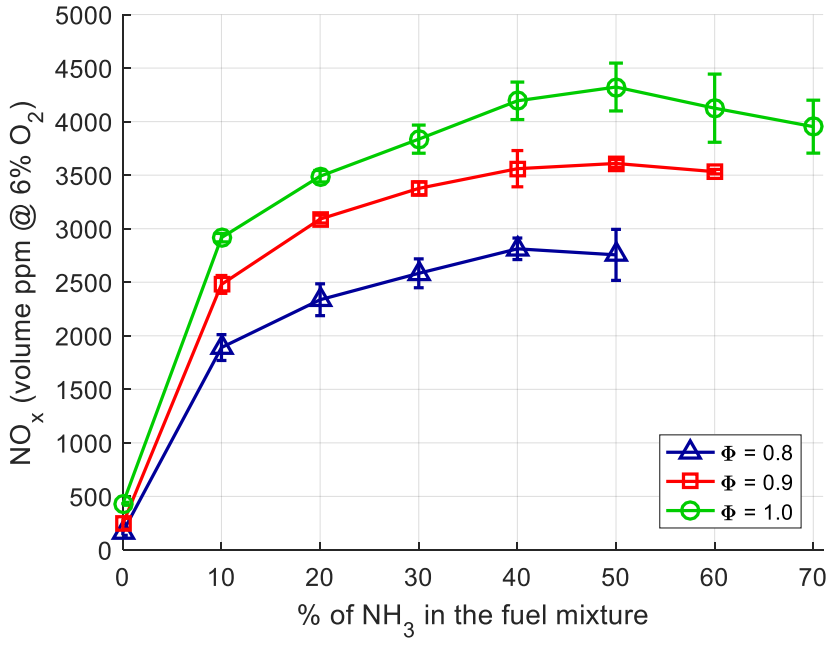


Figure 3.8 - $NO_x$ emissions as a function of the amount of $NH_3$ in the fuel mixture for a thermal input of 300 W.

As can be observed from Figure 3.8, the measurements seem to follow a consistent pattern, similar for each equivalence ratio. The $NO_x$ measurements start at very low values, for the combustion of only methane, and increase significantly as soon as ammonia is introduced. As the concentration of ammonia in the fuel mixture continues to increase, so does the $NO_x$ concentration, although at a progressively lower rate, until it reaches a peak, at around 50% of ammonia in fuel volume. The maximum value recorded is of around 4300 ppm, for $\phi = 1$. After this maximum, the values start slowly decreasing.

Focusing solely on the $NO_x$ concentrations for pure methane combustion, they are observably different from absolute zero. This should be due to dissociation of the nitrogen present in the air at high

temperatures, which will always contribute to the appearance of these oxides in the exhaust, even if the fuel has no nitrogen atoms. This is in contrast with the high $NO_x$ values registered for the adjacent condition with 10% of ammonia in fuel volume. Indeed, this great difference is due to a shift in the major source of $NO_x$, from the thermal dissociation of the nitrogen molecules in the air (thermal-$NO_x$), to the combustion of the nitrogen compounds in the fuel (fuel-$NO_x$), which have abundant N atoms and have a considerably higher rate of conversion.

Therefore, it is clear that the reactions involving the nitrogen atoms in ammonia are the primary source of $NO_x$. However, this conversion does not increase linearly with the ammonia concentration in fuel: as the $NH_3$ introduction increases, the $NO_x$ emissions slow down and then start decreasing. The reasoning behind this behaviour might be the saturation of ammonia, in a flame that is not hot enough, thus leading to an incomplete combustion. If that was the case, an increasing amount of unburnt ammonia would react with nitrogen oxides, reducing their concentration through selective non-catalytic reduction.

To understand if this mechanism is able to explain the $NO_x$ pattern, quantification of ammonia is needed. Testing was conducted with the GASTEC detector tubes, which allow for quantitative evaluation of $NH_3$ for concentrations starting at 10 ppm. Figure 3.9 shows an example of the results taken for the most extreme condition of 70% $NH_3$ in the fuel mixture, for $\phi$ = 1.


Figure 3.9 - GASTEC detector tubes: a) unused tube, b) tube after 5 pump strokes for a fuel mixture with 70% $NH_3$ with a thermal input of 300 W and $\phi$ = 1.

This result was taken with the maximum allowable number of strokes, which is 5. Comparing with Figure 2.6 it can be observed that the discoloration of the tube is homogeneous and there is an absence of two contrasting colours with a defined boundary. This means there is enough presence of unburnt ammonia to trigger the detection limit of 2 ppm in volume, although not enough to be measured quantitatively. For the other conditions, the homogeneous colour shifts were very similar, but their appreciation is subjective and carries high measuring uncertainty. Therefore, the overall conclusion is that, regardless of equivalence ratio and ammonia quantity in fuel, the $NH_3$ concentration at the exhaust is less than 10 ppm, but above 2 ppm.

Revisiting the temperature results for this installation, one of the hypotheses for the unexpected rise of temperature with increased ammonia was the possibility of $NH_3$ catalysis occurring at the thermocouple. It is now clear that the rather low amounts of unburnt ammonia at the exhaust are not enough to explain the temperature results. Even if some catalysis occurs, the energy transfer would still be negligible and not capable of producing the differences in temperatures observed. Therefore, this hypothesis is discarded.

Although presence of ammonia is proved at the exit, there is no possibility of calculating its effect on the measured $NO_x$ pattern, especially taking into account that the concentrations of $NO_x$ and $NH_3$ are separated by two orders of magnitude. Therefore, it is important to assess how the $NO_x$ patterns in Figure 3.8 fare against results found in the literature.

Regarding the conditions researched, the limitations of flame stability do not allow to observe how the $NO_x$ concentration pattern would develop, if ammonia were to reach 100% in fuel mixture volume. Nevertheless, the results gathered are enough for comparison with previously discussed graphs of ammonia/methane flames, namely Figure 1.5 and Figure 1.6. The patterns observed in these figures are in accordance to the results gathered: from the fast rise of $NO_x$ concentration with the introduction of ammonia, to the peak obtained midway and the decay of the curve afterwards. Both studies justify that the decline in emissions is due to reduction reactions between $NO_x$ and $NH_3$. Extrapolating to the present work, although unburnt $NH_3$ concentration is rather low, the measured ammonia in the exhaust may just be residual molecules that did not react with $NO_x$, since the pattern is the same as in the literature.

Note that, although the aforementioned literature graphs represent the concentration of ammonia in fuel in different types of percentages – one is in fuel energy and the other in moles of fuel –, this will only translate in a horizontal dilation or contraction of the curves, especially for the graph with the scale in energy fraction. Thus, these qualitative comparisons are valid and the $NO_x$ results are in agreement.

Additionally, when compared with Figure 1.5, the measured $NO_x$ values seem to be in the same order of magnitude. Note that, for this figure, the authors separated NO from $NO_2$. However, since $NO_2$ concentration is more or less constant and comparatively much lower, this means the $NO_x$ emissions (the sum of both) will have the same pattern as the NO, although with a slight vertical shift. Therefore, the previous statements are still true.

The similarities with the literature do not end there. Assessing the effect of equivalence ratio in the $NO_x$ concentration results (Figure 3.8), there is a clear reduction in the overall $NO_x$ values with the decrease in $\phi$. This concurs with Figure 1.3 and Figure 1.4, which show that a peak for $NO_x$ emissions is found approximately in the interval between $\phi$ = 0.9 and $\phi$ = 1.0. Additionally, both literature figures show that there is a reduction in $NO_x$ concentration as the equivalence ratio is further decreased. This is in accordance with the measured higher $NO_x$ concentrations for $\phi$ = 1.0 and the subsequent reduction for the remaining equivalence ratios.

It should be noted that the results in Figure 1.4 are for pure ammonia combustion, while the experimental results presented here are for $NH_3$-$CH_4$ blends. Nevertheless, Figure 1.3 is for ammonia/methane mixtures, and this pattern was already found in the analysis of [19], which employed ammonia-doped methane flames, as stated in the literature review. Furthermore, the previously discussed Figure 1.6, which concerns ammonia/methane combustion, also shows that the $NO_x$ concentrations for a fuel-lean condition of $\phi$ = 0.6 are substantially lower than those found for stoichiometry. Therefore, this pattern seems consistent, both among the literature and comparing with the gathered experimental data.

Continuing with the assessment of the exhaust gases, carbon monoxide is always an important pollutant to evaluate in the combustion of hydrocarbon fuels. Figure 3.10 represents the concentration of CO in the exhaust as a function of the percentage of ammonia in the fuel mixture, where each curve represents a different equivalence ratio.

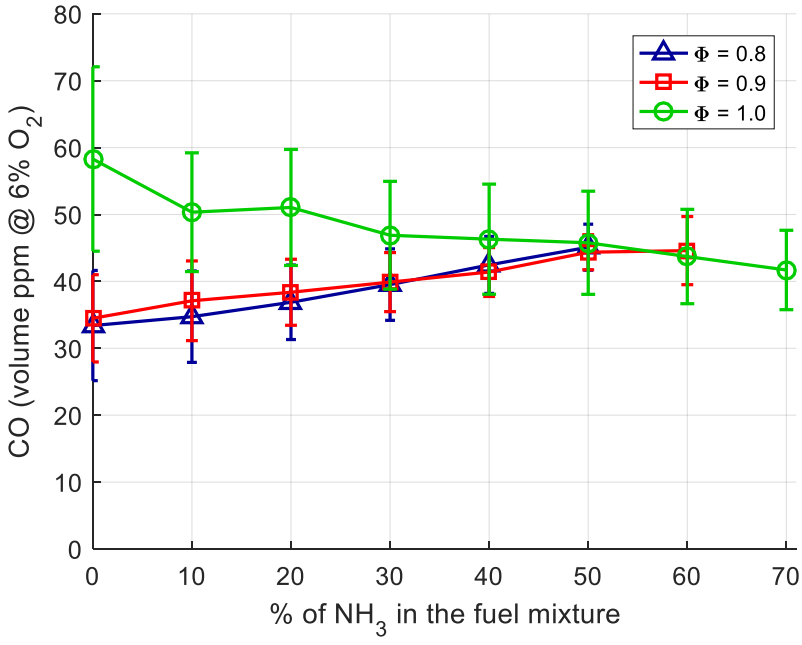


Figure 3.10 - CO emissions as a function of the amount of $NH_3$ in the fuel mixture for a thermal input of 300 W.

It can be observed that, for the lean conditions, the average CO concentration seems to increase as ammonia is introduced. However, bearing in mind the relative differences and the uncertainties found, these patterns may be considered virtual, since the results are rather low and very close. Furthermore, all average values for each equivalence ratio are below 60 ppm in volume. Contrasting with the documentation of the analyser, these values are quite near the detection threshold and are of the same order of magnitude than the measuring uncertainties specified by the manufacturer. Therefore, the only conclusion that should be taken from these results is that the combustion of the methane portion of the fuel is effectively complete, regardless of equivalence ratio and ammonia quantity. Consequently, the great majority of carbon atoms are integrated in $CO_2$.

The measurements of carbon-dioxide at the exhaust corroborate the complete combustion of methane, as the values are close to the expected. Figure 3.11 represents the $CO_2$ percentage in the flue gases as a function of the amount of ammonia in the fuel mixture, for each equivalence ratio. It can be observed that, regardless of equivalence ratio, the $CO_2$ concentration decreases with the increase of ammonia. This is expected since less methane is being burned, therefore, there is a lower amount of carbon-dioxide being produced.

Remounting to the temperature profiles obtained for this burner, it was theorized that the reason behind the rise in temperatures while ammonia presence in fuel grew might have been due to the differences in heat lost through radiation. The results for $CO_2$ seem to corroborate this hypothesis. In this way,

regardless of the equivalence ratio, as ammonia quantity increases, the concentrations of carbon-dioxide decrease, thus lowering the global emissivity of the exhaust gas. Therefore, taking into account the before mentioned influence of $CO_2$ and these observable changes in its concentration, it is quite possible that the change in emissivity might be behind the higher temperatures, since the consequent reduction in heat loss through radiation should be significant.

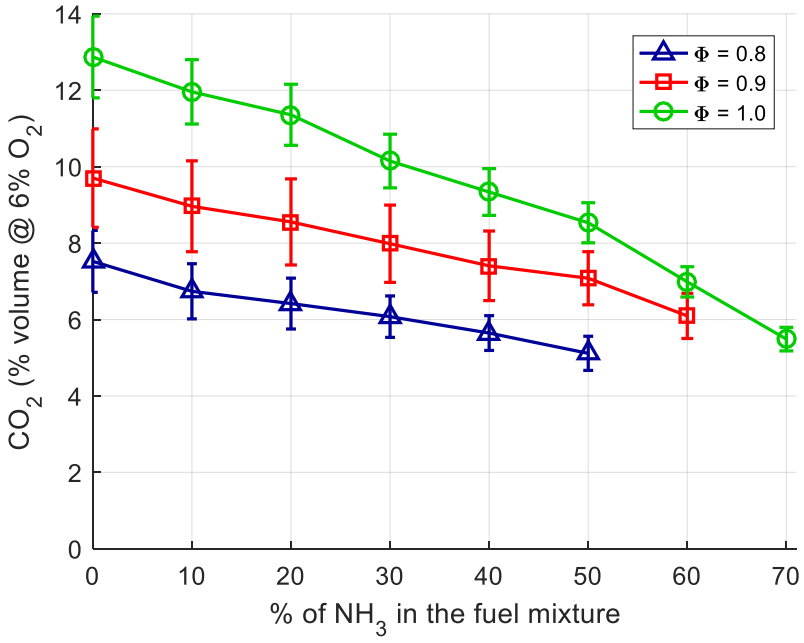


Figure 3.11 - $CO_2$ emissions as a function of the amount of $NH_3$ in the fuel mixture for a thermal input of 300 W.

This may also be the case when comparing the effect of excess air. It was seen that a decrease in the equivalence ratio would result in a rise in temperature profiles. Regarding the $CO_2$ results, as the equivalence ratio decreases, the overall concentration of $CO_2$ in the exhaust also decreases. This is because the amount of air increases, further diluting the products of the combustion. The lower $CO_2$ values would mean less heat lost through radiation, thus explaining the increased temperatures for lower equivalence ratios. Hence, the results are once more in accordance, and this hypothesis may be the reason behind the patterns found.

All curves show a very similar gradient and the uncertainty bars barely overlap adjacent equivalence ratios, indicating a concise spread pattern of the measurements.

Finally, the last species measured was oxygen. Figure 3.12 displays the percentage of $O_2$ in the exhaust gas as a function of the amount of ammonia in the fuel volume, and each curve represents a different equivalence ratio. As a global evaluation, the values for oxygen are barely affected with the differences of ammonia in fuel. This points to an effectively complete combustion, corroborated by the very low results gathered for CO and unburnt $NH_3$. In fact, observing the reproducibility spread of the $O_2$ values, a flat line could more or less fit within the uncertainties of each equivalence ratio.

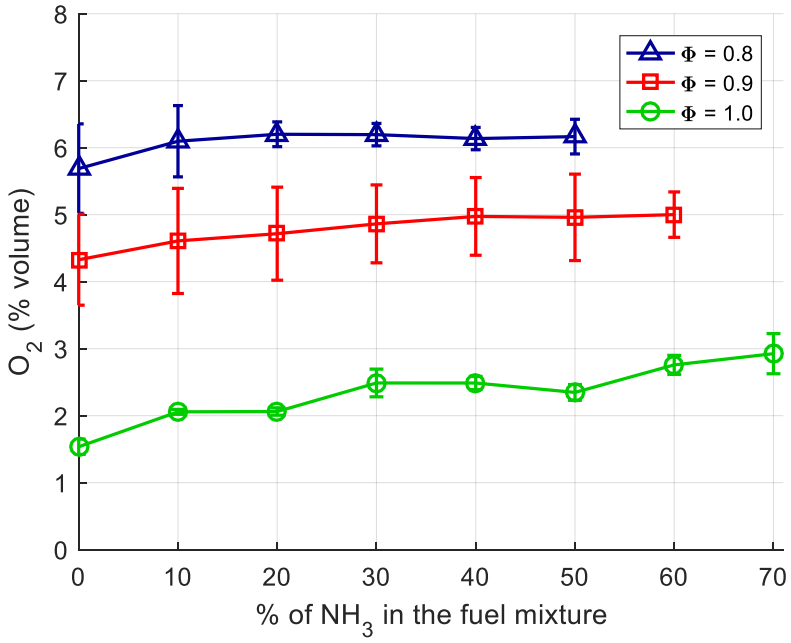


Figure 3.12 - $O_2$ emissions as a function of the amount of $NH_3$ in the fuel mixture for a thermal input of 300 W.

In the end, the results are rather close to what was expected, both prior to the experiments, and after discussing the other results.

The experimental results presented thus far were compared with numerical schemes to assess the quality of the predictions, given the same conditions. As was mentioned before, the mechanisms for the flat-flame installation were the ones from Okafor et al. [43] and Dagaut et al. [35]. Figure 3.13, Figure 3.14 and Figure 3.15 show the results for predicted $NO_x$ and CO emissions for the equivalence ratios of 0.8, 0.9 and 1, respectively, together with the experimental values, as a function of the quantity of $NH_3$ in the fuel mixture.

It can be seen that the $NO_x$ predictions follow the trends of the experimental results, increasing with the rise of ammonia quantity in the fuel mixture, at a progressively slower pace. This fit seems independent of the equivalence ratio and of the mechanism in question, since both are quite close to each other. The only significant difference that can be found regarding the patterns presented is for $\phi$ = 0.8 at 50% of ammonia in the fuel mixture, where the Dagaut mechanism predicts a sharp decrease in the $NO_x$ emissions. On the other hand, the Okafor mechanism still follows the pattern of the experimental values.

Patterns aside, comparing the absolute values predicted by the mechanisms with the experimental results, it can be observed that there is a difference in the scales presented for each. Indeed, the predicted values are always larger than the experimental ones, and the different scales were used for easier comparisons. As a general assessment, the predicted values are more or less double the experimental data. Therefore, although the mechanisms can capture the pattern of the $NO_x$ emissions, improvement is still needed for achieving comparable absolute values.

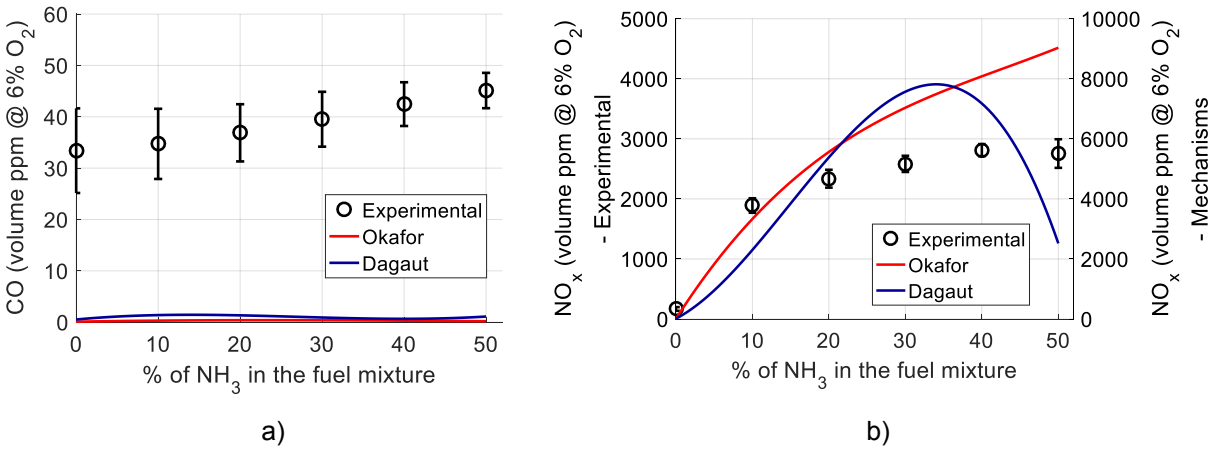


Figure 3.13 - Predictions and experimental data as a function of the amount of $NH_3$ in the fuel mixture for a thermal input of 300 W and $\phi$ = 0.8. a) CO emissions, b) $NO_x$ emissions.

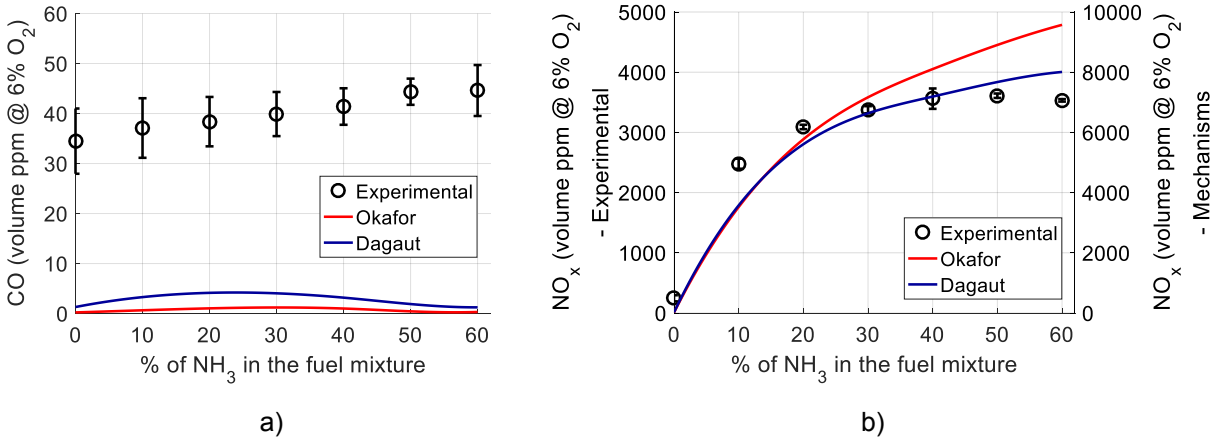


Figure 3.14 - Predictions and experimental data as a function of the amount of $NH_3$ in the fuel mixture for a thermal input of 300 W and $\phi$ = 0.9. a) CO emissions, b) $NO_x$ emissions.

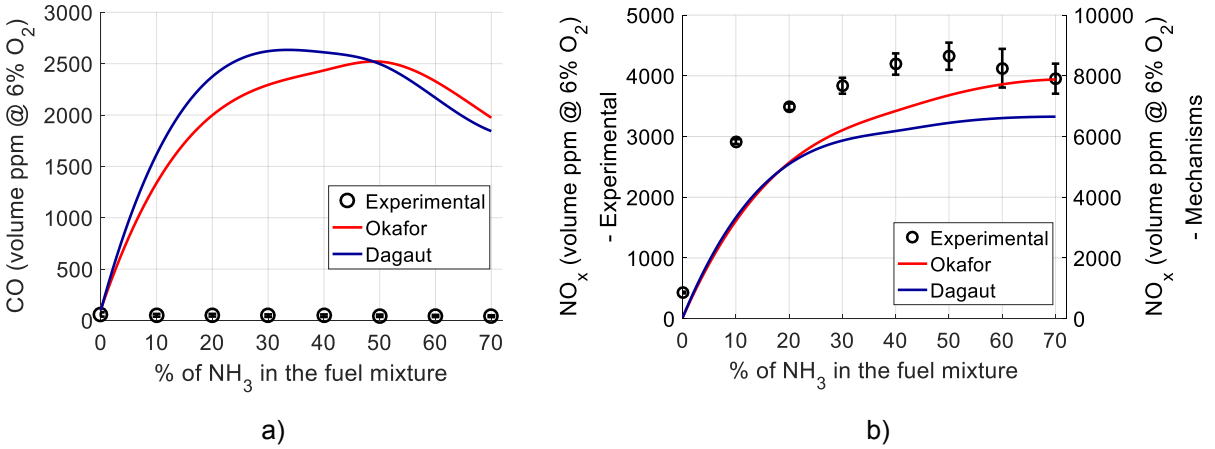


Figure 3.15 - Predictions and experimental data as a function of the amount of $NH_3$ in the fuel mixture for a thermal input of 300 W and $\phi$ = 1. a) CO emissions, b) $NO_x$ emissions.

Regarding the CO numerical results, there is a major difference when comparing the stoichiometric condition with the fuel-lean conditions, especially taking into account that the experimental values are rather low, regardless of equivalence ratio. For $\phi$ = 0.8 and 0.9, the predicted values are very low and

under 3 ppm, regardless of the mechanism. This is in accordance with the complete combustion of the methane present and close to the experimental data. However, for $\phi$ = 1, the numerical results are much higher than the experimental ones, reaching a maximum of around 1800 ppm. Although both mechanisms are close to each other, this is well above the experimental results of under 60 ppm. This over-prediction might be due to the reactions that the numerical simulations consider for stoichiometric conditions, which is the threshold between fuel-rich and fuel-lean. The CO results can have a difference of several orders of magnitude when going from one to the other. Therefore, numerical mechanisms should enhance the predictions of CO for the equivalence ratio of 1.0.

It should be noted that the unburnt ammonia emissions predicted for all conditions by any mechanism are negligible (< $10^{-3}$ ppm), which is in accordance with the experimental results gathered. These very low values were not interesting enough to be graphically represented.

Overall, the mechanisms showed a good fit to the experimental results, and none behaved better over the other, except for an outlier for $\phi$ = 0.8 with 50% of ammonia in the fuel mixture. The patterns seem to be well predicted and consistent. Nevertheless, research is still needed in order to approximate the absolute values of the predictions with the experimental results, so that the remaining discrepancies can be minimized.

## 3.2. Porous-Media Burner

### 3.2.1. Test Conditions

Recalling the literature review conducted in this thesis, porous burners had already shown great potential for burning high amounts of ammonia, even when using hydrogen as second fuel constituent, instead of methane [28]. Preliminary tests ran in the porous-media burner at IST corroborated these findings, as stable flames were achieved for several conditions. Methane/ammonia blends at different equivalence ratios were already the focus of the flat-flame burner. Therefore, the decision was to employ the porous-media setup in the investigation of different fuel blends, i.e. to study the differences between ammonia/hydrogen and ammonia/methane premixed flames burning with air, especially at high ammonia concentrations. The power and equivalence ratio values should be constant to minimize the variables at play. However, the search for these two numbers was difficult, since stable flames of both mixture types should be achievable for a considerable range of ammonia fractions in fuel.

This setup was used previously with power values from 400 W to 2740 W [45]. However, similarly to what was described in 3.1.1, the addition of ammonia easily produced blow-offs at high thermal power values, especially with methane. After testing several power limits for both blends, the value of 1200 W was the highest for which the amount of ammonia in fuel volume could still be above 70%, while maintaining a stable flame. Additionally, a low power value was already the study focus for the flat-flame burner. Thus, it was desirable to study the highest possible power for the porous-media burner, to gather data for a broader spectrum of conditions.

The next step was to find a suitable equivalence ratio that could stabilize flames with high ammonia concentrations, either combined with hydrogen or methane. As referenced previously, toxicity concerns limited the choice up to a maximum of $\phi$ = 1.0. However, that value was not suitable for stabilizing flames which included $H_2$. Hydrogen has a very low minimum ignition energy, about one order of magnitude lower when compared to fuels such as methane and propane [53]. This results in a very reactive combustion. In preliminary tests, flashback would occur, where the premixed flame would migrate upstream, towards the fuel source. The conclusion was that hydrogen combustion should not occur near stoichiometry, it should be more towards fuel-lean, since more air was needed to control the reaction and hold it in place. However, the decrease in equivalence ratio decreases the maximum amount of $NH_3$ that is achievable for both blends. A compromise was made by choosing an equivalence ratio of $\phi$ = 0.8, which is high enough not to hinder the maximum $NH_3$ fraction significantly, and at the same time low enough to not produce flashback, when operating with high amounts of hydrogen.

Methane/ammonia blends proved to be stable for a range of proportions starting in pure methane and ending in almost pure ammonia. However, at percentages of ammonia in fuel volume greater than 80%, ammonia could be detected in the laboratory due to its pungent scent. As a safety measurement, that was set as the maximum allowable amount of ammonia. An identical decision was made for the case of hydrogen/ammonia blends, in which a higher amount of ammonia could also be burned, although it exceeded the same safety concerns. However, for these mixtures a lower safety limit was also needed. The preoccupation in choosing the power and equivalence ratios values was not enough to guarantee combustion of high amounts of hydrogen. It was found that for a hydrogen fraction in fuel above of 50%, flashback would still occur. As a result, a mixture with 50% of ammonia in total fuel volume was chosen as the flame to be studied with the lowest amount of $NH_3$. Table 3.2 summarizes the test conditions of the porous-media burner.

Table 3.2 - Experimental conditions for the porous-media burner.

| Power | Fuel mixture | Ammonia in the fuel mixture (% in volume) |
|---|---|---|
| 1200 W | $NH_3$ - $H_2$ | 50, 60, 70, 80 |
| | $NH_3$ - $CH_4$ | 30, 50, 70, 80 |

The total number of studied flames is 8. Notice that the range of ammonia percentages studied for methane/ammonia blends is more spread-out, with the intent of measuring the emission patterns over a wider range of proportions.

Once again, an Excel spreadsheet was used to translate the input of power, equivalence ratio and ammonia fraction into the values to be inserted in the flow controllers. This made certain that the gas injections matched the desired conditions.

### 3.2.2. Temperature

The flames studied in this installation are not observable as in the flat-flame burner. However, due to the porosity structure of the burner, it is easy to conclude that they possess a rather complex and tri-dimensional shape. On the other hand, the thermocouples are placed along the vertical axis of the burner. Therefore, it must be taken into account that, in reality, there are horizontal temperature gradients that cannot be measured by the thermocouples. As a result, measured temperatures are only an approximation of the values that can be found for each horizontal plane where each probe is positioned. With that observation in mind, Figure 3.16 and Figure 3.17 show the temperature profiles of the flames studied in the porous-media, for ammonia/methane and ammonia/hydrogen blends, respectively. The temperatures are shown as a function of axial distance, where each curve represents different proportions of the constituents in the fuel.

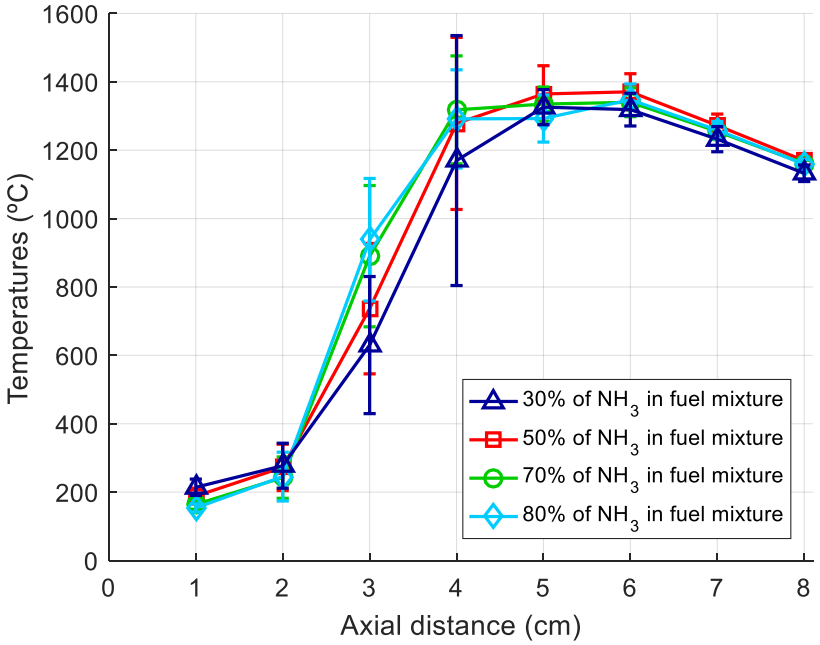


Figure 3.16 - Axial temperature for $NH_3$-$CH_4$ fuel mixtures with a thermal input of 1200 W and $\phi$ = 0.8.

For the $NH_3$-$CH_4$ mixtures, regardless of the amount of ammonia in fuel, between the first thermocouples there is a very low temperature gradient. However, moving upwards, there is a steep rise in temperature between second and fourth. This increase is slower from then on and a peak in temperatures is obtained between fifth and sixth thermocouples, for values of around 1350 °C. From that point upwards, the temperatures decrease, slowly and steadily.

From this pattern, some conclusions can already be drawn. Firstly, the flame front is located between the fifth and sixth thermocouples, where the temperature reaches its peak. The decay of temperature downstream is consistent with post-combustion heat loss. Additionally, there is a “zone of influence” upstream, where the combustion starts taking place, responsible for the steep temperature gradients found. It is also the region where the uncertainties are considerably larger than the rest. The reasoning

behind this is that, across several repetitions, the flame moved either down or upstream. Since this is an area where temperatures vary greatly with the vertical coordinate, even a slight drift of the flame front originates high fluctuations, which results in a larger spread of the values reflected by the reproducibility uncertainty. The rest of the uncertainties are considerably tighter, since temperature gradients in those positions are much lower. Moving more towards the pre-mixture source, this zone of influence fades away, as the temperatures and gradients are much lower.

One thing worth mentioning is the fact that this pattern seems mostly independent of the proportions of ammonia in fuel. Although there may appear to be some distinguishable patterns, it is clear that the curves are always so close that all uncertainties overlap. Therefore, no conclusions should be made regarding the influence of varying ammonia in the temperatures of these blends.

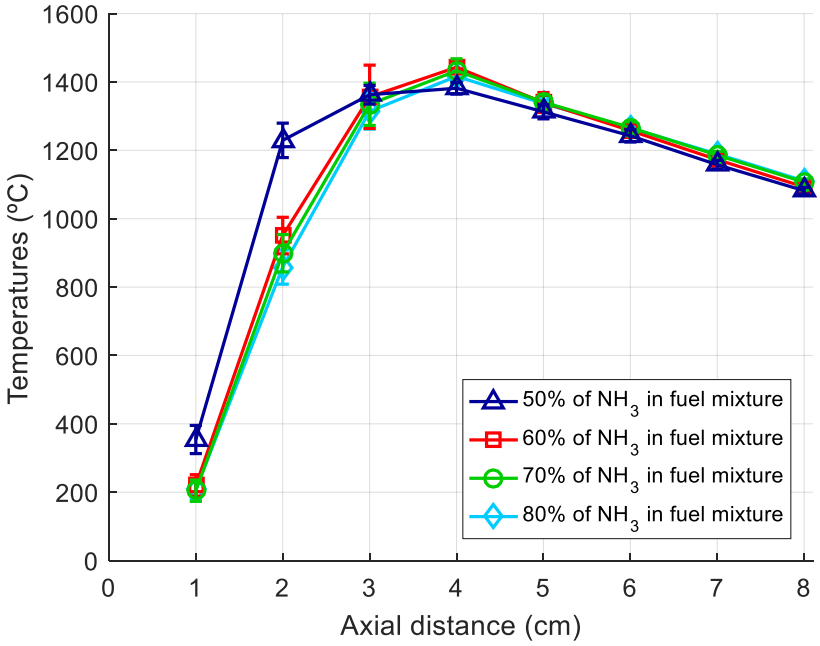


Figure 3.17 - Axial temperature for $NH_3$-$H_2$ fuel mixtures with a thermal input of 1200 W and $\phi$ = 0.8.

Observing the temperatures for the $NH_3$-$H_2$ blends in Figure 3.17, it can be seen that the patterns are close to the previous graph, albeit is starts immediately with a rather high temperature gradient. The values peak around the fourth thermocouple, at temperatures in the vicinity of 1400 °C. This is where supposedly the flame fronts rests. Afterwards, heat losses dictate the decrease in temperatures.

A clear difference for this graph is that the curve with 50% of ammonia in volume is clearly set apart from the rest: the temperatures seem shifted to the left. This should be due to the high energy density of hydrogen and the fact that this condition has the highest $H_2$ quantity. As was explained in section 3.2.1, this condition was set as the lower limit of ammonia quantity because of the reactivity of $H_2$. During the experimental procedures, this already proved to be a difficult fuel composition to maintain, since even the smallest deviation in the proportions could lead to the beginning of a flashback. Thus, these temperatures represent that same behaviour, as the flame shifts downstream with the increased presence of hydrogen. Additionally, the peak for this curve is neither as high nor as well-defined as the

rest. Indeed, the flame appears to be more spread out, reducing the spatial concentration of the chemical reactions and, thus, resulting in a lower maximum value.

As with the rest of the conditions, the results are very close to one another and the uncertainties overlap. Therefore, no objective conclusions can be drawn, except that the temperatures seem independent of the amount of ammonia in the mixture.

On another note, all reproducibility uncertainties are rather constricted, even in the region with high temperature gradients. This is in contrast with the $NH_3$-$CH_4$ mixtures.

The gathered data can be shown in a different manner to compare how different fuel constituents affect temperatures. Figure 3.18 represents the temperature as a function of axial distance for 2 flames with 70% of $NH_3$ in the fuel mixture, where each curve represents either the $NH_3$-$CH_4$ or the $NH_3$-$H_2$ blend. Note that, although the only shown condition is with 70% of ammonia in the fuel mixture, due to low variability of the temperatures, the comparisons between blends are very similar for 50% and 80% of ammonia.

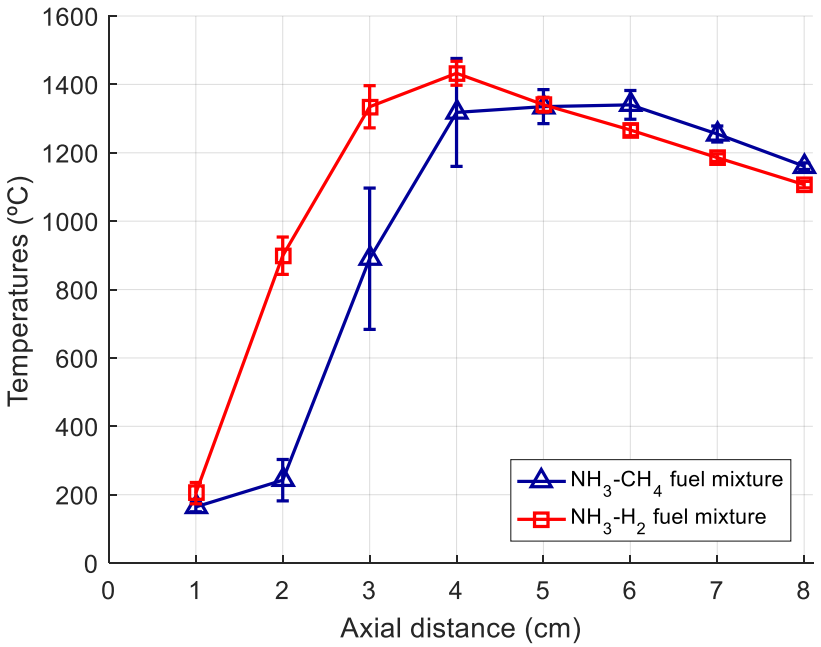


Figure 3.18 - Axial temperature for 70% of $NH_3$ in the fuel mixture with a thermal input of 1200 W and $\phi$ = 0.8.

Observing Figure 3.18, it is clear that the two main differences seem to be the flame position and the maximum value. As was mentioned before, hydrogen mixtures are more reactive and tend to induce flashback. Thus, this explains why the region with high temperature gradient and the flame front (peak) for this mixture are set more upstream. Regarding the differences in maximum values, although the power set for both mixtures is both constant and the same, methane and hydrogen have a great difference regarding its products: hydrogen does not produce carbon-dioxide. Therefore, the difference in the emissivity of the exhaust gases will be significantly lower for hydrogen/ammonia blends, when

comparing to methane/ammonia. Thus, for hydrogen mixtures, the heat loss through radiation should be considerably less, thus explaining the measured temperature differences.

As a final note to Figure 3.18, it is also worth mentioning that the recorded temperature patterns closely resemble the results of other studies conducted in this same burner [44], [45]. Therefore, the behaviour of the temperatures along the vertical axis seems to be more or less consistent across different fuels.

Similar to the process for the flat-flame burner, the temperatures measured in the porous-media burner were implemented in the Cantera code, to serve as a basis for the predictions of the gas species. However, since these temperatures profiles include the complete flame, there is no need to predict other virtual measurements. Therefore, the experimental temperature results serve as a direct input to the code. Figure 3.19 presents an example of the temperatures for the numerical simulation, which corresponds to a $NH_3$-$CH_4$ fuel mixture with 50% of ammonia in the fuel mixture.

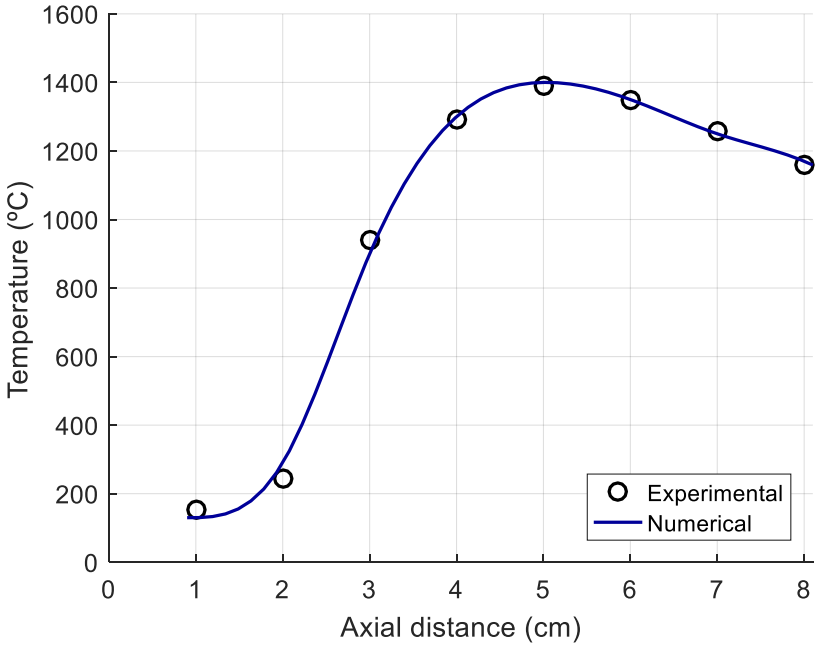


Figure 3.19 - Axial temperature profile used in Cantera, and the corresponding experimental values for a fuel mixture with 50% of $NH_3$ with a thermal input of 1200 W and at $\phi$ = 0.8.

As can be observed, the numerical temperatures almost completely resemble the experimental ones, smoothening the connections between results to achieve a valid profile. However, for convergence purposes, the code executes some small deviations from the experimental results. This procedure is the same for all the numerical simulations performed.

### 3.2.3. Gas Species Concentration

The same two measuring methods applied in the flat burner were also used in the porous-media. The sampling probe was positioned facing 20 cm away from the top of the porous core. Note that the

following results for all gas species concentrations – both experimental and numerical – are corrected for 6% of $O_2$ (with the exception of oxygen itself).

Figure 3.20 shows the concentrations of $NO_x$ as a function of ammonia in the fuel mixture. Each curve represents a different combination of fuel constituents.

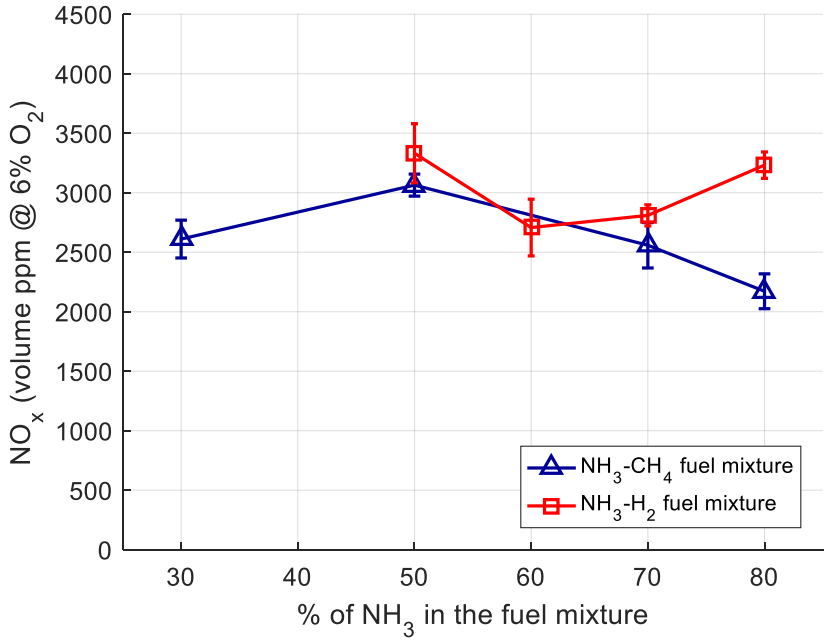


Figure 3.20 - $NO_x$ emissions as a function of the $NH_3$ in the fuel mixture, for $NH_3$-$CH_4$ and $NH_3$-$H_2$ mixtures, for thermal inputs of 1200 W and in $\phi$ = 0.8.

For ammonia/methane blends, there is no data for values lower than 30% of $NH_3$ in fuel because the concentrations of species for mixtures with high methane content had already been studied in the flat-flame burner. Moreover, due to the limitations expressed in 3.2.1, the profile obtained for the ammonia/hydrogen is shorter than the one of ammonia/methane. Nevertheless, contrasts are still easily found between the two types of mixtures.

For $NH_3$-$CH_4$, the $NO_x$ pattern should, presumably, start very low when only methane is present. As ammonia is gradually introduced, a maximum value can be seen in the graph for 50% $NH_3$ in fuel, to which corresponds approximately 3100 ppm vol. of $NO_x$ in the exhaust gases. From then forth, the values start to decline. This pattern fits closely to the ones found in the literature [25], [26], which were already discussed for the flat flame results. Thus, the trend seems to be consistent. Finally, the low reproducibility uncertainties point towards consistent results.

The $NO_x$ results have a different arrangement for the $NH_3$-$H_2$ blends, although they are definitely close to the values for $NH_3$-$CH_4$. A maximum of around 3400 ppm is found for the initial condition with 50% of ammonia in fuel. The values decrease to around 2700 ppm for 60% of $NH_3$ and barely rise for the following condition. However, this small increase continues, and for the final fuel constitution with 80% of ammonia, the values rise to about 3200 ppm.

Contrasting the $NO_x$ pattern for $NH_3$-$H_2$ with data from the literature, such as Figure 1.7, does not allow for extensive comparisons, since the range of $\%NH_3$ in fuel measured is shorter. Nevertheless, these literature results are within the same order of magnitude as the measurements, taking into account that $10^{-3}$ in mole fraction equals 1000 ppm vol.

Both $NO_x$ patterns should once again be related with the quantity of unburnt ammonia, since reactions between these species significantly alter their concentration at the exhaust. To assess $NH_3$ concentrations post-combustion, the GASTEC detector tubes were employed. In contrast with the measurements made for the flat-flame burner, in this case the results were conclusive and quantifiable, as they fitted within the measuring range. Figure 3.21 shows the values gathered for unburnt ammonia at the exhaust as a function of the quantity of $NH_3$ in the fuel mixture, for both types of fuel blends.

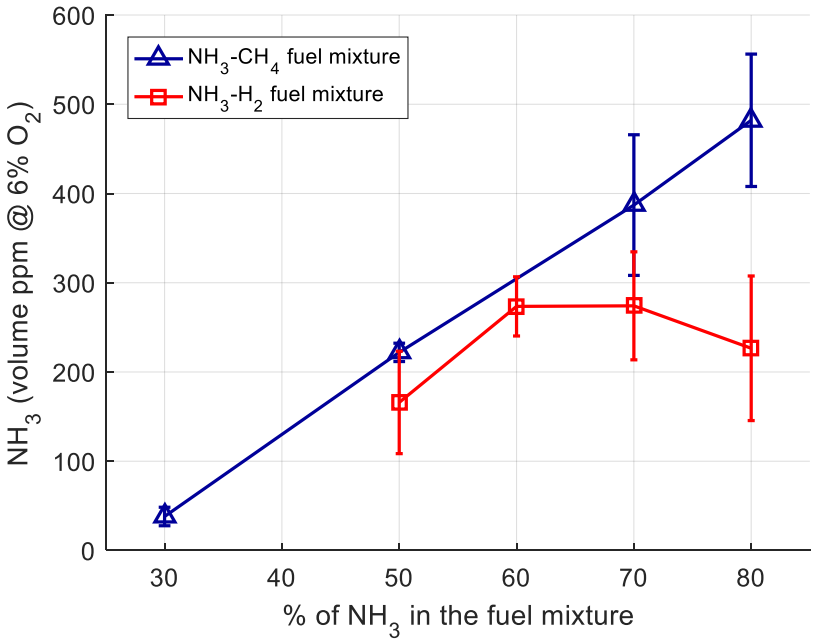


Figure 3.21 - $NH_3$ emissions as a function of the $NH_3$ in the fuel mixture, for $NH_3$-$CH_4$ and $NH_3$-$H_2$ mixtures, for thermal inputs of 1200 W and in $\phi$ = 0.8.

As an overall observation, it can be seen that the results are all below 500 ppm and that the $NH_3$-$H_2$ blends have less unburnt ammonia at the exhaust, which points to a more complete combustion of $NH_3$.

For $NH_3$-$CH_4$ blends, the pattern of unburnt ammonia follows almost a linear proportionality, maxing at around 480 ppm vol. for 80% of $NH_3$. As the authors of [25] and [26] mentioned, this should be the reason behind the $NO_x$ pattern: the gradual increase of ammonia in the flame is not completely combusted, and the increasing amount of $NH_3$ at the exhaust starts reacting with the $NO_x$ at a significant rate, explaining the decay of the $NO_x$ curve after around 50% of ammonia in fuel volume.

The same may happen for the $NH_3$-$H_2$ blends, although at a reduced rate. Comparing with $NH_3$-$CH_4$ for the same $\%NH_3$ in the fuel mixture, since less ammonia is present in the flue gases, there is less reduction of $NO_x$, which explains why the $NO_x$ results for the hydrogen blends were mostly higher.

The conclusion to take from the these results is that, at higher powers, the $NH_3$ and $NO_x$ emissions must be balanced: optimum ammonia combustion with low $NO_x$ may occur for high amount of ammonia in the fuel mixture, but, in these conditions, $NH_3$ emissions start being significant and warrant treatment.

The CO concentrations are once again measured to assess the combustion of the hydrocarbons. Figure 3.22 shows the CO emissions as a function of the quantity of ammonia in the fuel mixture, where each curve represents a different combination of fuel constituents.

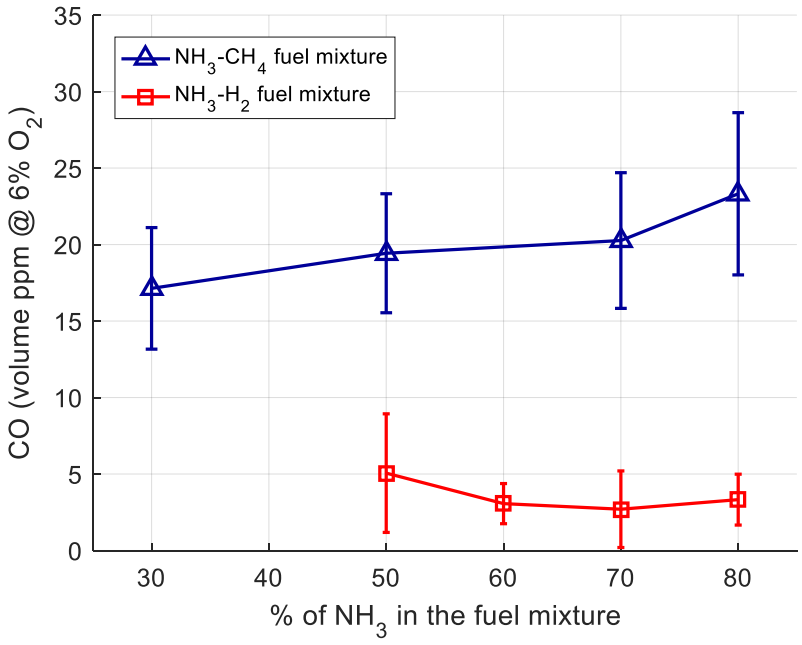


Figure 3.22 - CO emissions as a function of the $NH_3$ in the fuel mixture, for $NH_3$-$CH_4$ and $NH_3$-$H_2$ mixtures, for thermal inputs of 1200 W and in $\phi$ = 0.8.

The values obtained are rather low, with the averages being under 25 ppm vol. This points to a complete combustion of the methane in $NH_3$-$CH_4$ blends. Note that the values for hydrogen blends are not null, although no CO should be present. Nevertheless, they are under the detection threshold of the analyser. Therefore, these numbers just represent a background noise in the signal.

Remounting to the temperature results of this installation, it was previously theorized that the differences in maximum values between $NH_3$-$CH_4$ and $NH_3$-$H_2$ could be due to contrasting emissivity of the flue gases from one mixture to the other. It is therefore important to analyse the $CO_2$ emissions. Figure 3.23 displays the $CO_2$ concentrations as a function of the percentage of ammonia in the fuel mixture. The results for methane/ammonia are within expected, reducing the $CO_2$ concentration as ammonia in fuel increases due to less methane being burned. Additionally, the values gathered for hydrogen/ammonia blends are also the predicted: since no carbon is present in the mixture, the $CO_2$ concentration is null. These results corroborate the aforementioned hypothesis. Since the $CO_2$ concentrations for $NH_3$-$H_2$ mixtures are significantly inferior, this means the emissivity of the exhaust gas is also considerably smaller, thus having a reduced radiative heat loss. Therefore, these results are in accordance to the higher maximum temperatures found for hydrogen/ammonia mixtures.

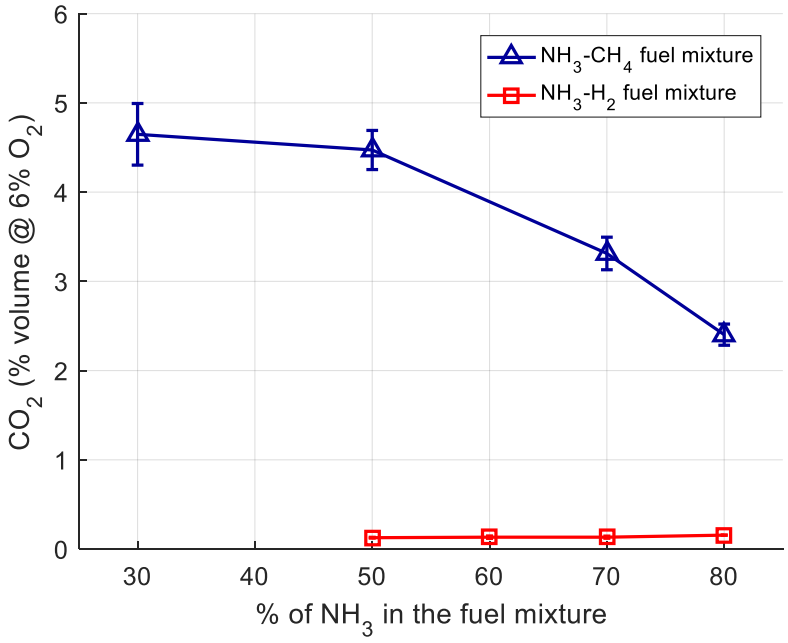


Figure 3.23 - $CO_2$ emissions as a function of the $NH_3$ in the fuel mixture, for $NH_3$-$CH_4$ and $NH_3$-$H_2$ mixtures, for thermal inputs of 1200 W and in $\phi$ = 0.8.

The final gas concentration measured was for oxygen. Figure 3.24 shows the $O_2$ concentrations as a function of the quantity of ammonia in the fuel mixture.

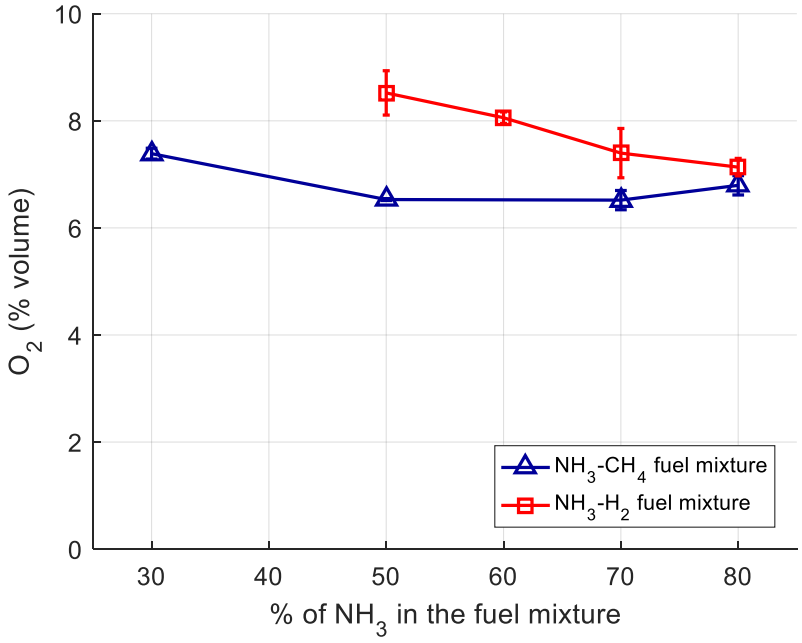


Figure 3.24 - $O_2$ emissions as a function of the $NH_3$ in the fuel mixture, for $NH_3$-$CH_4$ and $NH_3$-$H_2$ mixtures, for thermal inputs of 1200 W and in $\phi$ = 0.8.

These values are within expected regarding the stoichiometry involved and previously discussed results, which points towards a correct use of the desired equivalence ratios.

Similar to the work discussed for the previous installation, the experimental results gathered so far were compared with numerical simulations to understand if the gas species concentrations are well predicted. The mechanisms used for the porous-media burner were the ones by Okafor et al. [43] and Tian et al. [40]. Figure 3.25 and Figure 3.26 show the results of predicted $NO_x$ and CO emissions, for $NH_3$-$CH_4$ and $NH_3$-$H_2$, respectively, together with the experimental values, as a function of the quantity of $NH_3$ in the fuel mixture.

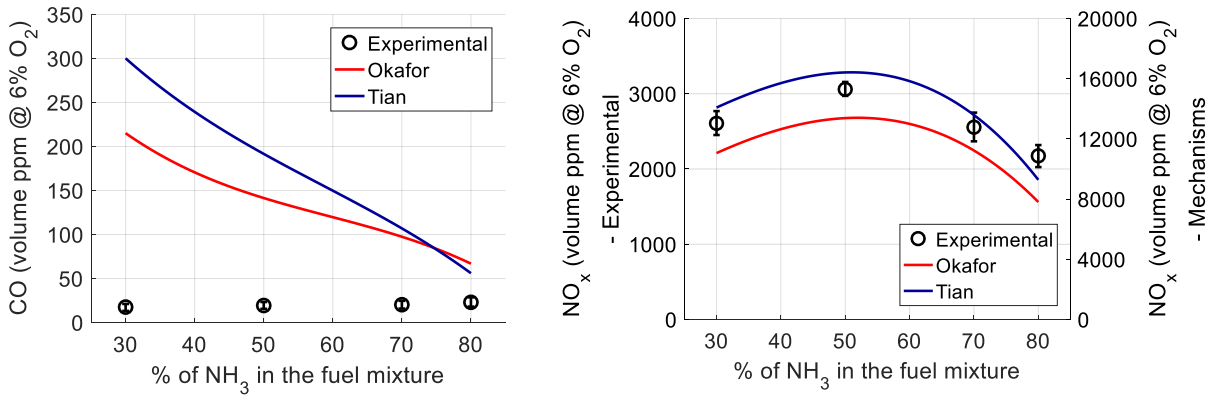


Figure 3.25 - Predictions and experimental data as a function of the amount of $NH_3$ in the $NH_3$-$CH_4$ mixture for a thermal input of 1200 W and $\phi$ = 0.8. a) CO emissions, b) $NO_x$ emissions.

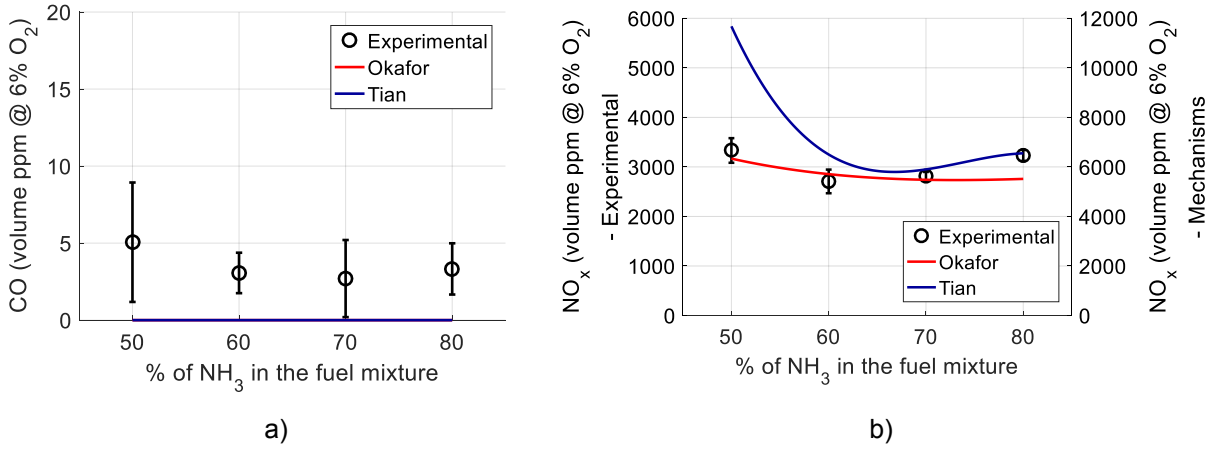


Figure 3.26 - Predictions and experimental data as a function of the amount of $NH_3$ in the $NH_3$-$H_2$ mixture for a thermal input of 1200 W and $\phi$ = 0.8. a) CO emissions, b) $NO_x$ emissions.

The numerical results for $NO_x$ emissions for the $NH_3$-$CH_4$ fuel mixtures seem to capture the experimental patterns rather well, and the monotony is consistent for both mechanisms. However, comparing the scales of the experimental measurements, the numerical data over-predicts the experimental one by more than 300%, although the differences are smaller for the Okafor model. Bearing in mind that the Okafor scheme is based off of Tian's, some improvement can be observed regarding the magnitude of the results. Moving the focus to the $NO_x$ predictions of the $NH_3$-$H_2$ fuel mixture, it can be observed that the mechanisms adopt a different relationship with the experimental data. The absolute differences are smaller than previously. Okafor's model has a good fit with the experimental results in terms of capturing the overall pattern, although there is an over-prediction of around 100%. Tian's model over-predicts the

experimental data a bit more, with emphasis on the condition of 50% of ammonia in the fuel mixture. Once again, the Okafor model demonstrates an improvement over the predecessor, both in terms of absolute differences and fitting to experimental patterns.

Regarding the numerical prediction of the CO concentrations, both mechanisms behaved similarly. For methane-ammonia blends, the models over-predicted the experimental results, although the maximum values did not exceed around 250 ppm. For Okafor they were even lower, showing an improvement over Tian once more. Additionally, the mechanisms showed a pattern consistent with the progressive withdrawal of methane from the fuel mixture. For hydrogen-ammonia blends, the simulations appear to under-predict the experimental data, resulting in values of less than 1 ppm vol. Nevertheless, the experimental values were regarded as background noise, as they were below the detection threshold of the analyser. Therefore, both experimental and numerical results agree that there is no carbon-monoxide in this scenario. Overall, the CO results are consistent with the experimental condition of a fuel-lean equivalence ration of 0.8.

It should be noted that the numerical results for unburnt $NH_3$ were negligible (< $10^{-2}$ ppm), regardless of the condition in question and mechanism, which is why they were not considered relevant enough to warrant a dedicated graph. These predictions are in contrast with the maximum experimental results for ammonia in the exhaust of around 500 ppm (for $NH_3$-$CH_4$). Therefore, some improvement is needed in the prediction of these traces.

## 3.3. The Path for an Ammonia-Based Economy

The research conducted in this thesis has focused on investigating properties of the combustion of ammonia and its mixtures with methane and hydrogen. The influence of several variables has been discussed, assessing how each one contributes to the formation and emission of pollutants. The conclusion was that optimum ammonia combustion with low $NO_x$ emissions occurs for low equivalence ratios and for high percentages of ammonia in the fuel mixture. However, this may also result in unburnt $NH_3$, when at higher powers. Therefore, these emissions must be balanced. The results were juxtaposed with numerical mechanisms, to assess the quality of the predictions and the improvements that are needed for refining the models. The simulations captured the overall emission patterns but failed to meet the values portrayed by the experimental work.

These results can now be contrasted with the present reality. As was mentioned in the beginning of this work, the focus has been to provide information on the underlying concepts of burning $NH_3$ as fuel. Therefore, the end goal is to introduce ammonia as a clean fuel alternative, capable of answering the urging necessity of reducing carbon pollution, while allowing for the fulfilment of the ever-rising global energetic needs. However, before ammonia can evolve from being considered just a potential alternative to actually being deployed in real-world scenarios, many aspects have to be researched and developed. This necessity is true both for fundamental studies and for practical settings. As an example, the mechanisms behind the release of $NO_x$ and/or unburnt $NH_3$ have to be fully understood and controlled, or else the use of ammonia merely implies trading one type of pollutants for others.

In present times, carbon-based pollution is liberated from many types of processes, spread throughout different sectors. Therefore, to gauge the potential of ammonia in substituting conventional fuels across several areas, it is important to understand how pollution is emitted in each sector of society. In doing so, research efforts can be guided for each specific scenario. Davis et al. [54] have analysed the major $CO_2$ emitting sectors and have divided them in two classes. The first is related to areas that should be relatively easier to decarbonize in the following decades. This includes the following:

- Light-duty transportation;
- Heating, cooling and lighting;
- Residential and commercial sector;
- Electricity (consistent).

The first three areas are being actively developed to implement (or have implemented already) electricity as the main source of energy, e.g. the advent of electric cars. Nevertheless, electricity itself is responsible for a significant amount of carbon-pollution. Therefore, a sustainable chain can be created where electricity is obtained from a varying mix of renewable energy sources, fuels that do not contain carbon, or, at the very least, non-renewable sources that can be introduced in a circuit with net-zero carbon emissions (e.g. nuclear power). On the other hand, [54] refers to a second group of sectors that are difficult to decarbonize, due to the inherent dependence on carbon-based fuels. Therefore, these areas should be the focus of the most crucial changes in the underlying power generation systems. They include:

- Aviation, long-distance transport, shipping;
- Production of carbon-intensive structural materials (e.g. steel, cement);
- Provision of reliable electricity supply for varying demand.

The sector involving aviation, long-distance transport and shipping is dependent on cheap, mobile energy sources that answer to weight and volume constraints for profitability. Batteries carry both products and reagents, which, from a weight/performance point of view, cannot match an oxidizing fuel that liberates the products into the atmosphere, reducing the weight along the trip. Additionally, electrified motor systems cannot compete against the ranges and refuel times that conventional motors offer, which is a relevant aspect when accounting for the strict schedules that characterize this sector. Although the growing trend of electricity-based light-transportation is evolving at a steady place, the freight industry will still rely heavily on energy-dense liquid fuels for quite a long time, which is why carbon-based fuels are still the major energy source for these services, by a great margin.

On the other hand, structural materials production is also hard to decarbonize, but not because of the fuels used in the industry, since the furnaces employed and the rest of the infrastructure can be electrified. It is due to the manufacturing of these products, in which the materials themselves release $CO_2$ due to the processes utilized. The solution should be to fundamentally alter the production process, or incur in minimizing carbon-pollution by diverting the resultant gases to other ends.

Finally, the last aspect considered difficult to decarbonize is the availability of a reliable electricity supply. Consistent electricity use can be effectively independent of fuel consumption, by resourcing to major renewable energies, like hydric power plants and windfarms. However, the extremely varying demand of electricity across days or seasons is currently being accommodated by the use of fossil fuels, due to their prompt availability and readiness of deployment.

Taking into account the wide spectrum of pollution-emitting services, ammonia has the potential to be implemented into a mixture of power sources that can answer the energetic needs of these sectors while inhibiting $CO_2$ emissions. In fact, the prolific research on ammonia as a source for power that are currently being developed [31] may pave the path for an ammonia-based economy, based in close symbioses between several processes in different sectors, in a sustainable manner. To envision this possibility, an example of such system is presented in Figure 3.27 and hereby discussed.

For ammonia to be considered a clean fuel, carbon-pollution must be withdrawn at the very start. The Haber-Bosch process is the main ammonia production process, where nitrogen and hydrogen are combined in a catalytic medium to synthesize $NH_3$. Although $N_2$ is captured from air, $H_2$ comes mostly from steam reforming of natural gas (or other carbon-fuels), which releases carbon-dioxide. To counter this, the process can include carbon capture and storage (CCS), which renders the production process $CO_2$ neutral [55]. Additionally, aqueous ammonia can be used to capture $CO_2$ from other sources in a standalone system with high efficiency and low investment [56]. This opens the doors to the overall reduction of carbon-pollution emanating from other industry sectors, facilitating net-zero systems. The captured carbon can then be implemented in the creation of synthetic hydrocarbons [54], which can be used in many applications, even in a dual-fuel approach, when ammonia alone is not suitable. Additionally, they can be employed in the production of ammonia, thus closing the circle.

On the other hand, ammonia production can be integrated with several renewable energy sources. Bicer et al. [8] demonstrated the feasibility of producing ammonia from biomass, municipal waste and hydropower. In addition, there have been successful studies were ammonia is synthesized purely from wet air, resourcing to solar/photovoltaic and wind to power the process [7], [57].

As an answer to the carbon-pollution inherent to the manufacture of structural materials, a sustainable system can be implemented between the steel industry and ammonia production. Ammonia is a known by-product of steel manufacturing plants [31], which can then be purified or used as a CCS system to reduce the amount of $CO_2$ being emitted.

It should also be taken into account that ammonia has been used for more than a century, although with other goals, such as a fertilizer, chemical feedstock and a refrigerant [8]. This existing infrastructure is of utmost importance, since it means there is already plenty experience in the production, handling and storage of ammonia. This is a necessary factor for accelerating the introduction of the chemical in any sector.

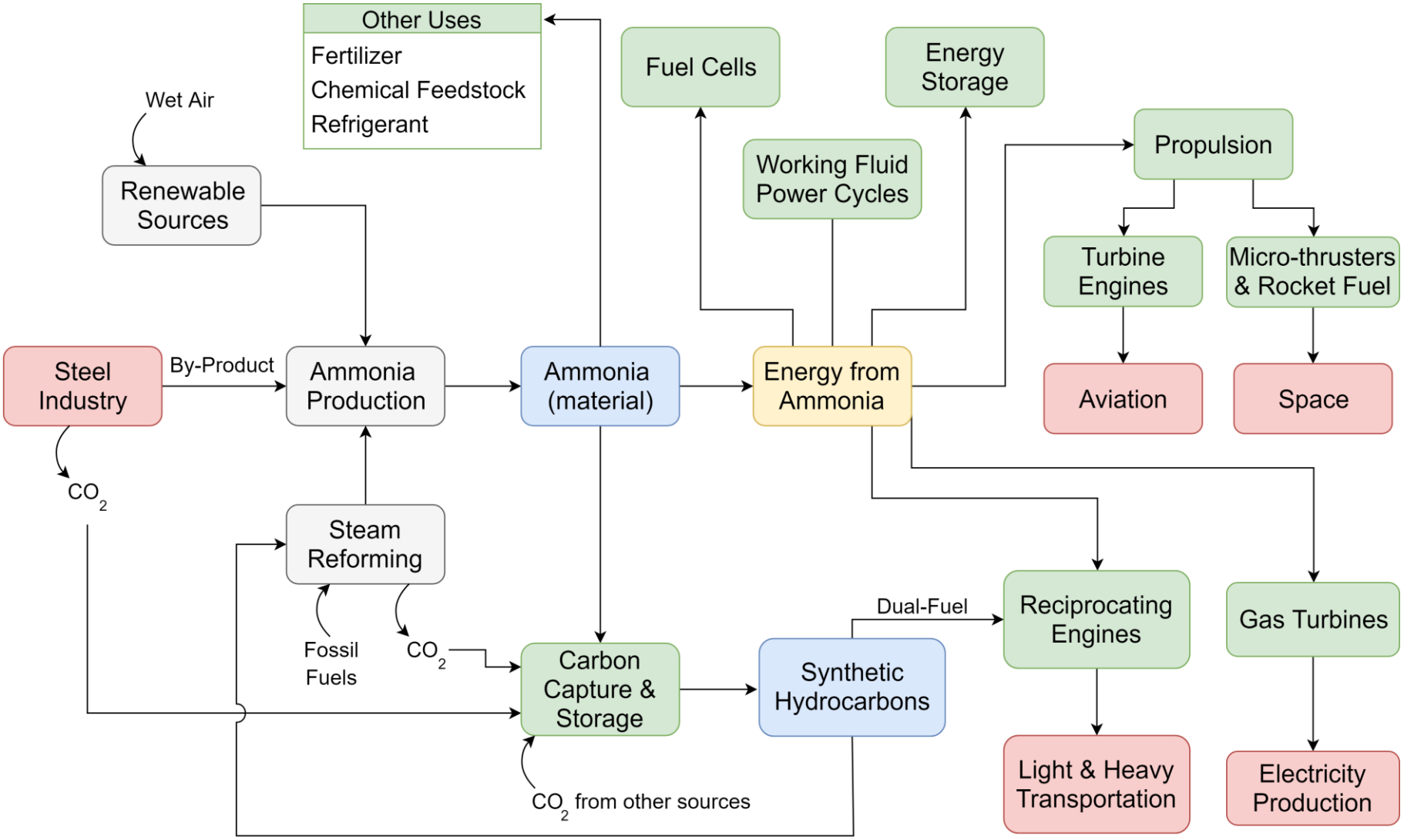


Figure 3.27 - Representation of a future ammonia-based economy with interconnected products and processes. Red - industry sectors; blue - fuels; grey - ammonia production; green - applications of ammonia.

Additionally, long-range ammonia pipelines are already available (in Europe and America), which are able to efficiently supply high quantities of the substance [8]. It can also be transported in existent pipelines for natural gas and oil with minimum modifications, which would result in a higher energy exchange due to different volumetric densities [8]. Thus, ammonia can easily be available anywhere in the world, without the need of expensive transportation.

With this potential in mind, one can envision how a wide spread use of ammonia for power generation could take place. Ammonia can be used as a liquid fuel in reciprocating engines for light- and heavy-duty transportation, as its energy density and performance metrics render it a viable alternative to gasoline and diesel. Some examples of these technologies were discussed previously [5], [6]. It can also be implemented in the production of electricity through the use of gas turbines [25]. In such scenario, renewable energy sources like hydropower, solar and wind would be in charge of minimum constant electricity supply, while ammonia could be used to manage the oscillations of energy demand throughout the days and seasons, thus ensuring a reliable and mixed electricity supply.

Regarding the aerospace industry, ammonia could also be used for propulsion purposes. In the aviation sector, ammonia-powered turbine engines can relieve the dependence on hydrocarbons, thus contributing to lower carbon-emissions of this sector, which was considered difficult to decarbonize [54]. For space applications, ammonia can be employed in micro-thrusters, for satellite control, or as a rocket fuel for spacecraft operation. A great example of this is the X-15 concept aircraft, which used a $NH_3$-LOX (liquid oxygen) rocket engine and set unofficial speed and altitude records in the 1960s [58].

Ammonia can also be directly used in fuel cells, and research has pointed out that cracking ammonia to use the resultant hydrogen is simpler than using $H_2$ directly, due to the differences with handling and storing precautions [59]. Furthermore, $NH_3$ can be used as a working fluid in power cycles [31]. Finally, ammonia can simply be used as an energy vector, facilitating the storage and exchange of energy across remote locations [8].

It should be taken into account that all of these possibilities may grow symbiotic relationships dependent on the scenario. Thus, ammonia can be used as fuel and refrigerant at the same time. This is the case of the X-15 example, in which the aircraft has a feeding system capable of diverting the $NH_3$ to be used as a fuel and to cool the exhaust of the engine simultaneously.

Another example could be of a remote location with no power grid. Ammonia could be transported to the designated place and have several uses. It could be employed to supply electricity through fuel cells, to fuel reciprocating engines for transportation and to supply cooling and heating through power cycles. Examples like this illustrate how ammonia can be regarded as a flexible substitute for hydrocarbons, while eliminating the $CO_2$ sources that were discriminated before.

In the end, the vision illustrated in Figure 3.27 is merely a representation of how the implementation of a sustainable fuel could shape the future of the energy industry. Nevertheless, the infrastructures that define these sectors are subject to slow-changes, which are more incremental than evolutionary. Therefore, there is great emergency in implementing sustainable projects that are not short-sighted:

they should focus not only in the problems of today, but also in those of tomorrow. The possible widespread use of ammonia as an energy source is a very serious contender in that regard.

It is hoped that the results provided in this work are able to be of assistance in this search to use ammonia as a viable alternative to carbon-based fuels. Experimental results on emissions – like the ones presented in this thesis – are of utmost importance to improve numerical tools, so that they are able to correctly predict the properties of ammonia combustion across a range of conditions. This contributes to a gradual development of cost-effective manners to assess the characteristics of future reactors, so that they may be optimal in maximizing efficiency and minimizing emissions. With that objective in mind, the following decades may give way to a significant change in the management of energy resources, so that ammonia may finally be regarded as an important player in the energy sector, capable of supporting a sustainable and carbon-free society.

# 4. Closure

## 4.1. Conclusions

It is widely known that the fossil fuels that supply most of the useful energy to our society also represent a great danger to the environment, especially bearing in mind that their combustion accounts for the majority of the energy production processes. As the supply demands grow larger, so does the necessity of decreasing the global pollution levels.

The use of ammonia as a fuel has been gathering attention due to its high potential of supplying carbon-free energy through a multitude of processes, especially combustion. However, research on the matter has not matured yet, and little data exists on the emissions of nitrogen-pollutants, namely nitrogen oxides ($NO_x$).

Therefore, the motivation behind the present work was to characterize the combustion of ammonia and its mixtures with methane and hydrogen in terms of pollutant emissions, in order to understand the fundamental reactions that occur, so that technologies could be developed to suppress polluting emissions. This information is also important for the validation of computational work.

This evaluation was conducted in two types of burners, assessing the impact of several variables on the combustion of ammonia. A fuel mixture of ammonia and methane, together with air, was employed in a flat-flame burner, which was used to gauge the effect of different equivalence ratios and of a varying percentage of ammonia in the fuel mixture. Additionally, a porous-media burner was used in the air-firing of methane-ammonia and hydrogen-ammonia fuel blends, to measure the influence of different fuel constituents, while also assessing the impact of changing the ammonia proportions for each mixture. Temperature and gas species concentration measurements were taken for each scenario, and compared with recent numerical models that were developed specifically for burning ammonia.

Temperature results for the flat-flame burner were quite interesting, since the increase of amount of $NH_3$ in the fuel mixture lead to a rise in temperatures, defying the norm. A similar contradiction was also found for the decrease of equivalence ratio, which also increased the temperatures. These patterns were concise and repeatable, which points to a certain mechanism between both fuel constituents, methane and ammonia, that was more complex than initially thought. The supposition presented argues that the decrease of carbon-dioxide in the exhaust, that occurs when methane is withdrawn and ammonia is added, significantly lowers the emissivity of the flue gases, thus reducing the heat lost through radiation and promoting a rise in temperatures.

Gas emissions for the flat-burner pointed towards a complete combustion of both fuel constituents. $NH_3$ values at the exhaust were found to be below 10 ppm, and for CO they were below 60 ppm, regardless of equivalence ratio or amount of ammonia in fuel.

The $NO_x$ results for this installation proved that ammonia is their major source, since they quickly rise as $NH_3$ is introduced. However, the pattern is not of proportionality, and a peak in emissions is obtained for around 50% of ammonia in the fuel mixture, decreasing afterwards. The effect of the equivalence ratio was also notable, as a decrease in $\phi$ lead to lower amounts of $NO_x$. Both of these trends are in agreement with the literature.

Regarding the temperature results of the porous-media burner, it was found that there is no quantifiable variance as the ammonia quantity in the fuel mixture changes, regardless of the constituents. Differences between methane/ammonia and hydrogen/ammonia blends were found to be mostly regarding flame front position, as the presence of hydrogen carried the flame front upstream, towards the source. Nonetheless, a higher maximum temperature was also found in hydrogen/ammonia blends, concordant with the fact that these mixtures do not emit carbon-dioxide. Thus the flue gases lose less heat through radiation, according to the previous supposition.

CO results for methane/ammonia blends in this burner proved that the combustion of the hydrocarbon was complete. However, for both types of mixtures, unburnt $NH_3$ was found at the exit, in traces up to 500 ppm. These values were lower for hydrogen/ammonia blends.

Results of $NO_x$ concentrations for the methane/ammonia blend in the porous-media setup were concordant with those found in the flat-flame burner. However, for $NH_3$-$H_2$, the results were higher and the variation with the fraction of $NH_3$ in the fuel mixture had a different pattern. However, this concurs with the lower $NH_3$ results for this blend, as these values mean there is less SNCR of the $NO_x$, and thus higher emissions. For the $NH_3$-$CH_4$ blend, the higher values of $NH_3$ at high ammonia fraction in the fuel mixture are also in accordance with the decrease of $NO_x$ after they have peaked, once more due to SNCR. This also means that, although low $NO_x$ is achieved for high ammonia quantities in the fuel mixture, $NH_3$ emissions can start becoming significant as well. These concentrations must be balanced when high power outputs are being employed.

The experimental results were compared with 3 numerical mechanisms, Okafor, Tian and Dagaut, in which the experimental temperatures also served as an input. For the flat flame burner, the $NO_x$ predictions managed to correctly capture the trends for each equivalence ratio. However, there was an absolute difference of about 100%, meaning there is still work needed to resemble the orders of magnitude that are featured here. CO predictions were concordant with the experimental results for the fuel-lean conditions, but the same was not true for the equivalence ratio of 1.0. Here, the numerical models over-predicted the experimental values by two orders of magnitude. This scenario leads to believe that the mechanisms need to be improved for stoichiometric conditions, although they already predict well for fuel-lean. On another note, $NH_3$ concentration at the exhaust was predicted as practically zero, for all conditions. This is accordance with the experimental counterpart.

Similar fittings were achieved for the porous-media setup. For methane/ammonia blends, the $NO_x$ patterns were well captured, but there is still a very significant absolute difference between the results and the predictions, even more in this burner. The same was true for hydrogen/ammonia blends. As for CO, it was correctly not detected for $NH_3$-$H_2$, and over-predicted in the $NH_3$-$CH_4$ mixtures, although only

by an order of magnitude, in this case. Once more the predicted $NH_3$ results were practically null, although this does not concur with the traces found in the experimental work.

As a whole, the numerical mechanisms were found to be mostly concise in the fitting of the patterns, correctly predicting the relative differences between adjacent conditions. Several improvements are observed when comparing the older models, Tian and Dagaut, with the most recent, Okafor. Indeed, the latter proved to be the best for practically all conditions tested here. However, there is still some development needed in terms of absolute values, as the differences were very significant.

It should be taken into account that these models were constructed with specific combustion conditions in mind, different than those featured here. However, the goal is to provide data of different scenarios, in order to fine-tune such mechanisms and allow for their strengthening. In this way, subsequent models will be capable of properly predicting emissions for a wide range of situations. Only after successful strenuous validation, will these numerical tools be suitable for the design of future ammonia-based reactors, in a multitude of configurations and applications.

With this objective in mind, the work presented here is a small step towards the development of technologies that will push for the wide acceptance and implementation of ammonia as a suitable substitute for fossil fuels. Complementarily, a future ammonia-based economy was presented and discussed, in which the flexibility of using ammonia in a variety of manners will be able to satisfy global energy demands, while also contributing to the active reduction of carbon-based pollution. Such is the future that this research aims to contribute for.

## 4.2. Future Work

As was previously discussed, research on ammonia as fuel is relatively new, and, consequently, there are many types of investigations that can be conducted and many technologies to develop until ammonia presents enough readiness to be applied extensively. Fundamental properties still need to be evaluated in scrutiny, as well as practical scenarios.

Regarding experimental research, swirl burners have showed great potential in combusting ammonia, due to their effectiveness in mixing the constituents. Development in this area will open doors to trials in industrial-size gas turbines, which may lead to feasible electricity production from ammonia. Therefore, scalability of these burners should also be investigated.

Emissions suppression should also be developed, as $NO_x$ is still a great barrier in implementing ammonia widely. SCR and SNCR processes should be evaluated in practical situations, and their deployment should also scale to large applications. Additionally, there should be an emphasis in using the ammonia that is already available in the fuel as a pathway to minimizing $NO_x$.

Finally, numerical mechanisms still need extensive development. GRIMech3.0 is an example of a mechanism that has been progressively enhanced and is now regarded as the best for predicting methane combustion for a wide range conditions. Such should be the objective in the case of ammonia.

Additionally, taking into account the multitude of models that already exist for ammonia combustion, efforts should be made towards a common denominator, because present investigations in this area are segregated among many different mechanisms.

# 5. References


[1] International Energy Agency, “Global Energy Statistics”. [Online]. Available: https://www.iea.org/statistics/. [Accessed: 03-Sep-2018].

[2] P. Coelho and M. Costa, *Combustão*, 2ª Edição. 2012.

[3] United Nations Framework Convention on Climate Change, “Paris Agreement”, *United Nations*, 2015. [Online]. Available: http://unfccc.int/files/essential_background/convention/application/pdf/english_paris_agreement.pdf. [Accessed: 03-Sep-2018].

[4] I. P. Jain, “Hydrogen the fuel for 21st century”, *Int. J. Hydrogen Energy*, vol. 34, no. 17, pp. 7368–7378, 2009.

[5] A. J. Reiter and S. C. Kong, “Combustion and emissions characteristics of compression-ignition engine using dual ammonia-diesel fuel”, *Fuel*, vol. 90, no. 1, pp. 87–97, 2011.

[6] C. Zamfirescu and I. Dincer, “Using ammonia as a sustainable fuel”, *J. Power Sources*, vol. 185, no. 1, pp. 459–465, 2008.

[7] R. Lan, K. A. Alkhazmi, I. A. Amar, and S. Tao, “Synthesis of ammonia directly from wet air at intermediate temperature”, *Appl. Catal. B Environ.*, vol. 152–153, pp. 212–217, Jun. 2014.

[8] Y. Bicer, I. Dincer, C. Zamfirescu, G. Vezina, and F. Raso, “Comparative life cycle assessment of various ammonia production methods”, *J. Clean. Prod.*, vol. 135, pp. 1379–1395, 2016.

[9] J. R. Bartels, “A feasibility study of implementing an ammonia economy”, Iowa State University, 2008.

[10] G. Thomas and G. Parks, “Potential Roles of Ammonia in a Hydrogen Economy”, *U.S. Dep. Energy*, 2006.

[11] S. Cornelius, “REFUEL Is Back on Track”, *Ammonia Energy*, 2017. [Online]. Available: http://www.ammoniaenergy.org/refuel-is-back-on-track/2017/. [Accessed: 05-Oct-2018].

[12] E. Kroch, “Ammonia - A fuel for motor buses”, *J Inst Pet.*, vol. 31, pp. 21–32, 2018.

[13] N. Akter, L. Han, D. Huaman, Y. J. Kang, and T. Kim, “NO and NH3Oxidation over Zeolite Materials”, *Mater. Today Proc.*, vol. 3, no. 2, pp. 550–555, 2016.

[14] W. Duo, K. Dam-Johansen, and K. Østergaard, “Kinetics of the gas-phase reaction between nitric oxide, ammonia and oxygen”, *Can. J. Chem. Eng.*, vol. 70, pp. 1014–1020, 1992.

[15] W. Henry, “Experiments on Ammonia, and an Account of a New Method of Analyzing It, by Combustion with Oxygen and Other Gases”, *Philos. Trans. R. Soc. London*, vol. 99, pp. 430–449, 1809.

[16] E. S. Starkman and G. S. Samuelsen, “Flame-propagation rates in ammonia-air combustion at high pressure”, in *Symposium (International) on Combustion*, 1967, vol. 11, no. 1, pp. 1037–1045.

[17] F. J. Verkamp, M. C. Hardin, and J. R. Williams, “Ammonia combustion properties and performance in gas-turbine burners”, *Symp. Combust.*, vol. 11, no. 1, pp. 985–992, Jan. 1967.

[18] D. T. Pratt, “Performance of Ammonia-Fired Gas-Turbine Combustors”, *Tech. Rep. No.9*, Contract DA-04-200-AMC-791(x), 1967.

[19] A. A. Konnov, I. V. Dyakov, and J. De Ruyck, “Probe sampling measurements of NO in CH4+O2+N2 flames doped with NH3”, *Combust. Sci. Technol.*, vol. 178, no. 6, pp. 1143–1164, 2006.

[20] C. Brackmann, E. J. K. Nilsson, J. D. Nauclér, M. Aldén, and A. A. Konnov, “Formation of NO and NH in NH3-doped CH4 + N2 + O2 flame: Experiments and modelling”, *Combust. Flame*, vol. 194, pp. 278–284, 2018.

[21] M. Barbas, M. Costa, S. Vranckx, and R. X. Fernandes, “Experimental and chemical kinetic study of CO and NO formation in oxy-methane premixed laminar flames doped with NH3”, *Combust. Flame*, vol. 162, no. 4, pp. 1294–1303, 2015.

[22] C. S. Mørch, A. Bjerre, M. P. Gøttrup, S. C. Sorenson, and J. Schramm, “Ammonia/hydrogen mixtures in an SI-engine: Engine performance and analysis of a proposed fuel system”, *Fuel*, vol. 90, no. 2, pp. 854–864, 2011.

[23] A. Valera-Medina *et al.*, “Ammonia, Methane and Hydrogen for Gas Turbines”, *Energy Procedia*, vol. 75, pp. 118–123, 2015.

[24] A. Hayakawa, Y. Arakawa, R. Mimoto, K. D. K. A. Somarathne, T. Kudo, and H. Kobayashi, “Experimental investigation of stabilization and emission characteristics of ammonia/air premixed flames in a swirl combustor”, *Int. J. Hydrogen Energy*, vol. 42, no. 19, pp. 14010–14018, 2017.

[25] O. Kurata *et al.*, “Performances and emission characteristics of NH3-air and NH3-CH4-air combustion gas-turbine power generations”, *Proc. Combust. Inst.*, vol. 36, no. 3, pp. 3351–3359, 2017.

[26] H. Xiao, A. Valera-Medina, and P. J. Bowen, “Study on premixed combustion characteristics of co-firing ammonia/methane fuels”, *Energy*, vol. 140, pp. 125–135, 2017.

[27] H. Nozari and A. Karabeyoğlu, “Numerical study of combustion characteristics of ammonia as a renewable fuel and establishment of reduced reaction mechanisms”, *Fuel*, vol. 159, pp. 223–233, 2015.

[28] H. Nozari, O. Tuncer, and A. Karabeyoglu, “Evaluation of ammonia-hydrogen-air combustion in SiC porous medium based burner”, *Energy Procedia*, vol. 142, pp. 674–679, 2017.

[29] A. Hayakawa, T. Goto, R. Mimoto, Y. Arakawa, T. Kudo, and H. Kobayashi, “Laminar burning velocity and Markstein length of ammonia/air premixed flames at various pressures”, *Fuel*, vol. 159, pp. 98–106, 2015.

[30] C. Duynslaegher, H. Jeanmart, and J. Vandooren, “Ammonia combustion at elevated pressure and temperature conditions”, *Fuel*, vol. 89, no. 11, pp. 3540–3545, 2010.

[31] A. Valera-Medina, H. Xiao, M. Owen-Jones, W. I. F. David, and P. J. Bowen, “Ammonia for power”, *Prog. Energy Combust. Sci.*, vol. 69, pp. 63–102, Nov. 2018.

[32] J. A. Miller and C. T. Bowman, “Mechanism and Modeling of Nitrogen Chemistry in Combustion”, *Prog. Energy Combust. Sci.*, vol. 15, pp. 287–338, 1989.

[33] A. A. Konnov, “Implementation of the NCN pathway of prompt-NO formation in the detailed reaction mechanism”, *Combust. Flame*, vol. 156, no. 11, pp. 2093–2105, 2009.

[34] C. Duynslaegher, F. Contino, J. Vandooren, and H. Jeanmart, “Modeling of ammonia combustion at low pressure”, *Combust. Flame*, vol. 159, no. 9, pp. 2799–2805, 2012.

[35] P. Dagaut, P. Glarborg, and M. U. Alzueta, “The oxidation of hydrogen cyanide and related chemistry”, *Prog. Energy Combust. Sci.*, vol. 34, no. 1, pp. 1–46, Feb. 2008.

[36] O. Mathieu and E. L. Petersen, “Experimental and modeling study on the high-temperature oxidation of Ammonia and related NOx chemistry”, *Combust. Flame*, vol. 162, no. 3, pp. 554–570, 2015.

[37] H. Xiao, A. Valera-Medina, and P. J. Bowen, “Modeling Combustion of Ammonia/Hydrogen Fuel Blends under Gas Turbine Conditions”, *Energy and Fuels*, vol. 31, no. 8, pp. 8631–8642, 2017.

[38] Y. Song, H. Hashemi, J. M. Christensen, C. Zou, P. Marshall, and P. Glarborg, “Ammonia oxidation at high pressure and intermediate temperatures”, *Fuel*, vol. 181, pp. 358–365, Oct. 2016.

[39] J. Otomo, M. Koshi, T. Mitsumori, H. Iwasaki, and K. Yamada, “Chemical kinetic modeling of ammonia oxidation with improved reaction mechanism for ammonia/air and ammonia/hydrogen/air combustion”, *Int. J. Hydrogen Energy*, vol. 43, no. 5, pp. 3004–3014, 2018.

[40] Z. Tian, Y. Li, L. Zhang, P. Glarborg, and F. Qi, “An experimental and kinetic modeling study of premixed NH3/CH4/O2/Ar flames at low pressure”, *Combust. Flame*, vol. 156, no. 7, pp. 1413–1426, 2009.

[41] P. Kumar and T. R. Meyer, “Experimental and modeling study of chemical-kinetics mechanisms for H2-NH3-air mixtures in laminar premixed jet flames”, *Fuel*, vol. 108, pp. 166–176, 2013.

[42] H. Xiao, A. Valera-Medina, R. Marsh, and P. J. Bowen, “Numerical study assessing various ammonia/methane reaction models for use under gas turbine conditions”, *Fuel*, vol. 196, pp.

344–351, 2017.

[43] E. C. Okafor *et al.*, “Experimental and numerical study of the laminar burning velocity of CH4–NH3–air premixed flames”, *Combust. Flame*, vol. 187, pp. 185–198, 2018.

[44] T. Carvalho, M. Costa, C. Casaca, R. C. Catapan, and A. A. M. Oliveira, “Destruction of the tar present in syngas by combustion in porous media”, *Energy and Fuels*, vol. 29, no. 2, pp. 1130–1136, 2015.

[45] R. W. Francisco, F. Rua, M. Costa, R. C. Catapan, and A. A. M. Oliveira, “On the combustion of hydrogen-rich gaseous fuels with low calorific value in a porous burner”, *Energy and Fuels*, vol. 24, no. 2, pp. 880–887, 2010.

[46] J. Li, H. Huang, N. Kobayashi, Z. He, and Y. Nagai, “Study on using hydrogen and ammonia as fuels: Combustion characteristics and NO x formation”, *Int. J. Energy Res.*, vol. 38, no. 9, pp. 1214–1223, Jul. 2014.

[47] British Standards Institution, “International thermocouple reference tables”. [Online]. Available: https://doi.org/10.3403/BS4937. [Accessed: 04-Oct-2018].

[48] REOTEMP Instruments, “Typr R Thermocouple”. [Online]. Available: https://www.thermocoupleinfo.com/type-r-thermocouple.htm. [Accessed: 04-Oct-2018].

[49] R. Imbihl *et al.*, “Catalytic ammonia oxidation on platinum: mechanism and catalyst restructuring at high and low pressure”, *Phys. Chem. Chem. Phys.*, vol. 9, no. 27, pp. 3522–3540, 2007.

[50] Cantera Developers, “Cantera”. [Online]. Available: https://cantera.org. [Accessed: 04-Oct-2018].

[51] M. J. Moran, H. N. Shapiro, D. D. Boettner, and M. B. Bailey, *Fundamentals of Engineering Thermodynamics*, 7th Edition. John Wiley & Sons, 2010.

[52] R. Mateus, “Analysis of radiation properties of gases and utilization in a pulverised coal combustion simulation model”, Instituto Superior Técnico, 2007.

[53] A. Kumamoto, H. Iseki, R. Ono, and T. Oda, “Measurement of minimum ignition energy in hydrogen-oxygen-nitrogen premixed gas by spark discharge”, *J. Phys. Conf. Ser.*, vol. 301, no. 1, 2011.

[54] S. J. Davis *et al.*, “Net-zero emissions energy systems”, *Science*, vol. 360, no. 6396, p. eaas9793, Jun. 2018.

[55] H. A. Haugen, N. H. Eldrup, A. M. Fatnes, and E. Leren, “Commercial Capture and Transport of CO2 from Production of Ammonia”, *Energy Procedia*, vol. 114, no. 1876, pp. 6133–6140, 2017.

[56] B. Zhao, Y. Su, W. Tao, L. Li, and Y. Peng, “Post-combustion CO2 capture by aqueous ammonia: A state-of-the-art review”, *Int. J. Greenh. Gas Control*, vol. 9, pp. 355–371, 2012.

[57] A. Sánchez and M. Martín, “Optimal renewable production of ammonia from water and air”, *J. Clean. Prod.*, vol. 178, pp. 325–342, 2018.

[58] R. W. Seaman and G. Huson, “The choice of NH3 to fuel the X-15 rocket plane”, *NH3 Fuel Association*, 2011. [Online]. Available: https://nh3fuel.files.wordpress.com/2013/01/2011-seaman-huson.pdf. [Accessed: 05-Oct-2018].

[59] A. Afif, N. Radenahmad, Q. Cheok, S. Shams, J. H. Kim, and A. K. Azad, “Ammonia-fed fuel cells: A comprehensive review”, *Renew. Sustain. Energy Rev.*, vol. 60, pp. 822–835, 2016.